GFRP DOWEL BARS FOR CONCRETE PAVEMENT

by

Susan L. Grieef

69.

A Thesis
Submitted to the Faculty of Graduate Studies
in Partial Fulfilment of the Requirements
for the Degree of

MASTER OF SCIENCE

Department of Civil & Geological Engineering
University of Manitoba
Winnipeg, Manitoba

ISBN 0-612-13156-4

Name _____

Dissertation Abstracts International and *Masters Abstracts International* are arranged by broad, general subject categories. Please select the one subject which most nearly describes the content of your dissertation or thesis. Enter the corresponding four-digit code in the spaces provided.

CIVIL ENGINEERING

SUBJECT TERM

0543 UMI

SUBJECT CODE

Subject Categories

THE HUMANITIES AND SOCIAL SCIENCES

COMMUNICATIONS AND THE ARTS
Architecture 0729
Art History 0377
Cinema 0900
Dance 0378
Fine Arts 0357
Information Science 0723
Journalism 0391
Library Science 0399
Mass Communications 0708
Music 0413
Speech Communication 0459
Theater 0465

EDUCATION
General 0515
Administration 0514
Adult and Continuing 0516
Agricultural 0517
Art 0273
Bilingual and Multicultural 0282
Business 0688
Community College 0275
Curriculum and Instruction 0727
Early Childhood 0518
Elementary 0524
Finance 0277
Guidance and Counseling 0519
Health 0680
Higher 0745
History of 0520
Home Economics 0278
Industrial 0521
Language and Literature 0279
Mathematics 0280
Music 0522
Philosophy of 0998
Physical 0523
Psychology 0525
Reading 0535
Religious 0527
Sciences 0714
Secondary 0533
Social Sciences 0534
Sociology of 0340
Special 0529
Teacher Training 0530
Technology 0710
Tests and Measurements 0288
Vocational 0747

LANGUAGE, LITERATURE AND LINGUISTICS
Language
- General 0679
- Ancient 0289
- Linguistics 0290
- Modern 0291

Literature
- General 0401
- Classical 0294
- Comparative 0295
- Medieval 0297
- Modern 0298
- African 0316
- American 0591
- Asian 0305
- Canadian (English) 0352
- Canadian (French) 0355
- English 0593
- Germanic 0311
- Latin American 0312
- Middle Eastern 0315
- Romance 0313
- Slavic and East European 0314

PHILOSOPHY, RELIGION AND THEOLOGY
Philosophy 0422
Religion
- General 0318
- Biblical Studies 0321
- Clergy 0319
- History of 0320
- Philosophy of 0322

Theology 0469

SOCIAL SCIENCES
American Studies 0323
Anthropology
- Archaeology 0324
- Cultural 0326
- Physical 0327

Business Administration
- General 0310
- Accounting 0272
- Banking 0770
- Management 0454
- Marketing 0338

Canadian Studies 0385
Economics
- General 0501
- Agricultural 0503
- Commerce-Business 0505
- Finance 0508
- History 0509
- Labor 0510
- Theory 0511

Folklore 0358
Geography 0366
Gerontology 0351
History
- General 0578
- Ancient 0579
- Medieval 0581
- Modern 0582
- Black 0328
- African 0331
- Asia, Australia and Oceania 0332
- Canadian 0334
- European 0335
- Latin American 0336
- Middle Eastern 0333
- United States 0337

History of Science 0585
Law 0398
Political Science
- General 0615
- International Law and Relations 0616
- Public Administration 0617

Recreation 0814
Social Work 0452
Sociology
- General 0626
- Criminology and Penology 0627
- Demography 0938
- Ethnic and Racial Studies 0631
- Individual and Family Studies 0628
- Industrial and Labor Relations 0629
- Public and Social Welfare 0630
- Social Structure and Development 0700
- Theory and Methods 0344

Transportation 0709
Urban and Regional Planning 0999
Women's Studies 0453

THE SCIENCES AND ENGINEERING

BIOLOGICAL SCIENCES
Agriculture
- General 0473
- Agronomy 0285
- Animal Culture and Nutrition 0475
- Animal Pathology 0476
- Food Science and Technology 0359
- Forestry and Wildlife 0478
- Plant Culture 0479
- Plant Pathology 0480
- Plant Physiology 0817
- Range Management 0777
- Wood Technology 0746

Biology
- General 0306
- Anatomy 0287
- Biostatistics 0308
- Botany 0309
- Cell 0379
- Ecology 0329
- Entomology 0353
- Genetics 0369
- Limnology 0793
- Microbiology 0410
- Molecular 0307
- Neuroscience 0317
- Oceanography 0416
- Physiology 0433
- Radiation 0821
- Veterinary Science 0778
- Zoology 0472

Biophysics
- General 0786
- Medical 0760

EARTH SCIENCES
Biogeochemistry 0425
Geochemistry 0996
Geodesy 0370
Geology 0372
Geophysics 0373
Hydrology 0388
Mineralogy 0411
Paleobotany 0345
Paleoecology 0426
Paleontology 0418
Paleozoology 0985
Palynology 0427
Physical Geography 0368
Physical Oceanography 0415

HEALTH AND ENVIRONMENTAL SCIENCES
Environmental Sciences 0768
Health Sciences
- General 0566
- Audiology 0300
- Chemotherapy 0992
- Dentistry 0567
- Education 0350
- Hospital Management 0769
- Human Development 0758
- Immunology 0982
- Medicine and Surgery 0564
- Mental Health 0347
- Nursing 0569
- Nutrition 0570
- Obstetrics and Gynecology 0380
- Occupational Health and Therapy 0354
- Ophthalmology 0381
- Pathology 0571
- Pharmacology 0419
- Pharmacy 0572
- Physical Therapy 0382
- Public Health 0573
- Radiology 0574
- Recreation 0575
- Speech Pathology 0460
- Toxicology 0383

Home Economics 0386

PHYSICAL SCIENCES
Pure Sciences
Chemistry
- General 0485
- Agricultural 0749
- Analytical 0486
- Biochemistry 0487
- Inorganic 0488
- Nuclear 0738
- Organic 0490
- Pharmaceutical 0491
- Physical 0494
- Polymer 0495
- Radiation 0754

Mathematics 0405
Physics
- General 0605
- Acoustics 0986
- Astronomy and Astrophysics 0606
- Atmospheric Science 0608
- Atomic 0748
- Electronics and Electricity 0607
- Elementary Particles and High Energy 0798
- Fluid and Plasma 0759
- Molecular 0609
- Nuclear 0610
- Optics 0752
- Radiation 0756
- Solid State 0611

Statistics 0463

Applied Sciences
Applied Mechanics 0346
Computer Science 0984
Engineering
- General 0537
- Aerospace 0538
- Agricultural 0539
- Automotive 0540
- Biomedical 0541
- Chemical 0542
- Civil 0543
- Electronics and Electrical 0544
- Heat and Thermodynamics 0348
- Hydraulic 0545
- Industrial 0546
- Marine 0547
- Materials Science 0794
- Mechanical 0548
- Metallurgy 0743
- Mining 0551
- Nuclear 0552
- Packaging 0549
- Petroleum 0765
- Sanitary and Municipal 0554
- System Science 0790

Geotechnology 0428
Operations Research 0796
Plastics Technology 0795
Textile Technology 0994

PSYCHOLOGY
General 0621
Behavioral 0384
Clinical 0622
Developmental 0620
Experimental 0623
Industrial 0624
Personality 0625
Physiological 0989
Psychobiology 0349
Psychometrics 0632
Social 0451

Nom _____

Dissertation Abstracts International est organisé en catégories de sujets. Veuillez s.v.p. choisir le sujet qui décrit le mieux votre thèse et inscrivez le code numérique approprié dans l'espace réservé ci-dessous.

_____ ☐☐☐ U·M·I

SUJET — CODE DE SUJET

Catégories par sujets

HUMANITÉS ET SCIENCES SOCIALES

COMMUNICATIONS ET LES ARTS
Architecture 0729
Beaux-arts 0357
Bibliothéconomie 0399
Cinéma 0900
Communication verbale 0459
Communications 0708
Danse 0378
Histoire de l'art 0377
Journalisme 0391
Musique 0413
Sciences de l'information 0723
Théâtre 0465

ÉDUCATION
Généralités 515
Administration 0514
Art 0273
Collèges communautaires 0275
Commerce 0688
Économie domestique 0278
Éducation permanente 0516
Éducation préscolaire 0518
Éducation sanitaire 0680
Enseignement agricole 0517
Enseignement bilingue et multiculturel 0282
Enseignement industriel 0521
Enseignement primaire. 0524
Enseignement professionnel 0747
Enseignement religieux 0527
Enseignement secondaire 0533
Enseignement spécial 0529
Enseignement supérieur 0745
Évaluation 0288
Finances 0277
Formation des enseignants 0530
Histoire de l'éducation 0520
Langues et littérature 0279
Lecture 0535
Mathématiques 0280
Musique 0522
Orientation et consultation 0519
Philosophie de l'éducation 0998
Physique 0523
Programmes d'études et enseignement 0727
Psychologie 0525
Sciences 0714
Sciences sociales 0534
Sociologie de l'éducation 0340
Technologie 0710

LANGUE, LITTÉRATURE ET LINGUISTIQUE
Langues
- Généralités 0679
- Anciennes 0289
- Linguistique 0290
- Modernes 0291

Littérature
- Généralités 0401
- Anciennes 0294
- Comparée 0295
- Médiévale 0297
- Moderne 0298
- Africaine 0316
- Américaine 0591
- Anglaise 0593
- Asiatique 0305
- Canadienne (Anglaise) 0352
- Canadienne (Française) 0355
- Germanique 0311
- Latino-américaine 0312
- Moyen-orientale 0315
- Romane 0313
- Slave et est-européenne 0314

PHILOSOPHIE, RELIGION ET THÉOLOGIE
Philosophie 0422
Religion
- Généralités 0318
- Clergé 0319
- Études bibliques 0321
- Histoire des religions 0320
- Philosophie de la religion 0322

Théologie 0469

SCIENCES SOCIALES
Anthropologie
- Archéologie 0324
- Culturelle 0326
- Physique 0327

Droit 0398
Économie
- Généralités 0501
- Commerce-Affaires 0505
- Économie agricole 0503
- Économie du travail 0510
- Finances 0508
- Histoire 0509
- Théorie 0511

Études américaines 0323
Études canadiennes 0385
Études féministes 0453
Folklore 0358
Géographie 0366
Gérontologie 0351
Gestion des affaires
- Généralités 0310
- Administration 0454
- Banques 0770
- Comptabilité 0272
- Marketing 0338

Histoire
- Histoire générale 0578
- Ancienne 0579
- Médiévale 0581
- Moderne 0582
- Histoire des noirs 0328
- Africaine 0331
- Canadienne 0334
- États-Unis 0337
- Européenne 0335
- Moyen-orientale 0333
- Latino-américaine 0336
- Asie, Australie et Océanie 0332

Histoire des sciences 0585
Loisirs 0814
Planification urbaine et régionale 0999
Science politique
- Généralités 0615
- Administration publique 0617
- Droit et relations internationales 0616

Sociologie
- Généralités 0626
- Aide et bien-être social 0630
- Criminologie et établissements pénitentiaires 0627
- Démographie 0938
- Études de l' individu et de la famille 0628
- Études des relations interethniques et des relations raciales 0631
- Structure et développement social 0700
- Théorie et méthodes. 0344
- Travail et relations industrielles 0629

Transports 0709
Travail social 0452

SCIENCES ET INGÉNIERIE

SCIENCES BIOLOGIQUES
Agriculture
- Généralités 0473
- Agronomie. 0285
- Alimentation et technologie alimentaire 0359
- Culture 0479
- Élevage et alimentation 0475
- Exploitation des pâturages 0777
- Pathologie animale 0476
- Pathologie végétale 0480
- Physiologie végétale 0817
- Sylviculture et faune 0478
- Technologie du bois 0746

Biologie
- Généralités 0306
- Anatomie 0287
- Biologie (Statistiques) 0308
- Biologie moléculaire 0307
- Botanique 0309
- Cellule 0379
- Écologie 0329
- Entomologie 0353
- Génétique 0369
- Limnologie 0793
- Microbiologie 0410
- Neurologie 0317
- Océanographie 0416
- Physiologie 0433
- Radiation 0821
- Science vétérinaire 0778
- Zoologie 0472

Biophysique
- Généralités 0786
- Medicale 0760

SCIENCES DE LA TERRE
Biogéochimie 0425
Géochimie 0996
Géodésie 0370
Géographie physique 0368
Géologie 0372
Géophysique 0373
Hydrologie 0388
Minéralogie 0411
Océanographie physique 0415
Paléobotanique 0345
Paléoécologie 0426
Paléontologie 0418
Paléozoologie 0985
Palynologie 0427

SCIENCES DE LA SANTÉ ET DE L'ENVIRONNEMENT
Économie domestique 0386
Sciences de l'environnement 0768
Sciences de la santé
- Généralités 0566
- Administration des hôpitaux 0769
- Alimentation et nutrition 0570
- Audiologie 0300
- Chimiothérapie 0992
- Dentisterie 0567
- Développement humain 0758
- Enseignement 0350
- Immunologie 0982
- Loisirs 0575
- Médecine du travail et thérapie 0354
- Médecine et chirurgie 0564
- Obstétrique et gynécologie 0380
- Ophtalmologie 0381
- Orthophonie 0460
- Pathologie 0571
- Pharmacie 0572
- Pharmacologie 0419
- Physiothérapie 0382
- Radiologie 0574
- Santé mentale 0347
- Santé publique 0573
- Soins infirmiers 0569
- Toxicologie 0383

SCIENCES PHYSIQUES
Sciences Pures
Chimie
- Généralités 0485
- Biochimie 487
- Chimie agricole 0749
- Chimie analytique 0486
- Chimie minérale 0488
- Chimie nucléaire 0738
- Chimie organique 0490
- Chimie pharmaceutique 0491
- Physique 0494
- PolymÈres 0495
- Radiation 0754

Mathématiques 0405
Physique
- Généralités 0605
- Acoustique 0986
- Astronomie et astrophysique 0606
- Électronique et électricité 0607
- Fluides et plasma 0759
- Météorologie 0608
- Optique 0752
- Particules (Physique nucléaire) 0798
- Physique atomique 0748
- Physique de l'état solide 0611
- Physique moléculaire 0609
- Physique nucléaire 0610
- Radiation 0756

Statistiques 0463

Sciences Appliqués Et Technologie
Informatique 0984
Ingénierie
- Généralités 0537
- Agricole 0539
- Automobile 0540
- Biomédicale 0541
- Chaleur et thermodynamique 0348
- Conditionnement (Emballage) 0549
- Génie aérospatial 0538
- Génie chimique 0542
- Génie civil 0543
- Génie électronique et électrique 0544
- Génie industriel 0546
- Génie mécanique 0548
- Génie nucléaire 0552
- Ingénierie des systèmes 0790
- Mécanique navale 0547
- Métallurgie 0743
- Science des matériaux 0794
- Technique du pétrole 0765
- Technique minière 0551
- Techniques sanitaires et municipales 0554
- Technologie hydraulique 0545

Mécanique appliquée 0346
Géotechnologie 0428
Matières plastiques (Technologie) 0795
Recherche opérationnelle 0796
Textiles et tissus (Technologie) 0794

PSYCHOLOGIE
Généralités 0621
Personnalité 0625
Psychobiologie 0349
Psychologie clinique 0622
Psychologie du comportement 0384
Psychologie du développement 0620
Psychologie expérimentale 0623
Psychologie industrielle 0624
Psychologie physiologique 0989
Psychologie sociale 0451
Psychométrie 0632

THE UNIVERSITY OF MANITOBA

FACUTY OF GRADUATE STUDIES

COPYRIGHT PERMISSION

GFRP DOWEL BARS FOR CONCRETE PAVEMENT

BY

SUSAN L. GRIEEF

A Thesis/Practicum submitted to the Faculty of Graduate Studies of the University of Manitoba in partial fulfillment of the requirements for the degree of

MASTER OF SCIENCE

ABSTRACT

Traditionally, plain steel or epoxy-coated steel has been used for dowel bars in concrete pavements. However, problems arising from corrosion of the steel have prompted recent investigations into alternative dowel materials. This thesis presents the results of an experimental program that was undertaken to determine the feasibility of using Isorod, a glass fiber reinforced plastic, as dowels in concrete pavements. A total of eight push-off specimens were tested with either steel or Isorod dowels that were either partially bonded or not bonded to the concrete. The tested specimens were designed to apply a pure shear load to the dowels to determine their behaviour and strength.

The results revealed that the dowels of all the specimens exhibited a kinking action, however, this occurred at significantly lower loads for the Isorod dowels than for the steel dowels. The Isorod dowels were not as stiff as the steel dowels in the pre-kinking stage and also experienced a decrease in load-carrying capacity after kinking began, which was contrary to the steel dowel behaviour. As well, the Isorod dowels split longitudinally as kinking commenced and later experienced a complete failure as the dowels sheared off at the concrete face.

From the models available for predicting the kinking strength of the dowels, the model that treated the embedded portion of the dowel as a beam on an elastic foundation gave accurate predictions. However, it was found that the kinking strength of the Isorod dowels was dependent on the tensile strength of the resin used in the composite and not the tensile strength of the composite itself. Using the dowel strength obtained from testing, the Isorod

dowel diameter required in an actual pavement was found to be significantly larger than that required for steel dowels.

The other aspect of this feasibility study that was investigated was a life-cycle cost comparison of five alternative dowel materials: plain steel, epoxy-coated steel, stainless steel, Isorod and C-bar. The most cost-effective dowel material was plain steel. Epoxy-coated steel dowels were slightly more expensive than the plain steel dowels. This was the result of the majority of the dowels being replaced due to factors other than those related to corrosion of the steel. The costs of Isorod, C-bar and stainless steel dowels were much too high to consider them as viable alternatives.

ACKNOWLEDGEMENTS

This research program was conducted under the direct supervision of Dr. S. H. Rizkalla, Department of Civil Engineering, University of Manitoba. The author wishes to thank Dr. Rizkalla for suggesting this research topic and for his guidance and advice throughout this investigation.

The author also wishes to thank Mr. S. Hilderman, Manitoba Department of Highways and Transportation for his continued assistance and information during this project. Thanks are also extended to Mr. B. Prentice, Transport Institute, University of Manitoba and Mr. K. Boyd, Winnipeg Streets and Transportation Department for their advice and information for the life-cycle cost comparison portion of this project.

The author wishes to express her gratefulness to Dr. B. Benmokrane, Université de Sherbrooke, for his assistance during several stages of the research program.

Special thanks are due to Mr. Scott Sparrow, Mr. Moray McVey, Mr. Ed Lemke, Mr. Kim Majury, Mr. Irwin Penner and Mr. Rob Graham, P. Eng. of the Department of Civil Engineering for their continued assistance during the laboratory portion of the work. Thanks are also extended to graduate students Mr. Craig Michaluk and Mr. Nolan Domenico for their assistance during construction and testing of the specimens.

TABLE OF CONTENTS

Page

CHAPTER 7

CHAPTER 8

LIST OF TABLES

LIST OF FIGURES

LIST OF SYMBOLS

A_s	Total area of steel crossing shear plane
c	Depth of crushed concrete from concrete face
d_b	Dowel bar diameter
d_{bi}	Isorod dowel bar diameter
d_{bs}	Steel dowel bar diameter
d_u	Ultimate dowel strength
d_{ui}	Isorod dowel strength
d_{us}	Steel dowel strength
D	Shear force applied to dowel
D_u	Ultimate dowel load
E_i	Modulus of elasticity of Isorod
E_s	Modulus of elasticity of steel
f_b	Bearing strength of concrete
f'_c	Compressive strength of concrete
$f_{t\ resin}$	Tensile strength of resin in GFRP
f_y	Yield strength of steel
F_u	Ultimate tensile load of Isorod
G_i	Shear modulus of Isorod dowel
G_s	Shear modulus of steel dowel
I_i	Moment of inertia of Isorod dowel

I_s	Moment of inertia of steel dowel
K	Elastic foundation stiffness
K_f	Concrete foundation modulus
l	Joint width
L_n	Distance from concrete face to n^{th} point of pressure reversal along dowel
M_p	Plastic moment of dowel
s	Dowel bar spacing
s_i	Isorod dowel bar spacing
s_s	Steel dowel bar spacing
t	Concrete pavement thickness
T	Dowel axial force
T_y	Tensile axial yield force of steel bar
V_c	Shear resistance of concrete
V_d	Shear strength of dowels
α	Angle of dowel to plane of loading
ß	Constant in equation for dowel length
γ	Constant in general equation for ultimate strength of dowel
γ_i	Constant in equation for ultimate strength of Isorod dowel
γ_s	Constant in equation for ultimate strength of steel dowel
Δ_i	Displacement of Isorod dowel
Δ_s	Displacement of steel dowel
θ	Kinking angle

μ	Coefficient of friction for concrete
χ	Distance from concrete face to point of maximum bending moment

CHAPTER 1

INTRODUCTION

1.1 GENERAL INFORMATION

In concrete pavements, dowel bars are used to transfer load from one slab to an adjoining slab across a joint. Dowel bars are typically smooth bars placed at mid-depth of the slab and they transfer the load without restricting horizontal movement of the joint, due to expansion and/or contraction. The bars provide horizontal and vertical alignment of the slabs, decrease slab deflection, lower concrete stress and also reduce the possibility of cracking, faulting and pumping of the pavement.[1]

Traditionally, dowels are made of mild steel and are normally 32 mm to 38 mm (1¼" to 1½") in diameter, 450 mm (18") long and spaced at 300 mm (12") on centre along the length of the transverse joint.[2] Since the dowels cross a joint exposed to environmental conditions, the dowels usually experience some corrosion, particularly in environments such as those encountered in Manitoba where salts are used for de-icing roads and highways in the winter. This corrosion restricts movement of the slab due to restricted movement of the dowel within the concrete as a result of expansion due to corrosion. This phenomenon is known as 'freezing' or 'binding' of the dowel. This behaviour can induce serious stresses in the concrete, causing cracking and chipping of the concrete at the joint locations. The corrosion may also cause failure of the dowels, leading to cracking of the concrete as well as excessive slab deflections under load resulting in a rough riding surface. Corrosion can also lead to premature failure of the joint with the result that more frequent repairs are needed.

To minimize the problem caused by corrosion, epoxy coated reinforcement is currently used. However, the effectiveness of the coating is highly dependent on whether it remains intact. The epoxy can chip off during placing and/or with wear during service. This can trigger the corrosion process and initiate the same problems discussed above.

Fiber reinforced plastic (FRP) presents a possible solution to this traditional problem as it has non-corrosive characteristics and may be applicable in the same fashion as normal reinforcement. However, since this is a relatively new material with completely different properties from steel, it is the purpose of this research to evaluate its behaviour and performance as compared to steel. FRP reinforcement consists of fibers which are oriented unidirectionally along the length of the reinforcement. Since the dowels will be loaded perpendicular to the fibers, their behaviour is unknown and it may be quite different than that of steel reinforcement.

1.2 OBJECTIVE

The main objective of this research was to examine the feasibility of using FRP dowels for concrete pavements. The proposed material was a glass fiber reinforced plastic (GFRP) dowel. The commercial name is Isorod which is produced by Pultrall Inc. in Thetford Mines, Québec. The main performance criteria which were evaluated were the load-displacement behaviour, the ultimate failure load and the mode of failure.

To achieve these objectives, specially designed tests were performed that subject the dowels to shear loading conditions equivalent to what could be induced in concrete pavement joints. Specially designed specimens were tested to induce pure shear conditions in the

dowels. Some of the specimens were reinforced with steel dowels. They were used as control specimens and provided a comparison to the behaviour of FRP dowels.

1.3 SCOPE

The experimental program consisted of testing push-off specimens to determine the behaviour and strength of the FRP dowels in pure shear as compared to that of steel. A review of the literature applicable to this experimental program is presented in Chapter 2. Detailed information of the test specimens and test setup are given in Chapter 3.

The results of these tests are presented in Chapter 4, while Chapter 5 contains an analysis and comparison of the behaviour of the specimens which determines whether the Isorod dowels perform similarly to the steel dowels. Then, design recommendations are made in Chapter 6 as to a method of strength prediction, as well as the diameter and length of Isorod dowel required for actual pavement thicknesses. The research program also includes a life-cycle cost comparison of alternatives to plain steel dowels such as epoxy-coated steel, stainless steel and Isorod dowels presented in Chapter 7.

CHAPTER 2

LITERATURE REVIEW

2.1 INTRODUCTION

This chapter contains a review of the literature relevant to this experimental program. The following sections discuss the methods available to resist shear loads, as well as the types of joints used in concrete pavements. The model used in the experimental program to simulate the behaviour of the dowels is also presented.

When concrete is used for pavement, cracking of the slab can be caused by several factors such as shrinkage during curing, temperature, moisture changes, subbase friction and traffic loadings.[1] In order to control the location and geometry of the cracks, joints are incorporated into the pavement. These joints act as inherent planes of weakness where cracks will occur, thereby preventing random cracking. However, design of the joint requires that a portion of a wheel load must be transferred across the transverse joint to the adjacent slab. Load transfer is typically accomplished by two mechanisms which can occur in a cracked or jointed slab: aggregate interlock and dowel action.

2.2 AGGREGATE INTERLOCK

Roughness of the concrete surface at a crack, which normally causes the aggregate to protrude, provides resistance to applied shear loads known as aggregate interlock. The resistance is provided through rubbing of the aggregates against one another along the crack interface. However, this mechanism occurs only when there is contact between the two rough

surfaces of the joint. Therefore, aggregate interlock becomes ineffective in large joint openings, which occur when the slabs contract significantly.

The shearing resistance due to aggregate interlock can be calculated, in the presence of dowels, using the shear friction theory as presented by both Birkeland[3] and Mast[4]. This theory relates the friction force developed along the cracked surface to the tensile force developed in a steel dowel crossing the crack. As slip occurs along the rough shear plane, the two faces are forced apart due to the protruding aggregate. This separation creates a tensile force in the dowel bar if it is bonded to the concrete. In turn, a compressive force is created in the concrete in equilibrium with the tensile force and it pushes the two faces back together.[5] This maintains a frictional resistance to slipping which resists the applied shear, as shown in Figure 2.1.

If the shear plane is under-reinforced, which is normally the case, the steel bars will eventually reach their yield point, f_y. Therefore, the tension force is equivalent to $A_s f_y$, where A_s is the total area of steel crossing the shear plane. As a result, the compressive force, which opposes the tensile force and pushes the faces together, is equal in magnitude to this tensile force. Therefore, the shear force, which is normal to the compressive force, can be calculated as the product of the compressive force and a coefficient of friction, μ, for concrete. The shear resistance can be estimated as:[6]

$$V_c = \mu A_s f_y \qquad (2.1)$$

The above represents the resistance of the concrete only. The total shear resistance is typically a combination of aggregate interlock and dowel action of the bar.

2.3 DOWEL ACTION

Dowel action is the second mechanism which provides resistance to the applied shear forces when dowel bars are provided across a joint. As the two concrete slabs move relative to one another, the dowels are subjected to a shearing action, which is commonly referred to as dowel action. The following sub-sections describe two different methods available to predict the amount of shear which can be resisted by the dowels. The first method is concerned with the behaviour of the portion of the dowel within the joint, while the second method deals with the behaviour of the portion of the dowel embedded in the concrete.

2.3.1 Dowel Action Mechanism

This method, which focusses on the dowel within the joint, assumes that the shear resistance of the dowels is dependent on the specific dowel action mechanism that develops and is a function of the total area of the bars crossing the joint.[7] Three different mechanisms can occur for steel dowels, and they are dependent on the joint width. These mechanisms are: kinking of the dowel, shear resistance of the bar and flexure of the dowel bar. Normally, shear and kinking mechanisms are the principal ones which occur. The three mechanisms are illustrated in Figure 2.2, which includes the following corresponding equations to evaluate each mechanism:

$$\textit{Flexure Mechanism} \qquad V_d = \frac{4\, d_b A_s f_y}{3\, \pi\, l} \tag{2.2}$$

$$\textit{Shear Mechanism} \qquad V_d = \frac{A_s f_y}{\sqrt{3}} \tag{2.3}$$

Kinking Mechanism $V_d = A_s f_y \cos \theta$ (2.4)

where A_s is the area of the dowel crossing the joint, d_b is the diameter of the dowel, f_y is the yield strength of the steel dowel, l is the joint width and θ is the kinking angle. These equations can be used only if the bars are not subjected to tensile forces.[8] In cases of combined shear and tensile loads, the shear strength will be less than the values predicted by the preceding equations.

2.3.2 Ultimate Strength of the Dowel

This theory states that the ultimate strength can be predicted based upon the beam on an elastic foundation theory using the portion of the dowel embedded in the concrete.[9] The theory was developed for steel dowels which were subjected to pure shear, with the dowel being modelled as a beam on an elastic foundation. The dowel bar is subjected to a shear force, D, at the concrete face and an axial force, T, along the length of the bar which has an angle α to the loading plane, as shown in Figure 2.3. This figure also shows the bearing stress distribution along the dowel as well as its bending moment distribution. A simplification of the applied loading and stress distribution is also shown to simulate the failure condition. The simplification assumes that the concrete is crushed to a distance, c, from the concrete face. The crushed zone can be evaluated using the following equation:[10]

$$c = \frac{0.05 f_y d_b}{fc'} \sin \alpha \qquad (2.5)$$

where f_c' is the compressive strength of the concrete.

From the end of the crushed zone to a distance χ within the concrete along the bar, which is where the maximum bending moment occurs, the bearing stress is assumed to be equivalent to the bearing strength of the concrete. According to this theory, the distance χ can be calculated using the following equation:

$$\chi = \frac{\pi}{\sqrt[4]{\frac{K}{E_s I_s}}} \tag{2.6}$$

where E_s is the modulus of elasticity of the steel dowel, I_s is the moment of inertia of the steel dowel and K is the elastic foundation stiffness, which is a function of the concrete foundation modulus, K_f, as follows:

$$K = K_f d_b \tag{2.7}$$

The typical value of K_f is approximately 10^6 psi/in (271.7 MPa/mm). The concrete foundation modulus is a constant for a given system and it depends on the concrete, the dowel material and diameter.[11]

The bearing strength of the concrete, f_b, can be calculated using the following equations:

$$f_b = \begin{cases} 154 \dfrac{\sqrt{f_c'}}{\sqrt[3]{d_b}} & \text{for } f_c' \text{ in psi and } d_b \text{ in inches} \\ 37.6 \dfrac{\sqrt{f_c'}}{\sqrt[3]{d_b}} & \text{for } f_c' \text{ in MPa and } d_b \text{ in mm} \end{cases} \tag{2.8}$$

These equations were obtained from a regressional analysis performed on results of tests

which measured the bearing strength of concrete at the instant of split cracking.[9]

For steel dowels, the bar is assumed to fail when the moment within the dowel reaches the plastic moment, Mp. This can be approximated for a round bar subjected to an axial force, T, as follows:

$$M_p = \frac{f_y d_b^3}{6}\left(1 - \frac{T^2}{T_y^2}\right) \tag{2.9}$$

where T_y is the axial yield strength of the dowel, which is simply equal to:

$$T_y = f_y \frac{\pi\, d_b^2}{4} \tag{2.10}$$

Using these equations and the equilibrium equation of forces at a distance χ, the expression given below can be obtained to predict the ultimate load, D_u, which the dowel bars can resist, as follows:[9]

$$D_u = 0.5 f_b (0.37\ \gamma\ d_b - c)^2 + \frac{0.45 f_y d_b^2}{\gamma}\left(1 - \frac{T^2}{T_y^2}\right) \tag{2.11}$$

$$\textit{where}\quad \gamma = \sqrt[4]{\frac{E}{K_f d_b}}$$

The basic theory of an infinitely long beam on an elastic foundation was originally derived by Timoshenko[12] and later applied to the specific case of a finite length dowel within concrete by Friberg.[13] For this specific case, Friberg developed a relationship to calculate the points along the dowel where there is a change in the direction of the pressure exerted on the

concrete. These points, L_n, can be calculated using the following equation:

$$\tan \beta L_n = \frac{2 + \beta l}{\beta l}$$

$$\text{where} \quad \beta = \sqrt[4]{\frac{K_f d_b}{4 E_s I_s}} \qquad (2.12)$$

where ß is a constant for a given system and l is the joint width. Friberg also concluded that the length of a dowel need not be larger than the second point of pressure change on each side of the joint.

2.4 TRANSVERSE JOINT TYPES

There are three standard types of transverse joints used in concrete pavements. They are the contraction joint, the construction joint and the isolation or expansion joint. Their use, construction and method of shearing resistance are explained in the following sub-sections.

2.4.1 Contraction Joints

Contraction joints are the most commonly used joint in concrete pavements and they are normally placed at every 5 to 6 m (18 to 20 feet) to permit movement of the slabs. The joints are crossed by a row of dowels which have been set up on 'baskets' or 'chairs' to hold them in place and at the proper elevation. The dowels are greased and the concrete is then cast. The greasing of the bar prevents the concrete from bonding and consequently allows movement of the slab. Once the concrete has set, a saw is used to cut approximately one third of the concrete thickness above the centre of the row of dowels.[1] This creates a plane

of weakness where the crack will form due to shrinkage of the concrete during curing. The crack allows dowel action to take place, and since the crack faces are rough, as shown in Figure 2.4(a), aggregate interlock will also be effective in resisting shear.

2.4.2 Construction Joints

Construction joints are made at the end of a day's work or when an unforseen interruption in casting occurs. Where the concrete stops, a board is put up to hold the concrete in place while it sets and the dowels are inserted into the concrete through pre-drilled holes in the board. Before casting begins again, the board is removed and the free end of the dowel is greased.[1]

For this type of joint, the greasing of one end still allows some slab movement even though the other end is bonded to the concrete. Since the board creates a relatively smooth surface, as shown in Figure 2.4(b), aggregate interlock becomes ineffective across the joint. Therefore, only dowel action can be used to develop the shear resistance.

2.4.3 Isolation or Expansion Joints

Isolation or expansion joints are used to separate a pavement from another structure, such as a bridge or manhole. They can also be used at large intersections where a lane meets the large expanse of concrete, as the intersection will have differing amounts and directions of expansion than the lane. The joint is usually 12 mm to 25 mm (½" to 1") wide with a filler in the space. The bars are set up similarly to those at contraction joints and the filler is placed at the centre of the joint. However, in this case only one half of the bar is greased, so that

after casting, only one half of the bar is bonded to the concrete. As shown in Figure 2.4(c), the greased end is also fitted with an expansion cap to allow movement of the slab.[1] Like the construction joint, the load will be resisted by the dowel action only. However, because the joint space is larger, the dowel action may be developed by a different mechanism than that for the other types of joints.

2.5 PROPOSED TEST MODEL

As the main objective of this research focuses on the behaviour of the dowels, the test model is designed to eliminate aggregate interlock components for shear resistance across the joints. The model reflects the actual method used to set the dowels in the field. For the three types of joints described, there are essentially only two dowel configurations which need to be modelled. The first is the case of the contraction joint, where the bar is not bonded to the concrete at all. The second configuration applies to the other two joint types, where one half of the bar is bonded to the concrete and the other half is not. Since the dowels are not bonded to the concrete or are only partially bonded, the test model is different from those which have been tested and recorded in the literature. Due to the lack of aggregate interlock and the lack of bond between the dowel and the concrete, the shear friction theory cannot be used to predict the shear strength of the proposed specimens. Lack of bond also affects the equations for dowel action given in Equations 2.2 to 2.4. The lack of bond may also affect the predicted values from Equation 2.11. Therefore, the actual shear strength obtained from the test may differ from the values predicted by the equations available in the literature.

CHAPTER 3

EXPERIMENTAL PROGRAM

3.1 INTRODUCTION

This chapter reviews the experimental program conducted to determine the shear properties and behaviour of dowels in concrete pavements. A description of the specimens and their construction and the materials used, as well as the testing procedure and the instrumentation used on the specimens is included.

The experimental program conducted at the Structural Engineering and Construction Research and Development Facility of the University of Manitoba consisted of investigating the behaviour of dowels in pure shear, which involved testing push-off test specimens. A typical push-off test specimen consisted of two 'L'-shaped concrete panels, with one in an inverted configuration, that were connected together at a joint with dowel bars, as shown in Figure 3.1. The two panels were loaded in compression at the ends to induce a pure shear loading condition at the joint. The test specimen was designed to simulate the typical loading condition on the dowels similar to those in the field at the concrete pavement joints.

The specimens were loaded to failure to determine the mode of failure and ultimate strength of the dowels, as well as the load-deflection relationship under service loading conditions that are typically experienced in concrete pavement joints. The various parameters considered in this investigation were the material of the dowels and the degree of bonding of the dowel bar to the concrete. A total of eight specimens were tested. Four specimens used steel dowels and the other four had Isorod dowels. For each material, two specimens had

dowels partially bonded to the concrete and two specimens included non-bonded dowels. The test program is described in Table 3.1. The specimen notation used was composed of two letters designating the dowel material (ST for steel or IS for Isorod), a letter designating the degree of bonding (N for no bonding on either side of the dowel or P for bonding on one side of the dowel) and finally a number indicating the first or second specimen of that type. All specimens had two 450 mm long dowels with a diameter of 19 mm, which crossed the 12.7 mm wide joint.

3.2 SPECIMEN DESCRIPTION

Each specimen consisted of two panels connected by two dowels, as shown in Figure 3.1. The specimens had an overall width of 913 mm, an overall height of 975 mm and a thickness of 250 mm. The dimensions of each panel are given in detail in Figure 3.2, which also shows the locations of the dowels crossing the joint. Figure 3.3 shows the location of the dowels with respect to the specimen and the stirrups used for reinforcement. The locations of the dowels were selected to avoid contact with the surrounding stirrups.

3.3 MATERIALS

3.3.1 Concrete

Each specimen was made with concrete supplied from a local ready-mix concrete company. The concrete was to have a nominal compressive strength of 40 MPa at 28 days with a maximum aggregate size of 14 mm. A slump of 20 mm was required before the addition of a superplasticizer. Once the chemicals had been added to improve workability,

a slump of 180 mm was required, as determined by a standard slump test. At the time of casting, six cylinders were also cast. Three cylinders were used for determining the modulus of elasticity of the concrete while the other three were used for determining the compressive strength at the time of testing. As well, three small beams were cast to determine the tensile strength of the concrete.

The compressive strength, modulus of elasticity and tensile strength of the concrete which were measured at the time of testing are presented in Table 3.2 for all of the tested specimens. The concrete strength was found to be significantly higher than the specified nominal strength of 40 MPa.

3.3.2 Reinforcement

Reinforcement was placed in each specimen to allow the concrete to resist the applied loads without cracking. The same layout of reinforcement was provided for each panel. The steel reinforcement had a nominal specified yield strength of 400 MPa and a modulus of elasticity of approximately 200 GPa. The 10M size of deformed reinforcing bars were used to reinforce the panels, as shown in Figure 3.4. Detailed dimensions of the three types of reinforcing used are given in Figures 3.5 and 3.6. The actual stress-strain curve for the steel, shown in Figure 3.7, was obtained from tensile tests performed on lengths of the reinforcing bar. Results showed that the actual yield strength averaged 435 MPa with a standard deviation of 4.1 MPa, a strain at yield of 0.246% and a modulus of elasticity of 176.8 GPa.

3.3.3 Dowels

The dowels used in this program were similar to the actual dowels used in practice, but had smaller diameters to accommodate laboratory testing. Two 19.1 mm (¾") diameter dowels, that were 450 mm long, crossed the joint. The steel dowels were made of 44W steel, that consisted of plain round bars with a yield strength of approximately 360 MPa and a modulus of elasticity of approximately 200 GPa. From the tension tests that were performed on samples of the steel used for the dowels, the yield strength was calculated to be 356.5 MPa with a standard deviation of 2.9 MPa, a yield strain of 0.182% and a modulus of elasticity of 199 GPa, as seen in Figure 3.8.

The glass fiber reinforced plastic rod (Isorod) consists of continuous longitudinal strands of glass fibers which are bound together with a thermosetting polyester resin in a process called pultrusion. Normally, a helical winding of the same type of fibers is applied to the surface with a resin, and a coating of sand is then added to improve bond. This produces a material similar in appearance to deformed steel reinforcement. However, the rod that is used for dowels does not have the additional wrapping or sand coating so that the rod has a smooth surface.

According to the data supplied by the manufacturer,[14] which is based on information obtained from material testing, the stress-strain characteristics of this and other fiber reinforced plastics (FRPs), are perfectly linear up to failure. For Isorod, failure occurs at an ultimate tensile strength of 690 MPa and at an ultimate strain of 1.8%. Isorod has a tensile modulus of elasticity of 42 GPa and a Poisson's ratio of 0.28. The results of punching shear tests show that Isorod has a punching shear strength of 184 MPa. Like all other FRPs, Isorod

is non-corrosive and non-electromagnetic. However, the resin may show signs of breakdown if there is prolonged exposure to ultra-violet light.[15] It has a specific gravity of 2.0 which is approximately 25% that of steel. From preliminary fatigue tests that have been performed, it has been found that Isorod can withstand slightly fewer cycles than steel bars at higher upper limits.[16] However, the manufacturer is considering using a different resin in the material which should improve the fatigue endurance. As the fibers within the bar are oriented only longitudinally, the material behaves anisotropically. The effect of this can be seen in the large variation of the longitudinal and transverse coefficients of thermal expansion, which are 9.0 x 10^{-6}/°C and 52.9 x 10^{-6}/°C, respectively. The longitudinal coefficient of thermal expansion of Isorod is much closer to that of concrete than is the coefficient of expansion of steel.

In order to determine the properties of the Isorod used for the dowels, tension tests were performed. However, standard tension tests that are used for steel could not be used for FRP materials, as the anchorage grips used in the tests cut into the Isorod specimen and caused it to fail prematurely in the anchorage. Therefore, a method of testing smooth Isorod bars was developed at the Université de Sherbrooke in Sherbrooke, Québec. The 500 mm long sample to be tested was prepared by lightly sandblasting 150 mm of each end to roughen the surface. The roughened ends were then encased in a resin (West System Epoxy Resin 105 with Hardener 205). Once the resin had set and cured, each end of the sample was inserted into a grip that was placed into a conical coupler, as shown in Figure 3.9. This coupler was used to apply load to the specimen and acted as an adaptor to allow for mounting of the specimen into a testing machine.

Tension tests were done on three samples of 19.1 mm diameter Isorod to determine the actual behaviour. Failure occurred at or near the anchorage in all of the tests. A typical failure is shown in Figure 3.10, which shows the test setup as well as the brittle failure of the material. The ultimate tensile strength, modulus of elasticity and strain at ultimate are given in Table 3.3 for the three samples tested. The results of these tests are also shown in Figure 3.11 which gives an average ultimate tensile strength of 696 MPa at a strain of 1.542% with an average modulus of elasticity of 43.37 GPa.

3.4 CONSTRUCTION OF THE SPECIMENS

The specimens were cast in the Structural Engineering and Construction Research and Development Facility at the University of Manitoba. Both panels of a specimen were cast simultaneously to eliminate possible variation of the concrete strengths in each panel. A wood form was used for casting the two panels in a horizontal position. Photographs showing the formwork and the first specimen before and after casting are shown in Figure 3.12.

To create the joint between the panels, 12.7 mm (½") thick styrofoam was used. The bottom fit in a groove routered into the plywood base and the top ends were attached to the form through a 2x4 cap. Before each casting, the forms were cleaned, reassembled and lubricated. Then the reinforcement, which had been tied into cages, was positioned in the forms on plastic chairs that provided a 20 mm concrete cover for the specimen. The dowels were then inserted through holes in the styrofoam and tied in place to prevent shifting during casting. Then, one or both halves of the dowels were oiled to prevent bonding.

Once the concrete was placed in the forms and consolidated with a hand-held vibrator, the surface of the specimen was trowelled to give a smoother surface. Then, lifting inserts were positioned at the locations shown in Figure 3.13. The inserts were later used to attach a temporary strongback designed to hold the panels in place during transportation and preparation for testing. Then, a plastic tarp was placed over the specimens to assist in keeping the concrete moist during drying and curing. The specimens remained under the tarps for three days and water was periodically added to the surface if it became too dry. The tarp was taken off, the sides of the form were removed and the specimens were allowed to air cure for a minimum of four more days before they were moved off the form bases and allowed to air cure in the laboratory for a minimum of 28 days before testing.

3.5 INSTRUMENTATION

During testing, several types of instrumentation were used to monitor and record the behaviour of the specimen. The following sub-sections describe the instrumentation used to measure strains, displacements and load, as well as the computer system used to record the information obtained.

3.5.1 Strain Measurements

Electrical resistance strain gauges were used to measure the strains that occurred in the dowel bars. The gauges used were N11-FA-5-120-11, which were manufactured by SHOWA Measuring Instruments Co. Ltd. of Japan. They were 10 mm long and had a 120 ohm resistance. The installation followed the standard set by the manufacturer, where the

surface was cleaned, the strain gauge was glued to the dowel, the lead wires of the strain gauge were connected to a cable and then coatings were applied to the strain gauge and lead wires to protect them from moisture during casting.

3.5.2 Displacement Measurements

The displacement of the panels during testing was measured using two types of devices: linear variable differential transducers (LVDTs) and demec points. All were mounted on the top surface of the specimen and were used to measure the displacement in the direction of applied loading as well as any possible lateral movements of the panels. Two LVDTs were used to measure the displacement of the panels in the direction of the applied load at the locations of the dowels. One LVDT was placed across the joint and at the centerline of the panels to measure any lateral movements of the two panels. Demec points were used as a means of verifying the LVDT readings. Sets of demec points were placed across the angled spaces at the ends of the panels to measure displacement. An additional set was placed near the centerline of the panels to verify lateral displacement. The locations of both the LVDTs and the demec points are shown in Figure 3.14.

3.5.3 Testing Machine

An MTS 1000 kN actuator was used to test the specimens. An MTS load cell was attached to the end of the actuator that measured the load applied to the specimens. The actuator and load cell were connected to an MTS control panel that controlled and monitored the load and stroke applied by the actuator. As well, to verify that the load was being resisted

by the dowels and not by friction of the specimen on its riding surface, an additional load cell was placed at the far end of the specimen.

3.5.4 Data Acquisition System

A data acquisition system was used to monitor the readings obtained from the LVDTs, strain gauges, load cell and the load and stroke applied by the actuator. The system comprised a Hewlett Packard Vectra 386/25 computer with a Validyne 16 channel data acquisition board. All data was simultaneously recorded in files and displayed on the screen in both graphical and numerical forms using a data acquisition software package called Labtech Notebook (version 7.2.0). All the information recorded during testing was later transferred to diskettes for further analysis.

3.6 TESTING PROCEDURE

After a specimen had cured sufficiently, it was prepared for testing. The styrofoam was removed from the joint to allow for visual inspection of the dowels during the test. Also, holes were drilled in the top surface of the specimen to attach the LVDT holders. The strongback was then attached to the specimen to enable it to be transported to the setup that was created in order to test the specimens. The test setup is described in the sub-section below. As well, the sequence that was followed to prepare for testing is explained in this section.

3.6.1 Test Setup

The specimens were tested horizontally while resting on a raised platform. The platform consisted of a layer of cinder blocks which supported a "sandwich" of plywood, sheet metal and aluminum rollers, as seen in Figure 3.15. The rollers between the sheet metal provided a smooth, frictionless riding surface that allowed the specimen to move freely as it was being pushed together, while the plywood provided rigidity to support the specimen. To allow for each panel to move independently, the rollers crossing the joint were cut in half. As well, the top layers of sheet metal and plywood were cut to the shape of separate panel pieces so that movement would not be restricted. The cinder blocks were needed to raise the specimen so that its mid-height was at the same height as the centerline of the actuator.

The actuator was attached to a concrete reaction wall at one end, and applied a load against the specimen via a load cell at the other end as seen in the plan view of the test setup shown in Figure 3.16. The actuator was aligned to ensure that the load was applied along the line of the joint to create pure shear in the dowels. Another load cell was placed between the far end of the specimen and a steel spacer that rested against an abutment anchored to the floor. At both ends, the load cells pressed upon steel bearing plates that helped to more evenly distribute the load on the specimen.

Figures 3.15 and 3.16 show the system devised to restrain the panels from moving laterally outward during testing. It consisted of a steel plate on each side of the specimen that had two steel tie ends attached vertically to it, as well as a small steel angle welded on at the bottom. The small angle was bolted to an anchored hollow structural steel section below it, that was anchored to the floor. The vertical tie ends, that extended above and below the

specimen, were then used to hold the specimen together through the use of steel tie rods that ran across the top and bottom of the specimen. Since movement occurred throughout the test in the specimen panel upon which the actuator applied load, a set of rollers was inserted between a steel plate that rested against the side of the specimen and the restraint device through which the steel tie rods ran. When the nuts on the threaded ends of the tie rods were tightened, it provided a system that would restrict all lateral movements but would not move with the specimen during the test.

3.6.2 Testing Sequence

Once the specimen was aligned in the test setup, the steel strongback was removed and the restraint system was put in place. The LVDTs and demec points were then mounted on the top concrete surface. The load cell was then placed between the specimen and the steel spacer. The LVDTs, the strain gauges, the load cell and the load and stroke from the actuator were then connected to the data acquisition system and their initial readings were taken to zero all of the instrumentation. Initial readings were also recorded manually for the demec points.

The test, which was stroke controlled, was then run and the data acquisition system recorded all readings except for the demec point readings which were taken manually at 5 kN increments. The test was stopped when significant displacements had occurred (approximately 20 mm, the width of the angled space at the joint) or if there was a large drop in the load-carrying capacity of the specimen. After testing, photographs were taken of the specimen and of the failed dowel bars in the joint.

CHAPTER 4

TEST RESULTS

4.1 INTRODUCTION

This chapter presents the results of the specimens tested in the experimental program. The results include the responses of the specimens obtained from the various types of instrumentation used during testing. This includes the load measured by the actuator, the load measured by the end load cell, the two LVDTs and two sets of demec stations used to measure displacement in the direction of loading, the LVDT and set of demec points that measured lateral displacement and the strain measured by the strain gauges attached to the dowel bars.

4.2 TEST RESULTS

A total of eight specimens were tested in the experimental program. The notation of the specimens are given in section 3.1. Specifications of each specimen are given in Table 3.1. In general, all eight specimens experienced a common kinking behaviour that represents one of the three possible dowel action mechanisms discussed previously in sub-section 2.3.1 and Figure 2.2. The following sub-sections provide the specific results of the load-displacement behaviour of each of the tested specimens. The load and displacement where kinking commenced and the maximum load and corresponding displacement are summarized in Table 4.1 for all tested specimens.

Test results indicated that the strain gauges placed on the dowels at the joint did not provide useful information. This was attributed to the kinking action that occurred at the location of the gauges causing damage, malfunction of the gauges and meaningless results. Therefore, the results are not presented.

As described in sub-section 3.5.2, an LVDT and a set of demec points were used to measure lateral movements of the panels. Configuration of the test setup was designed to restrict all outward movements of the panels to simulate the prototype pavement behaviour and the presence of very stiff concrete on either side of a joint. Additional means of measuring the lateral displacements were used after testing the first specimen. The measurements were obtained by attaching a strain gauge to one of the top tie rods of the restraint system. The force exerted in the tie rod for the seven specimens are given in Appendix A in Figures A1 to A7. Strain gauge readings were converted to force using the elastic modulus of the tie rod material (E=200 MPa). The results indicated that the forces exerted in the tie rod were very small, with the largest force having a magnitude in the range of one to two kiloNewtons. This indicates that the lateral constraint did not exert significant forces and consequently did not affect the behaviour. It should be noted that the readings of the strain gauge were not always consistent with that obtained by the LVDT and demec point. This may be due to the small magnitude of the strains and the accuracy of the strain gauge at these low values. The load-lateral displacement measurements obtained from the LVDT and set of demec points from each test are shown in Figures A8 to A15 of Appendix A.

Although there were some differences between the results of the LVDT and set of demec points for the eight tests performed, the trend observed was that outward movement

did not occur in the specimens. The readings of the demec stations indicated that a minor inward movement took place in all of the specimens prior to kinking and a large inward movement after kinking began. This movement is due to the pulling action of the dowels that caused large displacements of the panels toward each other after kinking. It should be noted that this inward movement is considered to be acceptable behaviour for these types of tests but does not represent the prototype due to the large stiffness and rigidity of the pavements. Since this movement did not occur in the tests before kinking and normally the dowels will not kink under load during the serviceability of the pavements, test results of the specimens are acceptable and represent actual conditions before kinking.

A load cell was placed at the far end of the specimen to monitor the load being transmitted through the specimen. The measured load applied by the actuator and the load measured by the end load cell are shown in Figures A16 to A23 of Appendix A. The insignificant difference between the two values indicates that the roller system used to support the specimens did not resist significant load and allowed full freedom of movement of one panel relative to the other. The measured load applied by the actuator was used in load-displacement graphs, as the differences were minor.

4.2.1 Specimen IS-N-1

This specimen was considered to be the pilot specimen for this program and was used to check the adequacy of the test setup. The specimen used Isorod dowels that were not bonded to the concrete on either side. The load was applied using stroke control at a slow rate of loading to determine the appropriate rates for these types of specimens. The test

started at a stroke rate of 0.1 mm/min and increased at the stage where large displacement occurred. The final stroke rate was 0.2 mm/min. Based on this test, it was decided that this slow stroke rate of 0.1 mm/min is adequate to determine the behaviour before kinking. The faster rate of 0.2 mm/min or higher was found to be useful to speed up the test and sufficient to determine the behaviour for the latter part of each test.

The measured load-displacement relationship using two LVDTs in the direction of the applied load is shown in Figure 4.1. The same displacement measured using the two sets of demec points is shown in Figure 4.2. Due to the limited range of the demec gauge, the demec readings were only recorded up to a load of 25 kN. To extend the range of demec readings for the subsequently tested specimens, a demec bar was created that incorporated eight points from which sequential readings could be taken. This demec bar allowed the use of a series of demec points to continue measuring the displacement as it exceeded the range of the previous point. Figure 4.3 is an illustration of the demec bar and the multiple ranges that could be achieved by this device. From this figure, it can be seen that the demec points were located at a distance that allowed a series of readings to be taken before exceeding the range of the point at a given range. This system was used to relate the readings from sequential ranges.

From Figures 4.1 and 4.2, it can be seen that the specimen initially exhibited linear behaviour up to a load of 30 kN and a displacement of 1.61 mm. Kinking of the dowel caused a drop in the load to 24 kN and significant displacements occurred at this lower load level. The load-carrying capacity of the specimen then increased to a maximum load of 34 kN before failure occurred and the dowels could no longer carry significant load. The

maximum displacement measured before failure was 10.3 mm. The specimen was then removed from the test setup and the panels were separated to examine the failed dowels. It was noted that the dowels were sheared off at the concrete faces accompanied by a longitudinal split, as shown in Figure 4.4.

4.2.2 Specimen IS-N-2

This specimen had the same characteristics as the previous specimen with Isorod dowels that were not bonded to the concrete on either side. The test began at the initial stroke rate of 0.1 mm/min and was increased to a final rate of 0.4 mm/min. The load-displacement behaviour obtained from the LVDTs and the demec bars are given in Figures 4.5 and 4.6, respectively. Demec bar readings were recorded throughout the test with the last reading recorded at 25 kN just prior to the second peak where failure occurred.

The behaviour pattern was almost identical to that of the previous specimen, with slight differences in the magnitude of the capacity before kinking. The first peak occurred at a load of 26 kN and displacement of 1.54 mm. The load dropped to a value of 20 kN, where an approximate displacement of 2 mm occurred. The second peak occurred at a load level of 27 kN and a maximum displacement of 9.2 mm was noted prior to failure of the dowels.

4.2.3 Specimen ST-N-1

This specimen used steel dowels that were not bonded to the concrete on either side. For the initial stage, a stroke rate of 0.1 mm/min was used and it was increased to a final rate of 0.4 mm/min. The test was terminated due to the configuration of the specimen which did

not allow any further movement in the direction of the applied load. The measured load-displacement of the two LVDTs and the demec stations are given in Figures 4.7 and 4.8 respectively. This specimen was tested before the demec bar was in use so that the demec point readings were only recorded up to a load of 75 kN. These figures show that the specimens were initially very stiff in comparison to the Isorod specimens and behaved linearly up to a load of 78 kN and a displacement of 1.25 mm. As the kinking mechanism started, the applied load increased slowly due to the large displacement range for this type of reinforcement. The test was stopped at a load of 107 kN and a displacement of 19.5 mm due to the limited space between the panels in the direction of the applied load. At this stage of the test, the concrete around the dowels was crushed. After the test was completed, the specimen was removed from the test setup and the panels were separated to inspect the kinking behaviour of the dowels and the concrete surface. The crushed surface and dowels for the ST-N-1 specimen are shown in Figure 4.9.

Displacement measurements indicated a slight rotation of the specimen due to imperfection of the end steel plate of the spacer. The problem was eliminated for subsequent specimens by placing a bag of plaster of paris between the spacer and the abutment. This allowed the spacer to rest evenly against the abutment and prevented rotation of the specimens.

4.2.4 Specimen ST-N-2

This specimen was identical to specimen ST-N-1 with steel dowels not bonded to the concrete on either side. No problems were encountered during testing and readings were

taken from the demec bar up to a load 98 kN. The same initial stroke rate of 0.1 mm/min was used and the rate was increased in the post-kinking stage to a rate of 0.8 mm/min. The load-displacement behaviour shown in Figures 4.10 and 4.11 was obtained from the LVDTs and demec bar readings, respectively. These figures show similar behaviour to that exhibited by the previous specimen with steel dowels. The specimen behaved linearly up to the kinking stage which occurred at a load of 81 kN and a displacement of 0.85 mm. The load-carrying capacity then gradually increased up to a maximum load of 103 kN and a displacement of 18.9 mm. The test was stopped due to the limitation of the space between the two panels in the direction of the applied load. Crushing of the concrete around the dowels was also observed for this specimen.

4.2.5 Specimen IS-P-1

This specimen had Isorod dowels with one side bonded to the concrete while the other side was not. The stroke rate was increased from 0.1 mm/min for the initial stage of testing to a final rate of 0.4 mm/min after kinking. This specimen was tested before usage of the demec bar, therefore, demec readings could be recorded for the first 30 kN only. The load-displacement relationships obtained from the LVDTs and demec points are shown in Figures 4.12 and 4.13, respectively. These figures show that this specimen exhibited the same behaviour pattern seen in the other specimens with Isorod dowels. The specimen behaved linearly up to a load of 34 kN and a displacement of 1.25 mm at which point kinking began. The load-carrying capacity then dropped to 28 kN and large displacements occurred. The

specimen was able to carry load up to a maximum value of 40 kN and displacement of 9.3 mm before failure of the dowels.

4.2.6 Specimen IS-P-2

This specimen was identical to the IS-P-1 specimen and was connected with Isorod dowels which were bonded to the concrete on one side only. The stroke rate was increased during the test from the initial rate of 0.1 mm/min to a final rate of 0.4 mm/min for the post-kinking stage. The load-displacement behaviour exhibited during the test is shown in Figures 4.14 and 4.15 for the LVDTs and the demec bars, respectively. Demec readings were recorded up to a load of 26 kN, that occurred on the rising limb of the second peak. The same behaviour was observed for this specimen as for the other specimens with Isorod dowels. The first peak occurred at a load of 26 kN and a displacement of 1.66 mm. After kinking, the load dropped to 22 kN with an approximate displacement of 2 mm. The second peak occurred at a load of 32 kN and the maximum displacement of 9.0 mm was noted before complete failure of the dowels.

4.2.7 Specimen ST-P-1

The specimen was connected by steel dowels bonded to one side of the concrete. The same initial stroke rate was used on this specimen as for all the other tests. The initial rate of 0.1 mm/min was increased to a rate of 0.6 mm/min in the post-kinking stage of the test. Demec point readings were obtained up to a load of 95 kN. Figures 4.16 and 4.17 show the load-displacement behaviour measured by the two LVDTs and demec points, respectively.

The specimen exhibited a stiff, linear behaviour up to a load of 80 kN and a displacement of 1.0 mm, followed by a significant reduction of the stiffness due to kinking. At a load of 105 kN and a displacement of approximately 6 mm, a reduction in the load-carrying capacity of 10 kN was observed, as shown in Figure 4.16. The load slowly increased again to a maximum value of 113 kN at a displacement of 18.2 mm before termination of the test due to closing of the gap between the two panels. During this latter stage of the test, crushing of the concrete around the dowels was observed.

4.2.8 Specimen ST-P-2

This specimen is a duplicate of specimen ST-P-1 that had steel dowels bonded to the concrete on one side only. The stroke rate was increased from 0.1 mm/min to a maximum of 0.8 mm/min for the latter stage of the test. The load-displacement behaviour of the LVDTs is shown in Figure 4.18, while Figure 4.19 shows the measurements obtained from the demec bars that were used to record the displacement up to a load of 110 kN. The behaviour pattern that occurred in the other specimen of this type was also exhibited in this specimen. Kinking began at a load of 85 kN and a displacement of 1.07 mm and a similar drop in the load-carrying capacity from 110 kN to 98 kN occurred at a displacement of approximately 7 mm. As the load slowly increased, the concrete around the dowels was crushed, which was consistent with the behaviour of the previous specimen with steel dowels. The maximum recorded load was 103 kN with a displacement of 17.9 mm before closing the gap between the panels.

When this specimen was tested, one step of the pre-test preparatory sequence was omitted and it affected the beginning of the test. Clamps were normally used to restrain the top layer of plywood from moving while each specimen was being placed on the test setup. However, these clamps were not removed before the test of this specimen began. They were noticed and removed after 40 kN of load had already been applied to the specimen. The initial behaviour was slightly affected by the unreleased roller system, however, after release, the specimen behaved similarly to the other specimen of this type, ST-P-1.

CHAPTER 5

DISCUSSION OF RESULTS

5.1 INTRODUCTION

This chapter analyzes and discusses the experimental test results presented in Chapter 4. The following sections include a general description and a comparison of the behaviour of the specimens connected by steel and Isorod dowels tested in this program, as well as a discussion of their shear strength and the effect of bond on their behaviour.

5.2 SPECIMEN BEHAVIOUR

The following sub-sections describe the behaviour of the specimens with steel and Isorod dowels. In each sub-section the average kinking load and maximum load are given for each type of specimen as well as an explanation of the mechanisms involved in the kinking process and the effect of any irregularities experienced during the test of each specific specimen.

5.2.1 Specimens With Steel Dowels

Four specimens with steel dowels were tested in this experimental program. Two specimens were connected with unbonded dowels (ST-N specimens), while the other two specimens were connected with dowels bonded to the concrete from one side only (ST-P specimens). Figure 5.1 shows the load-displacement behaviour of the two ST-N specimens obtained from the LVDTs, as well as their average values. The average of the demec

readings for these two specimens is also shown in this figure and it can be seen that the demec readings are in excellent agreement with those obtained from the LVDTs. The load-displacement behaviour obtained from the LVDTs for the two ST-P specimens, their average and the demec point reading average are shown in Figure 5.2. The preceding figures show that the steel dowels, which had a high initial stiffness, behaved linearly up to an average of approximately 80 kN with an average displacement of 1.05 mm for the ST-N specimens. Kinking began at a slightly higher load, averaging 83 kN, and at a slightly smaller displacement of 1.04 mm for the ST-P specimens, as can be seen in Figure 5.3. After kinking, there was a significant reduction in the stiffness of the specimen, accompanied by large displacements due to bending of the dowels at the concrete faces. As the displacements increased, the dowels exerted more pressure on the surrounding concrete. Eventually, the concrete bearing pressure reached its capacity, causing crushing of the concrete around the dowels. The tests were stopped at an average load of 105 kN and an average displacement of 19.2 mm for the ST-N specimens and an average load of 108 kN with an average displacement of 18.0 mm for the ST-P specimens because the gap between the two panels of the specimens closed.

As mentioned in Chapter 4, the first of the ST-N specimens experienced some rotation during testing. The effects of this rotation can be seen when comparing the load-displacement behaviour of the two specimens in Figure 5.1. The curve of the first specimen is quite rounded at the kinking point due to the rotation, whereas there is a sharp bend in the curve for the second specimen where rotation was prevented.

The second ST-P specimen behaved slightly differently than the first due to the initial restraint explained in sub-section 4.3.8. The effect of the initial restraint on the load-displacement behaviour resulted in a slight difference in the slope of the curve from the start of the test to 40 kN as compared to that after 40 kN, as shown in Figure 5.2.

Figure 5.3 indicates that the dowels of the partially bonded steel specimens (ST-P) carried slightly more load than those where the dowels were not bonded (ST-N) until a displacement of approximately 6 to 7 mm and a load of 105 to 110 kN was reached. At this point, there was a drop in the load-carrying capacity of approximately 10 kN. This drop was due to the breaking of the bond between the concrete and the one side of the dowel. After this point, the behaviour became very similar to that of the ST-N specimens although the ST-P specimens were still able to carry slightly more load.

5.2.3 Specimens With Isorod Dowels

A total of four specimens with Isorod dowels were tested in this program. Two specimens had dowels unbonded to the concrete on either side (IS-N specimens) and two specimens had dowels bonded to the concrete on one side only (IS-P specimens). The load-displacement behaviour obtained from the LVDTs of the two IS-N specimens as well as their average and the average demec readings are shown in Figure 5.4. The same information for IS-P specimens is given in Figure 5.5. These figures show that the readings obtained from the demec points agree very well with those obtained from the LVDTs. A comparison of the behaviour of the IS-N and IS-P specimens is given in Figure 5.6. From this figure, it can be seen that the dowels in the IS-N specimens had a linear behaviour up to an average load of

28 kN and displacement of 1.58 mm. The IS-P specimens were able to carry a slightly larger average load of 30 kN at a slightly smaller displacement of 1.46 mm before kinking began. After kinking, the load dropped down to an average of 22 kN for the IS-N specimens and 25 kN for the IS-P specimens as the dowels split longitudinally. The separation occurred within the resin of the Isorod in the embedded portion of the dowel as the compression zone of the rod separated from the tension zone. At this stage, the two portions of the dowel acted independently and kinking occurred. The load-carrying capacity then increased as the glass fibers of the composite material were able to carry a component of the load in tension. The average maximum load achieved for the IS-N specimens was 30.5 kN and an average maximum displacement of 9.75 mm occurred at failure. The IS-P specimens were able to carry a slightly larger maximum average load of 36 kN and had an average maximum displacement of 9.15 mm at failure.

5.3 ISOROD VERSUS STEEL BEHAVIOUR

Figures 5.7 and 5.8 give comparisons of the behaviour of steel and Isorod dowels for the unbonded and partially bonded cases for the two types of dowels. Firstly, and most prominently, it is noted that the Isorod dowels carry a considerably smaller load than the steel dowels. This is due to the fact that the composite material of the Isorod consists of unidirectional fibers and has very little resistance perpendicular to the fibers, which corresponds to shear. The material also has a very low modulus of elasticity in comparison to steel. Therefore, steel dowels are much stiffer than Isorod dowels and are capable of carrying much more load before kinking. A comparison of the shear strengths is given in

Section 5.5. The smaller load-carrying capacity of the Isorod means that a larger diameter dowel is required to carry the same load as a steel dowel. Calculations to determine the required Isorod dowel diameter are given in the following chapter.

Secondly, the Isorod dowels exhibit a larger displacement at the kinking point. On average, the Isorod has a 50% larger displacement than the steel dowels for the unbonded cases and there is a 41% increase in displacement for partially bonded Isorod dowels as compared to the steel dowels. This is due to the lower modulus of elasticity of Isorod, which is only 20% of that of steel.

The third difference noted is that the Isorod has a decrease in load after kinking, which does not occur in the steel dowels. This decrease could be serious for actual pavements as it is accompanied by large and permanent displacements. Further, it was noted that the Isorod dowels split longitudinally when kinking commenced. In practice, this point should not be reached as the split in the resin will expose the glass fibers to an alkali attack from the salt water that leaks into a joint.[15] Therefore, if Isorod dowels are to be used, it must be assured that the load where kinking commences would not be reached under typical service loads.

As expected, test results indicated that failure of the Isorod dowels occurred at a smaller displacement in comparison to the steel dowels. Isorod dowels experienced a complete failure at an average displacement of 9.45 mm for all cases, whereas the steel dowels did not fail, even with displacements of 18 to 19 mm. The tests were stopped at this point because of the configuration of the specimens that allowed only a maximum displacement of 20 mm in the direction of the applied load.

5.4 EFFECT OF BOND

The comparisons of the unbonded and partially bonded specimens for both steel and Isorod are presented in Figures 5.3 and 5.6, respectively. In general, bonding of one side of the dowel slightly increased the load-carrying capacity while decreasing the corresponding displacement. Due to the lower modulus of elasticity of Isorod in comparison to steel, the effect of bonding was more noticeable on its load-carrying capacity. The increase in the displacements of the unbonded specimens were in the range of 15% and 8% for steel and Isorod dowels, respectively. The partially bonded steel dowels were able to carry an average of 3.8% more load in comparison to the unbonded dowels. The increase for the Isorod case was in the range of 7%. The load capacity increase of the partially bonded steel dowels occurred up to the point of bond failure, after which the behaviour of the partially bonded specimens was almost identical to that of the unbonded specimens. This behaviour was not observed for the Isorod specimens and the bond continued to affect the behaviour up to complete failure. This resulted in a smaller displacement of the partially bonded Isorod dowels at failure in comparison to unbonded dowels.

5.4 SHEAR STRENGTH

In order to determine the shear strength of the dowels, the total applied load was assumed to be equally shared by the two dowels. In this investigation, the load that corresponds to kinking was assumed to represent the strength of the joint. In the following sub-sections, the shear strength obtained from testing is compared to the strength predicted by two equations that were presented in Chapter 2. The comparisons are done for both the

Isorod and steel dowels.

5.4.1 Isorod Dowel Shear Strength

Based on a nominal diameter of 19 mm, the kinking strength, p_k, of a single Isorod dowel from each specimen is shown in Table 5.1. The table also shows the average strength for each type of specimen and for the material used for the dowels. From these values, it is noted that the kinking strength of Isorod (51.1 MPa) is approximately only 28% of the punching shear strength of 184 MPa obtained from previous studies.[14] This is consistent with the lower shear strength expected when the load is applied along a wider joint, as this prevents a pure shear condition from developing.

The predicted values in Table 5.1 were derived using Equation 2.4; $v_d = f_y \cos \theta$. The kinking angle, θ, was calculated using the displacements measured at the commencement of kinking, given previously in Table 4.1, and a joint width of 12.7 mm. It can be seen that the predicted values are higher than the values obtained from testing the Isorod dowels when the tensile strength of the dowel is used. As well, the values calculated using the tensile strength of the resin within the composite are considerably lower than the actual test values.

The differences in predicted and actual dowel strengths are due to several factors. The first factor is the form of the equation available to predict kinking. It is desirable to have an equation that predicts the strength at which kinking will commence. However, Equation 2.4 determines the strength of the dowel at some point after kinking has started. The kinking strength is a function of the degree of kinking that has occurred, which means that the

strength increases towards the yield or tensile strength as the kinking angle approaches zero, which is the point where kinking commences. However, the actual dowel strength at kinking was less than the tensile strength. This indicates that the equation does not produce reasonable predictions of the strength at which kinking commences.

The second factor only applies to composite dowels, since the other component of the equation for kinking is the tensile strength of the material. However, for Isorod the first peak occurs when the resin cracks and the bar splits longitudinally. Therefore, the strength obtained should be a function of the tensile strength of the resin, which is considerably lower than the tensile strength of Isorod. However, as seen in Table 5.1, when using the tensile strength of the resin, which is approximately 11000 psi (75.8 MPa), the equation predicts a much lower shear strength of 8.9 MPa than that observed in the tests. Therefore, this equation does not correctly predict the kinking strength of composite materials, even when modifications are made to account for the actual behaviour of the material.

The second model available to predict dowel strength, Equation 2.11, depends on the bearing strength of the concrete as well as the plastic moment that can develop in the dowel before failure, as shown below:

$$D_u = 0.5 f_b (0.37 \gamma d_b - c)^2 + \frac{0.45 f_y d_b^2}{\gamma} \left(1 - \frac{T^2}{T_y^2} \right)$$

$$\textit{where} \quad \gamma = \sqrt[4]{\frac{E}{K_f d_b}}$$

For the specimens considered in this program, the equation can be simplified by ignoring the dowel tensile resistance as both types were unbonded or only bonded from one side. The

depth of the crushed concrete zone, c, can be reduced to zero as crushing occurred after the kinking stage. Using the area of the bar as $\pi d_b^2/4$, Equation 2.11 can be reduced and simplified to predict the strength, d_u, as follows:

$$d_u = \frac{0.637 f_b}{d_b^2}(0.37 \gamma d_b)^2 + \frac{0.57 f_y}{\gamma} \qquad (5.1)$$

Therefore, the simplified equation can be used for steel dowels without making any further modifications since steel can develop a plastic hinge. However, Isorod is a linearly elastic material up to failure and therefore a plastic hinge will not form. Using the tensile strength of Isorod in place of the yield strength of the steel, the equation will predict much larger loads than those the dowels actually carried, as seen in Table 5.2. However, it was noted during the tests on the specimens with Isorod dowels that failure began when the dowel split longitudinally due to the cracking of the resin. This is due to the tensile strength of the resin, which is approximately 7% of the tensile strength of the composite bar, being mainly responsible for the shear strength of the dowel bar. Therefore, the tensile strength of the resin was used in the equation rather than the tensile strength of the composite material. By making this modification, the predicted dowel strengths, d_u, shown in Table 5.2, are obtained. The predicted values agree very well with the actual strengths obtained. Equation 2.11 seems to be an acceptable equation for predicting dowel strength for Isorod dowels if the tensile strength of the resin is used.

5.4.2 Steel Dowel Shear Strength

The kinking strength of each of the steel specimens tested, as well as the average strength for each type of specimen and for the material, are shown in Table 5.3. When the strengths of the steel dowels are compared to those of the Isorod dowels in Table 5.1, it can be seen that the steel dowels are approximately 2.8 times stronger than the Isorod dowels. Table 5.3 also shows the predicted kinking strength obtained from both prediction equations. Equation 2.4 predicted a strength that is considerably lower than the actual strength obtained from testing. However, the strengths obtained from Equation 2.11 are very close to the actual strengths obtained from testing. Therefore, Equation 2.11 is also acceptable for predicting the strength of steel dowels based on the yield strength of the steel.

CHAPTER 6

DESIGN RECOMMENDATIONS

6.1 INTRODUCTION

This chapter provides design recommendations for glass fiber reinforced plastic (GFRP) dowels. The recommendations are based on testing one type of dowel known commercially as Isorod and produced in Thetford Mines, Québec. Design equations are presented that can be used to predict the strength of FRP as well as steel dowels. Design recommendations will determine the required diameter and length of an Isorod dowel that could provide comparable behaviour to steel dowels. Based on this study, a relationship between pavement thickness and dowel diameter is proposed for Isorod dowels. Application of Isorod as tie bars for concrete pavements is also explored and design recommendations are provided to determine tie bar spacing, length and diameter of Isorod.

6.2 STRENGTH PREDICTION

In order to have dowels with sufficient load-carrying capacity to withstand the loads that are expected to occur in concrete pavements, it is necessary to have an equation able to predict the load where kinking will commence in the dowel. In the previous chapter, it was found that an accurate prediction of the kinking load was possible for both steel and Isorod dowels using an equation that considered both the bearing strength of the concrete and the moment that could be developed in the embedded portion of the dowel. The following equation, originally proposed for steel,[9] could adequately be used to predict the dowel

strength, d_u, for GFRP using the tensile strength of the resin, which is normally in the range of 7 to 10 percent of the tensile strength of the GFRP bar.

$$d_u = \frac{0.637 f_b}{d_b^2}(0.37 \gamma_s d_b)^2 + \frac{0.57 f_y}{\gamma_s} \quad for\ steel$$

$$d_u = \frac{0.637 f_b}{d_b^2}(0.37 \gamma_i d_b)^2 + \frac{0.57 f_{t\,resin}}{\gamma_i} \quad for\ FRP \qquad (6.1)$$

$$where \quad f_b = 37.6 \frac{\sqrt{f_c'}}{\sqrt[3]{d_b}} \quad \gamma_s = \sqrt[4]{\frac{E_s}{K_f d_b}} \quad \gamma_i = \sqrt[4]{\frac{E_i}{K_f d_b}}$$

The concrete foundation modulus, K_f, is a constant for a given system and depends on the concrete strength, the dowel material used and the diameter of the dowel bar.[11] Therefore, a different value of K_f should theoretically be used for the systems that have Isorod dowels as compared to those with steel dowels. However, the dowel strength, d_u, will not change significantly with different values of K_f as the fourth root of K_f is used to calculate γ. This minimizes the effect on the dowel strength equation and therefore, the same K_f value can be used for both the steel and Isorod systems without a significant error in the results occurring.

These equations are simplified versions of the original, Equation 2.11, discussed in Chapter 2. This expression is for unbonded and partially bonded dowels. Therefore, the term that considers the effect of the tensile force in the dowel in the original equation is not included here. The term related to the depth of crushed concrete was also eliminated as the concrete did not crush at the commencement of kinking. Crushing of the concrete only occurred after a significant deformation had taken place due to kinking.

The results indicated that the tensile strength of the resin, and not that of the composite material, governs the shear strength of FRP dowels based on the kinking mechanism as the failure mode. It was found that the fibers within the FRP provide residual strength after the initial peak resistance and do not contribute significantly to the initial strength of the FRP dowel when subjected to shear. Isorod uses a polyester resin, a very versatile type of resin, however, some resins are available with higher tensile strengths. One of these that is widely used, is a vinyl ester resin that has a higher tensile strength than polyester resin, as well as possessing better resistance to aggressive media, high temperatures, corrosion and fatigue.[17] It is expected that using a vinyl ester resin as the matrix for Isorod may greatly enhance its performance as dowels in concrete pavements.

6.3 REQUIRED DOWEL DIAMETER

The current design practice of concrete pavements requires that a single dowel should carry a single wheel load as a vehicle crosses a joint. To determine a standard service load expected to act on a dowel, the equivalent single-axle load (ESAL) is used.[2] This is a standardized load acting on an axle of a truck or trailer and is taken as 18 kips (80 kN). Therefore, one wheel will carry one half of an ESAL, or 40 kN. The dowel diameter required to carry this load was calculated based on the average shear strength from the experimental program (51.1 MPa for Isorod and 142.8 MPa for steel) and was found to be 19 mm for steel dowels and 31.6 mm for Isorod dowels.

It was noted in the previous chapter that the Isorod dowels exhibited a larger displacement than steel dowels at the kinking point. Therefore, the required Isorod dowel

area should be increased to obtain displacement performance of the pavement similar to that with steel dowels. To determine the factor that should be applied, the displacements up to kinking were compared for the unbonded and partially bonded steel and Isorod dowels. Ratios of Isorod to steel displacements (Δ_i/Δ_s) were taken at 25%, 50%, 75% and 100% of the kinking strength for the eight specimens tested. The displacement ratios obtained can be seen in Figures 6.1 and 6.2. These figures also show the ratio of moduli of elasticity (E_s/E_i) which is approximately equal to 4.49 and would theoretically be used for flexure. The ratio of moduli of shear (G_s/G_i), which is approximately equal to 4.52, is also shown and would theoretically be used for pure shear. However, it can be seen that the maximum displacement ratios obtained from the tests are approximately 2.6 for the unbonded specimens and 2.3 for the partially bonded specimens. These values are much lower than those predicted by theory. This may be due to the development of the kinking mechanism that was neither pure flexure nor pure shear. The lack of bond of the dowel to the concrete may also contribute to this difference. Therefore, the theoretical values would give larger dowel areas than required. The displacement ratios obtained from testing should therefore be used to determine the required Isorod dowel area. However, since the results of these tests are limited and there may be variation in further tests of this type, a conservative displacement ratio of approximately 3 will be used for further calculations. This could lead to an Isorod dowel diameter of 55 mm located at the same spacing as the steel dowels. However, reducing the spacing could allow for a more reasonable and practical diameter.

Normally, the 38 mm (1½") steel dowels used for a 250 mm (12") thick pavement can carry twice the specified load of one half of an ESAL. Using the same safety factor on the

basic Isorod dowel requires a 63 mm diameter dowel. This is slightly larger than the 55 mm diameter dowel required to match the steel displacements, as discussed in the previous paragraph. Therefore, in a 250 mm thick pavement, an Isorod dowel with a diameter of 63 mm (2½") could be adequate to match the performance and the strength of the steel dowel and meet the required safety factor of twice the minimum required dowel diameter.

When dowels are installed in actual pavements, a wire frame, or 'basket', is used to hold a row of dowels in the proper location before the pavement is cast. The frame, which raises the dowels to the proper elevation, is normally fastened to the sub-base of the road to prevent movement. The dowels rest on top of the frame within steel loops that restrain the dowels from moving out of alignment. Typically, one end of each steel dowel is tack welded to the wire frame. It should be noted that an alternative method should be used to secure the FRP dowels to the supporting system during casting. The current welding technique used to fasten the steel dowels is certainly not applicable.

6.4 REQUIRED DOWEL LENGTH

As there is a difference between the elastic moduli of Isorod and steel, the length of dowel required will also differ. The equation that can be used to calculate the distance to the points of pressure change was presented previously in sub-section 2.3.2 and Equation 2.12. From this equation, the required dowel length can be found as twice the distance to the second point of pressure reversal in addition to the joint width. The required dowel length was calculated for steel and Isorod dowels by using a 25 mm (1") maximum joint width. It was found that a length of 420 mm is required as a minimal length for steel dowels. The

standard length used in practice is typically 450 mm (18") which is slightly larger than the minimum required.

For the same dowel diameter as steel, the minimum Isorod dowel length was calculated and found to be 293 mm. However, as a larger Isorod diameter is required to provide comparable shear strength to steel, a minimum dowel length of 418 mm is required for the GFRP dowels spaced the same as the steel dowels. Therefore, the same length of 450 mm (18") is recommended for Isorod dowels.

6.5 DOWEL SPACING

It has been noted in previous sections that a large diameter is required for the Isorod dowels to be comparable to the 38 mm (1½") diameter steel dowels that are spaced at 300 mm (12") along the transverse joints. However, smaller dowels could be used if they were spaced at closer intervals. In order to determine the dowel diameters required for various spacings, a relationship must be developed that relates the spacing and diameter of Isorod dowels to those of steel dowels. To obtain such a relationship, it is assumed that the shear force per unit length (D_u/s) that a dowel could carry is the same for both Isorod and steel dowels. The shear force, D_u, can be found since it is a function of the dowel shear strength at kinking, d_u, and the dowel diameter, d_b, as follows:

$$D_u = d_u \frac{\pi d_b^2}{4} \tag{6.2}$$

Therefore, by relating the shear force per unit length for Isorod and steel, the following

equation can be used to find the Isorod dowel spacing, s_i, for a given Isorod dowel diameter, d_{bi}:

$$s_i = \frac{d_{ui}}{d_{us}} \left(\frac{d_{bi}}{d_{bs}} \right)^2 s_s \qquad (6.3)$$

where d_{us} and d_{ui} are the shear strengths for steel and Isorod dowels respectively (d_{us} = 142.8 MPa and d_{ui} = 51.1 MPa), d_{bs} is the steel dowel diameter (38 mm) and s_s is the steel dowel spacing (300 mm).

For the same diameter used for steel dowels (38 mm), Isorod dowels would require a spacing of approximately 100 mm (4"). However, this close spacing may be considered unacceptable as a large number of dowels would be required. By rearranging the relationship derived above, it can be calculated that an Isorod dowel diameter of 45 mm (1¾") would be required for a more reasonable dowel spacing of 150 mm (6").

Previous studies have shown that the dowel strength attainable can be increased if smaller diameter bars are used in the joint. This is due to the more even distribution of bearing stress in the concrete as a larger number of bars is required.[7] The potential beneficial effect on the dowel strength by using smaller dowels has not been considered here and may improve the shear behaviour of Isorod dowels.

6.6 RATIOS OF PAVEMENT THICKNESS TO DOWEL DIAMETER

In practice, there is a general guideline used to determine the dowel size required for a given concrete pavement thickness. It states that the dowel diameter, d_b, can be found as ⅛ of the pavement thickness, t, (ie. $d_b = t/8$) however, the expression can only be used if t and d_b are expressed in inches.[2] Therefore, the information presented in this section is given in imperial units. The relationship described above can be applied to pavements in the range of 6 to 12 inches thick, which is normally used for concrete pavements. For pavements that are less than 6" thick, the dowel diameter required for a 6" thickness is used.[1]

Based on the experimental tests, a general guideline is established for Isorod dowels. It was determined in section 6.3 that a 2½" (63 mm) diameter Isorod dowel is required for an equivalent 1½" (38 mm) diameter steel dowel in a 12" (250 mm) thick pavement. Using the values for pavement thickness (12") and Isorod dowel diameter (2½"), a constant of 4.8 was obtained. This could be a relatively cumbersome value to use as the calculated diameters may not always be readily available in practice. Therefore, Table 6.1 was created which gives the actual Isorod dowel diameter required for different pavement thicknesses as well as the diameter closest to the actual one that is readily available. This table also includes the diameter of steel dowels required for the same thicknesses of pavements for comparison. It is noted from the table that the diameters required for the thinnest pavement listed (6" or 150 mm) are still equal to the minimum diameters required to carry the standard service load of one half of an ESAL.

CHAPTER 7

LIFE-CYCLE COST COMPARISON

7.1 INTRODUCTION

Use of fiber reinforced plastic (FRP) dowels could provide a possible solution to deterioration of concrete pavement joints currently caused by corrosion of steel dowels. Since FRP is a relatively new material for structural engineering components, they are, as expected, more expensive than steel dowels. However, their use for concrete pavement applications could enhance the lifetime of the pavement. Use of steel dowels typically causes corrosion and requires replacement during the useful life of the concrete pavement. The high cost of the FRP dowels in comparison to steel may suggest that their use as an alternative material may not be acceptable. However, it has been reported that the initial cost may not be the most critical issue for long-term investments such as pavements.[18] Therefore, this investigation is conducted to determine the cost-effectiveness of FRP dowels for concrete pavement. The life-cycle cost analysis considers not only the initial cost of the dowels but also the maintenance and/or repair costs which are incurred over the life of the pavement.[18] This chapter presents a life-cycle cost analysis of five alternative dowel materials. The materials considered are: plain steel, epoxy-coated steel, stainless steel, Isorod and C-bar. The latter material is a new GFRP made by Marshall Industries Composites Inc. of Lima, Ohio. This GFRP was not available when the testing program began and was therefore not included. However, C-bar is reported to have an improved shear strength as compared to Isorod with a much lower cost (approximately 35% higher than epoxy-coated steel).[19]

Therefore, it is included in this cost comparison to show that some types of GFRPs may be more cost-effective than others. The following sections present the data and assumptions which were used, as well as the actual analysis and comparison of the five dowel material alternatives.

7.2 TIME AND COST INFORMATION

Evaluation of a life-cycle cost analysis of a structural system requires consideration of tangible and intangible costs. The direct tangible costs are the actual costs of materials, installation and repair which must be considered. The indirect or the intangible costs include other considerations,[20] such as traffic delays, congestion during repairs, increased noise levels for residents during construction or repairs and increased damage to vehicles due to failed joints and consequently a rough riding surface. Due to the difficulty of assigning monetary values to these parameters, only the direct tangible costs will be considered in this analysis.

The study included information regarding costs and time periods obtained from the Manitoba Department of Highways and Transportation[21] and the Winnipeg Streets and Transportation Department.[22] Since the volume of traffic on Manitoba highways did not warrant the use of dowels, the information obtained from the Department of Highways was only related to the lifespan of the concrete pavement rather than the dowels. However, it should be noted that many of the undowelled pavements are now experiencing premature faulting due to an increase in traffic volume. The Department of Highways is currently considering the use of dowels for concrete pavement joints.

7.2.1 Pavement Lifespan

In order to perform a reasonable and accurate life-cycle cost analysis, the same time period must be considered for all alternative materials used for the dowels. The life of the concrete pavement from construction time to the time when an overlay is required was considered as the length of time over which this analysis would be performed. It is assumed that the life cycle of dowels is limited by the time at which the pavement requires an overlay. This is certainly due to the fact that after placing an overlay, the dowels will not function as they were originally designed. The information obtained from both the city and the province confirms that concrete pavements normally last 25 to 35 years before an overlay is required. This lifespan varies with several factors, the most prominent one being the volume of traffic which the pavement experiences over its lifetime.

7.2.2 Repair Timing

The records indicated that normally after approximately 20 years of the pavement lifespan, joints require repairs as a result of clear signs of distress. At this time, approximately 30% to 50% of the joints are replaced with a full-depth repair.[22] This repair consists of removing the concrete around the joint down to the subbase. The area removed is normally the full width of one lane and 1 m to 1.5 m long.[22] Holes are drilled into the sides of the transverse faces of the concrete and one half of the length of the dowels are grouted into the holes. These dowels provide load transfer capabilities to the patched area after casting of the concrete and prevent faulting or settling of the patch.[23] Full-depth repairs are done on

another 15% to 20% of the joints at the end of the pavement lifespan before the overlay is placed.[22]

These full-depth repairs are presently being done in Winnipeg pavements where plain steel dowels have previously been used for dowels. It has only been within the past 15 years that epoxy-coated dowels have been used in Winnipeg. For most of this period, they have been used in pavement repairs and not in new pavements. Therefore, there is no information available regarding the lifespan of the epoxy-coated dowels or whether fewer full-depth repairs are required.

In theory, if stainless steel or GFRP were used for dowels, corrosion would not occur and the dowels would last the lifespan of the concrete pavement without requiring repairs. However, it was found that joint distress can be due to factors other than those associated with dowels. The distress may also be caused by heavy repeated loads, thermal stresses, loss of slab support or excessive compressive stresses within the slab due to incompressibles within the joint which restrict slab movement.[23] The actual percentage of joints which experience distress due to the factors mentioned above is quite difficult to determine, however it can be approximated to be within the range of 80% to 90% of all joints which are replaced.[22] Therefore, this percentage of joints must be replaced regardless of the dowel material used.

7.2.3 Dowel and Repair Costs

It can be seen from the previous discussion that there are three costs which must be included in the analysis. The first cost to be considered is the dowel cost when the pavement

is initially constructed. At this point, it can be assumed that the labour, installation and concrete costs will be the same for all five cases since the pavement must be constructed regardless of the material used for the dowels. Therefore, the only cost which needs to be considered is the cost of the dowels themselves. It was mentioned previously in Chapter 1 that dowels are placed along the transverse joints at a spacing of 300 mm. Therefore, a standard highway pavement lane width of 3.7 m will require 13 dowels across the lane. Table 7.1 gives the average costs for the five types of dowels as a unit cost as well as the cost for the dowels of a joint in a pavement lane (13 dowels). This table shows that the initial dowel costs for the stainless steel and GFRP are considerably higher than the plain steel and epoxy-coated steel. The selected stainless steel dowels (Grade S316) have approximately the same strength as the plain steel for comparison reasons. These costs are based on a 450 mm (18") long dowel with a diameter of 38 mm (1½") for the three types of steel dowels being considered. However, a larger diameter of 63 mm (2½") must be used for the Isorod dowel, as determined previously in Chapter 6. Since the actual shear strength of C-bar dowels in unknown, it is assumed that it is approximately the same as that of the Isorod dowels and therefore the same diameter is required. For both GFRP bars, a 63 mm diameter dowel spaced at 300 mm was used, however, a more practical diameter of 38 mm spaced at 100 mm could have been used, resulting in approximately the same costs. At present, the largest GFRP reinforcement which is made is a 25.4 mm (1") diameter bar. Therefore, the costs for 63 mm (2½") diameter dowels were extrapolated from the average cost per cubic meter of the sizes which are presently manufactured. It should be noted that the GFRP costs shown here are those for small quantities. As with most other materials which are purchased, the

cost per dowel will decrease when they are mass produced.

The second and third costs to be considered are the costs of the full-depth repairs after 20 years and at the end of the pavement lifespan. These costs should include both the cost of the dowels and that of the concrete required for the repairs. According to tender prices submitted to the Winnipeg Streets and Transportation Department for previous repairs of this type, the cost of installing a dowel, which includes drilling the hole and grouting the dowel in place, averages $6.75 per epoxy-coated dowel. By comparing the cost of an epoxy-coated dowel shown in Table 7.1 to the installed cost shown above, the cost of installation can be estimated to be $1.78 per dowel. This installation cost can then be added to the costs per dowel shown in Table 7.1 for the other alternatives, to obtain the costs of dowels for the repair work, shown in Table 7.2. Since two joints are required for each concrete patch, each joint to be repaired will be replaced by two new joints. Consequently, a total of 26 dowels are required for each joint which is replaced. The dowel cost per joint (26 dowels) is also shown in Table 7.2.

The cost of removing the concrete from the affected area and re-casting the concrete as a patch must also be included in the cost of a full-depth repair. The typical tender prices submitted to the Streets and Transportation Department give an average cost of $85/m^2 for concrete repair. Assuming that an average area for a full-depth repair is one lane width (3.7 m) by approximately one meter long, each joint repair requires 3.7 m^2 of concrete repair. For this average area, the removal and replacement of the concrete will cost $314.50. This cost is added to the dowel cost for a repaired joint to give the total cost of a joint repair, as given in Table 7.2.

7.3 LIFE-CYCLE COST COMPARISON

There are several methods of analysis which can be used to determine the most cost-effective dowel material alternative. In the following sub-sections, the Present Worth method will be used to perform the life-cycle cost comparison. As well, a break-even analysis will be performed to determine the material costs at which all five alternative dowel materials could become equal.

In order to perform these analyses, an appropriate interest rate must be used. In most life-cycle cost analyses a discount rate is used, which can be found by using the interest rate less the inflation rate. However, for highways, which are government funded and considered riskless investments, and are normally considered as long-term investments, the inflation rate is not normally considered.[18] This is mainly due to the inability to accurately predict the inflation rate over a long period of time, such as the lifespan of a pavement. Therefore, a constant dollar is used for all estimations of the costs, and the uninflated cost at the baseline year is used for all time periods throughout the analyses. Discount rates typically used for government-funded analyses are in the range of 4%.[18,24] Discount rates of 3% and 5% will be investigated to determine the effect of the discount rate on the selection of the different dowel material alternatives.

A typical kilometer of pavement will be considered in this life-cycle cost comparison. In Manitoba, a pattern is used for contraction joint locations.[21] From this pattern, it can be calculated that approximately 218 contraction joints must be initially constructed in one kilometer of highway. Due to the variability in the percentage of joints which are typically replaced, an average percentage will be used for these analyses. Since the majority of joints

which require replacement have deteriorated due to factors other than those related to the dowels themselves, it is assumed that approximately the same percentage of joints with epoxy-coated steel dowels will require replacement as those with plain steel dowels. Therefore, for plain and epoxy-coated steel dowels, an average of 40% of the joints (87 joints) will be replaced after 20 years and 17.5% of the joints (38 joints) will be replaced at the end of the lifespan of the pavement. As mentioned previously in sub-section 7.2.2, the distress caused in an estimated 85% of the joints which are replaced is due to factors other than those related to the dowels. Therefore, 85% of the number of joints listed above for the plain and epoxy-coated dowels must be replaced for the stainless steel and GFRP dowels. This results in 74 joints with stainless steel or GFRP dowels requiring replacement after 20 years and a further 32 joints to be replaced at the end of the pavement lifespan. The costs for these replacements are illustrated in the timeline shown in Figure 7.1.

7.3.1 Present Worth Analysis

The most common type of analysis method used to compare alternatives is the Present Worth method. This method converts future expenses to a base of present costs.[18] In other words, it determines the amount which would need to be invested now, at a given compound interest rate, to equal the expenses which will be incurred in the future.

Tables 7.3 and 7.4 show the present worth costs for the five different alternatives with two different pavement lifespans (25 and 35 years) for 3% and 5% discount rates respectively. From these tables, it can be seen that Isorod dowels are the most expensive of all the alternatives, regardless of pavement lifespan and discount rate. This high cost precludes

Isorod dowels from being considered as a viable alternative. As well, the cost of stainless steel dowels is only slightly lower than that of the Isorod dowels and therefore the stainless steel dowels are also too expensive to be considered as a cost-effective alternative. The C-bar dowels have a considerably lower cost compared to Isorod and stainless steel but are still approximately 2½ times the cost of the plain and epoxy-coated steel dowels. Therefore, plain steel or epoxy-coated steel dowels remain the most cost-effective choices for dowel material with plain steel dowels being the least expensive of the two alternatives. According to this analysis, it is not cost-effective to use epoxy-coated dowels as a replacement for plain steel dowels. This is a result of the majority of dowels being replaced due to factors other than those associated with the corrosion of the steel dowels.

7.3.2 Break-Even Analysis

By comparing the total costs of the plain steel and epoxy-coated steel dowels to those of the stainless steel and GFRP dowels, the break-even point can be calculated. This point is the cost at which two alternatives become equal and either one could be chosen, assuming the decision is based solely on cost.[25] Table 7.5 shows the dowel costs at which stainless steel or GFRP dowels would become equal to plain steel and epoxy-coated steel dowels. However, the table shows that even though the break-even cost varies with both the discount rates and pavement lifespans, there is only a small range in the calculated costs. Therefore, if the initial cost of a stainless steel or GFRP dowel were in the range of $6 per dowel, it would be comparable to epoxy-coated steel dowels, and if the cost dropped further to approximately $4, it could be used in place of plain steel dowels. These costs average 26%

higher than the plain steel dowels and 19% higher than the epoxy-coated steel dowel costs. This is the result of slightly fewer joints requiring replacement when stainless steel or GFRP dowels are used.

Since both Isorod and C-bar are relatively new products, they may experience cost decreases in the future with increased use. As well, if the shear strength is improved to allow for the use of a smaller diameter dowel or if the dowel design is improved so that less material is required, the cost of the dowel will be drastically reduced. As mentioned previously in Chapter 6, other types of GFRP which are manufactured in the United States, such as C-bar, may be more suitable and more cost-effective than Isorod.

CHAPTER 8

CONCLUSION

8.1 SUMMARY

The objective of this research program was to examine the feasibility of using glass fiber reinforced plastic (GFRP) dowels in concrete pavements. This was achieved by testing eight push-off specimens in shear and by performing a life-cycle cost comparison of various alternative dowel materials.

The variables which were investigated in this program were the dowel material (steel and Isorod) and the degree of bonding of the dowel to the concrete (unbonded and partially bonded). The research focussed mainly on the load-displacement behaviour, the dowel action mechanism which occurred and the load at which it commenced, the ultimate failure load and the mode of failure.

Based on the results of this experimental program, the following findings and conclusions can be drawn:

1) A kinking dowel action mechanism occurred in all specimens. This began at significantly lower loads for the Isorod dowels as compared to the steel dowels.

2) The specimens with steel dowels were initially very stiff but lost much of this stiffness once kinking began. However, the steel dowels were able to carry additional load within the post-kinking stage.

3) The specimens with Isorod dowels have significantly less stiffness in comparison to the steel dowels, as evident by the larger displacements. When kinking began, there

was a decrease in the load-carrying capacity as a result of a longitudinal split of the dowels.

4) The Isorod dowels experienced a complete failure after they had regained the strength which was lost when splitting of the dowels occurred. The dowels sheared off at the concrete face at failure, due to the brittle behaviour of GFRP material.

5) The effect of bonding one end of the dowel to the concrete slightly increased the load-carrying capacity while slightly decreasing the corresponding displacement.

6) A model which focusses on the embedded portion of the dowel and uses the analogy of a beam on an elastic foundation gives an accurate prediction of the strength at which kinking commences. For the steel dowels, the yield strength of the steel can be used in the equation which is developed, however, the tensile strength of the resin used in the composite material should be used for the GFRP dowels. Therefore, it is desirable to use an FRP which has a high resin tensile strength such as those made with vinyl ester, as opposed to those with a polyester resin. This would result in a smaller diameter of dowel being required.

7) From the results of the tests, it was determined that the Isorod dowel diameter can be calculated from t/4.8 compared to t/8 for steel, where t is the pavement thickness, in inches.

8) From the life-cycle cost comparison which was done, it was determined that plain steel dowels were the most cost-effective choice. Epoxy-coated steel dowels were slightly more expensive, but the costs of the stainless steel and GFRPs were much too high to be considered as viable alternative dowel materials.

8.2 FURTHER RESEARCH SUGGESTIONS

From the test results and conclusions of this research program, the following points present some suggestions for areas of further research:

1) Research should be done to determine the actual load transfer capabilities of GFRP dowels in concrete pavements. This can be done in laboratory tests by simulating wheel loads which cross joints of model pavement slabs which rest on model subgrades. As well, the optimal spacing of the dowels can be determined.

2) Other GFRPs which have a smooth surface should be investigated for their potential use as dowels. There are presently many glass FRPs which are being produced in the United States and some may have a better shear resistance than the Isorod which was tested. By using a stronger resin and/or a transverse wrapping of chopped glass fibers within the bar, the shear behaviour can be greatly improved. These types of GFRPs may be better suited for use as dowel bars.

REFERENCES

1. Portland Cement Association, Design and Construction of Joints for Concrete Highways (IS060.01P), *Concrete Paving Technology*, Portland Cement Association, Stokie, Illinois, 1991.

2. American Association of State Highway and Transportation Officials, AASHTO Guide for Design of Pavement Structures - 1993, American Association of State Highway and Transportation Officials, Washington, D. C., 1993.

3. Birkeland, Philip W. and Halvard W. Birkeland, "Connections in Precast Concrete Construction", *Journal of the American Concrete Institute: Proceedings*, Vol. 63, No. 3, March 1966, pp. 345-368.

4. Mast, Robert F., "Auxiliary Reinforcement in Concrete Connections", *Journal of the Structural Division: Proceedings of the American Society of Civil Engineers*, Vol. 94, No. ST6, June 1968, pp. 1485-1504.

5. Hofbeck, J. A., I. O. Ibrahim and Alan H. Mattock, "Shear Transfer in Reinforced Concrete", *Journal of the American Concrete Institute: Proceedings*, Vol. 66, No. 2, February 1969, pp. 119-128.

6. Mattock, Alan H. and Neil M. Hawkins, "Shear Transfer in Reinforced Concrete - Recent Research", *PCI Journal*, Vol. 17, No. 2, March-April 1972, pp. 55-75.

7. Paulay, T., R. Park and M. H. Phillips, "Horizontal Construction Joints in Cast-in-Place Reinforced Concrete", *Shear in Reinforced Concrete - Volume 2, ACI Special Publication SP-42*, American Concrete Institute, Detroit, Michigan, 1974.

8. Park, R. and T. Paulay, Reinforced Concrete Structures, John Wiley & Sons, Inc., New York, New York, 1975.

9. Soroushian, Parviz, Kienuwa Obaseki, Maximo C. Rojas and Jongsung Sim, "Analysis of Dowel Bars Acting Against Concrete Core", *Journal of the American Concrete Institute: Proceedings*, Vol. 83, No. 4, July-August 1986, pp. 642-649.

10. Dulacska, Helen, "Dowel Action of Reinforcement Crossing Cracks in Concrete", *Journal of the American Concrete Institute: Proceedings*, Vol. 69, No. 12, December 1938, pp. 754-757.

11. Porter, Max L., Bradley W. Hughes, Bruce A. Barnes and Kasi P. Viswanath, Non-Corrosive Tie Reinforcing and Dowel Bars for Highway Pavement Slabs (Report HR-343), Engineering Research Institute, Iowa State University, Des Moines, Iowa, November 1993.

12. Timoshenko, S. and J. M. Lessels, Applied Elasticity, Westinghouse Technical Night School Press, East Pittsburg, Pennsylvania, 1925.

13. Friberg, Bengt F., "Design of Dowels in Transverse Joints of Concrete Pavements", *Proceedings: American Society of Civil Engineers*, Vol. 64, Part 2, 1938, pp. 1809-1828.

14. Isorod - Glass-fiber Composite Rebar for Concrete: Technical Data, Pultrall Inc., Thetford Mines, Québec, February 1992.

15. Taylor, D. A., N. P. Mailraganam, A. H. Rahman, D. Guenter and M.S. Cheung, "Evaluation of Fibre-Reinforced Plastic Reinforcing Bars for Structural Application in Concrete", Proceedings of the 1994 CSCE Annual Conference, Winnipeg,

Manitoba, June 1-4, 1994, Vol. 2, pp. 573-582.

16. Chaallal, O. and B. Benmokrane, "Physical and Mechanical Performance of an Innovative Glass-fiber-reinforced Plastic Rod for Concrete and Grouted Anchorages", *Canadian Journal of Civil Engineering*, Vol. 20, No. 2, 1993, pp. 254-268.

17. Murphy, John, The Reinforced Plastics Handbook, Elsevier Advanced Technology, Kidlington, Oxford, U.K., 1994.

18. Peterson, Dale E., Life-Cycle Cost Analysis of Pavements, National Cooperative Highway Research Program Synthesis of Highway Practice No. 122, Transportation Research Board, Washington, D.C., 1985.

19. Faza, Salem, Marshall Industries Composites Inc., Lima, Ohio, U.S.A., Personnal Correspondence, March 1996.

20. Toichoa, Gabriel R., and Barry E. Prentice, "Economic Analysis of Linseed Oil as a Concrete Sealer", obtained from Mr. Barry Prentice of the Transport Institute, University of Manitoba.

21. Hilderman, Stan, Manitoba Department of Highways and Transportation, Personal Correspondence, June 1994 to June 1995.

22. Boyd, Ken, Winnipeg Streets and Transportation Department, Personal Correspondence, June 1995.

23. American Concrete Pavement Association, Guidelines for Full-Depth Repair, *Concrete Paving Technology*, American Concrete Pavement Association, Arlington Heights, Illinois, 1989.

24. Brown, Robert J. and Rudolph R. Yanuck, Introduction to Life Cycle Costing, Prentice-Hall, Inc., Englewood Cliffs, New Jersey, 1985.

25. Riggs, James L., William F. Rentz, Alfred L. Kahl and Thomas M. West, Engineering Economics - First Canadian Edition, McGraw-Hill Ryerson Ltd., Toronto, Ontario, 1986.

Table 3.1: Push-off Test Program

Bonding Condition	Dowel Type	Specimen Notation	Test Date
Dowels Not Bonded	Isorod	IS-N-1	Oct 31/94
		IS-N-2	May 2/95
	Steel	ST-N-1	Feb 15/95
		ST-N-2	Mar 8/95
Dowels Partially Bonded	Isorod	IS-P-1	Feb 28/95
		IS-P-2	May 1/95
	Steel	ST-P-1	Mar 6/95
		ST-P-2	Mar 13/95

Table 3.2: Concrete Properties

Specimen	Compressive Strength (MPa)	Modulus of Elasticity (GPa)	Tensile Strength (MPa)
IS-N-1	63.5	32.34	7.20
IS-N-2	56.8	34.34	4.73
IS-P-1	60.6	37.8	6.23
IS-P-2	56.8	34.34	4.73
ST-N-1	60.1	37.8	6.23
ST-N-2	60.0	33.8	6.62
ST-P-1	60.6	37.8	6.23
ST-P-2	60.0	33.8	6.62

Table 3.3: Isorod Properties Obtained from Tension Tests

Isorod Sample	Tensile Strength (MPa)	Strain at Ultimate (%)	Modulus of Elasticity (GPa)
1	731	1.618	43.45
2	706	1.587	43.73
3	651	1.420	42.83
Average	696	1.542	43.37
Standard Deviation	33.4	0.087	0.38

Table 4.1: Load and Displacement Summary

Specimen	At Kinking		Maximum	
	Load (kN)	Average Displacement (mm)	Load (kN)	Average Displacement (mm)
IS-N-1	30	1.61	34	10.3
IS-N-2	26	1.54	27	9.2
IS-P-1	34	1.25	40	9.3
IS-P-2	26	1.66	32	9.0
ST-N-1	78	1.25	107	19.5*
ST-N-2	81	0.85	103	18.9*
ST-P-1	80	1.00	113	18.2*
ST-P-2	85	1.07	103	17.9*

* Displacement at which angled space between panels was closed.

Table 5.1: Isorod Dowel Shear Strength Comparison With Equation 2.4

Specimen	Test Results			Calculated Using $f_{t\,bar}$		Calculated Using $f_{t\,resin}$	
	p_k (MPa)	$p_{k\,type}$ (MPa)	$p_{k\,mat}$ (MPa)	v_d (MPa)	v_d/p_k	v_d (MPa)	v_d/p_k
IS-N-1	52.9	49.4	51.1	87.5	1.65	9.5	0.18
IS-N-2	45.9			83.8	1.83	9.1	0.20
IS-P-1	60.0	52.9		68.2	1.14	7.4	0.12
IS-P-2	45.9			90.2	1.97	9.8	0.21

Table 5.2: Isorod Dowel Shear Strength Comparison With Equation 2.11

Specimen	Test Results			Calculated Using $f_{t\,bar}$		Calculated Using $f_{t\,resin}$	
	p_k (MPa)	$p_{k\,type}$ (MPa)	$p_{k\,mat}$ (MPa)	d_u (MPa)	d_u/p_k	d_u (MPa)	d_u/p_k
IS-N-1	52.9	49.4	51.1	261.4	4.94	53.8	1.02
IS-N-2	45.9			259.9	5.67	52.2	1.14
IS-P-1	60.0	52.9		260.7	4.35	53.1	0.89
IS-P-2	45.9			259.9	5.67	52.2	1.14

Table 5.3: Steel Dowel Shear Strength Comparison

Specimen	Test Results			Calculated Using Equation 2.4		Calculated Using Equation 2.11	
	p_k (MPa)	$p_{k\ type}$ (MPa)	$p_{k\ mat}$ (MPa)	v_d (MPa)	v_d/p_k	d_u (MPa)	d_u/p_k
ST-N-1	137.6	140.2	142.8	34.9	0.25	140.7	1.02
ST-N-2	142.8			23.8	0.17	140.6	0.98
ST-P-1	141.1	145.5		28.0	0.20	140.9	1.00
ST-P-2	149.9			29.9	0.20	140.6	0.94

Table 6.1: Required Dowel Diameters for Various Pavement Thicknesses

Pavement Thickness		Isorod Dowel			Steel Dowel	
		d_{actual}	$d_{available}$		d_{actual}	
inches	mm	inches	inches	mm	inches	mm
12	300	2½	2½	63.5	1½	38
11	275	$2^{5}/_{16}$	2⅜	60	1⅜	35
10	250	$2^{1}/_{16}$	2⅛	54	1¼	32
9	225	1⅞	1⅞	47.5	1⅛	28.5
8	200	1⅔	1¾	44.5	1	25
7	175	$1^{7}/_{16}$	1½	38	⅞	22
≤6	150	1¼	1¼	32	¾	19

Table 7.1: Initial Costs of the Five Alternative Dowel Materials

Alternative Dowel Material	Cost Per Dowel	Dowel Cost Per Joint
Plain Steel	$3.37	$43.81
Epoxy-coated Steel	$4.97	$64.61
Stainless Steel	$44.75	$581.75
Isorod	$46.54	$605.02
C-bar	$18.44	$239.72

Table 7.2: Repair Costs of the Five Alternative Dowel Materials

Alternative Dowel Material	Cost Per Dowel	Dowel Cost Per Repaired Joint	Total Cost Per Repaired Joint
Plain Steel	$5.15	$133.90	$448.40
Epoxy-coated Steel	$6.75	$175.50	$490.00
Stainless Steel	$46.53	$1209.78	$1524.28
Isorod	$48.32	$1256.32	$1670.82
C-bar	$20.22	$525.72	$840.22

Table 7.3: Present Worths of the Five Alternative Dowel Materials for a Discount Rate of 3%

Alternative Dowel Material	Initial Cost	Repair Cost (20 years) (PW)	Repair Cost (25 years) (PW)	Repair Cost (35 years) (PW)	Total Cost for 25 Year Lifespan (PW)	Total Cost for 35 Year Lifespan (PW)
Plain Steel	$9550	$21599	$8138	$6055	$39287	$37205
Epoxy-coated Steel	$14084	$23603	$8893	$6617	$46581	$44305
Stainless Steel	$126821	$62452	$23296	$17334	$212570	$206608
Isorod	$131894	$64359	$24007	$17863	$220261	$214117
C-bar	$52258	$34425	$12841	$9555	$99525	$96239

PW = Costs expressed in terms of present worth.

Table 7.4: Present Worths of the Five Alternative Dowel Materials for a Discount Rate of 5%

Alternative Dowel Material	Initial Cost	Repair Cost (20 years) (PW)	Repair Cost (25 years) (PW)	Repair Cost (35 years) (PW)	Total Cost or 25 Year Lifespan (PW)	Total Cost for 35 Year Lifespan (PW)
Plain Steel	$9550	$14702	$5031	$3089	$29285	$27342
Epoxy-coated Steel	$14084	$16066	$5498	$3375	$35650	$33527
Stainless Steel	$126821	$42511	$14403	$8842	$183737	$178176
Isorod	$131894	$43809	$14843	$9112	$190548	$184817
C-bar	$52258	$23433	$7939	$4874	$83632	$80566

PW = Costs expressed in terms of present worth.

Table 7.5: Break-Even Costs for Stainless Steel or GFRP Dowels When Compared to Plain Steel and Epoxy-Coated Steel Dowels

Discount Rate (%)	Pavement Lifespan (years)	Break-Even Costs When Compared To:	
		Plain Steel Dowels	Epoxy-Coated Steel Dowels
3	25	$4.39	$6.09
	35	$4.34	$6.03
5	25	$4.14	$5.81
	35	$4.08	$5.74

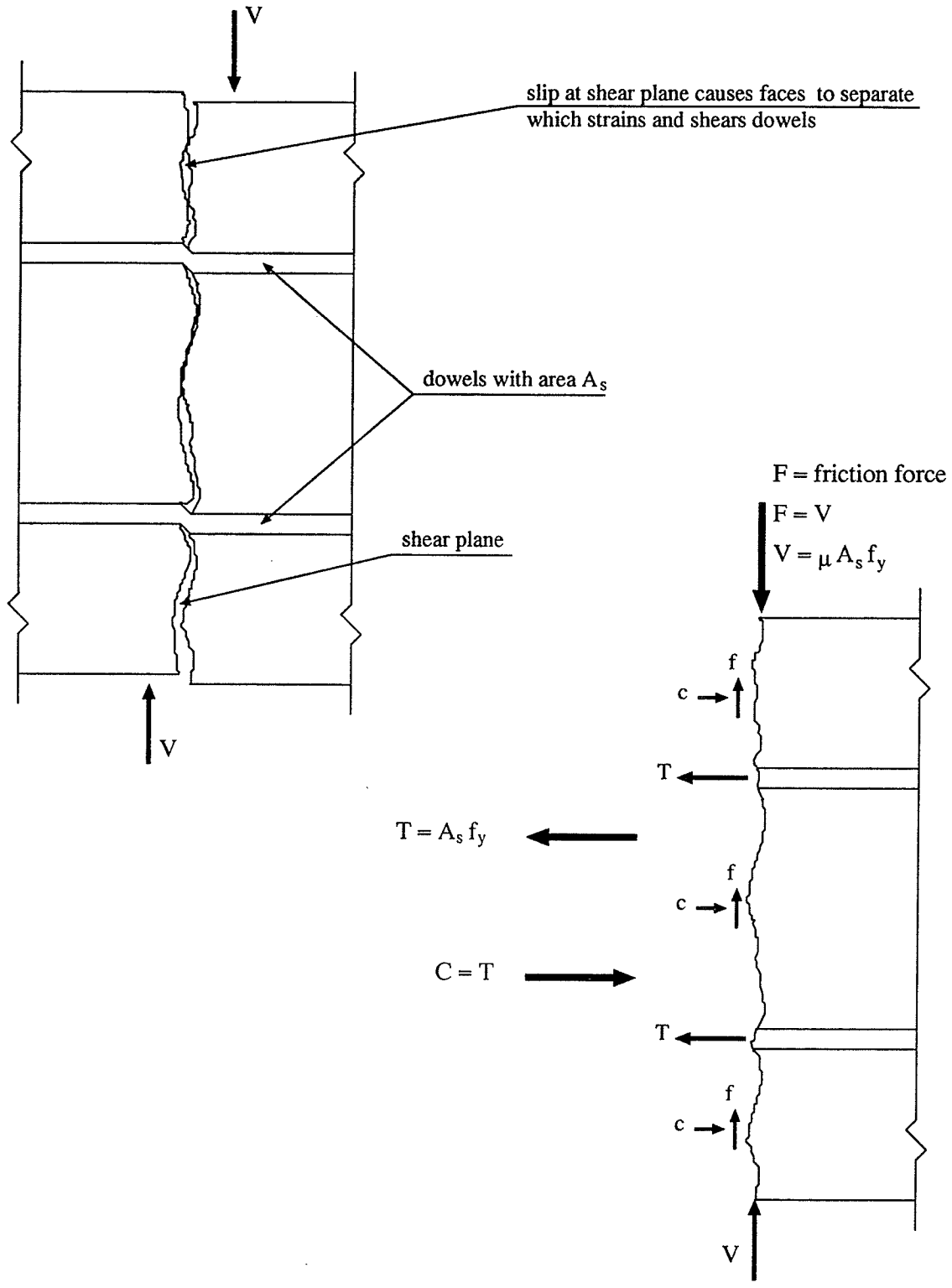

Figure 2.1: Shear Friction Theory

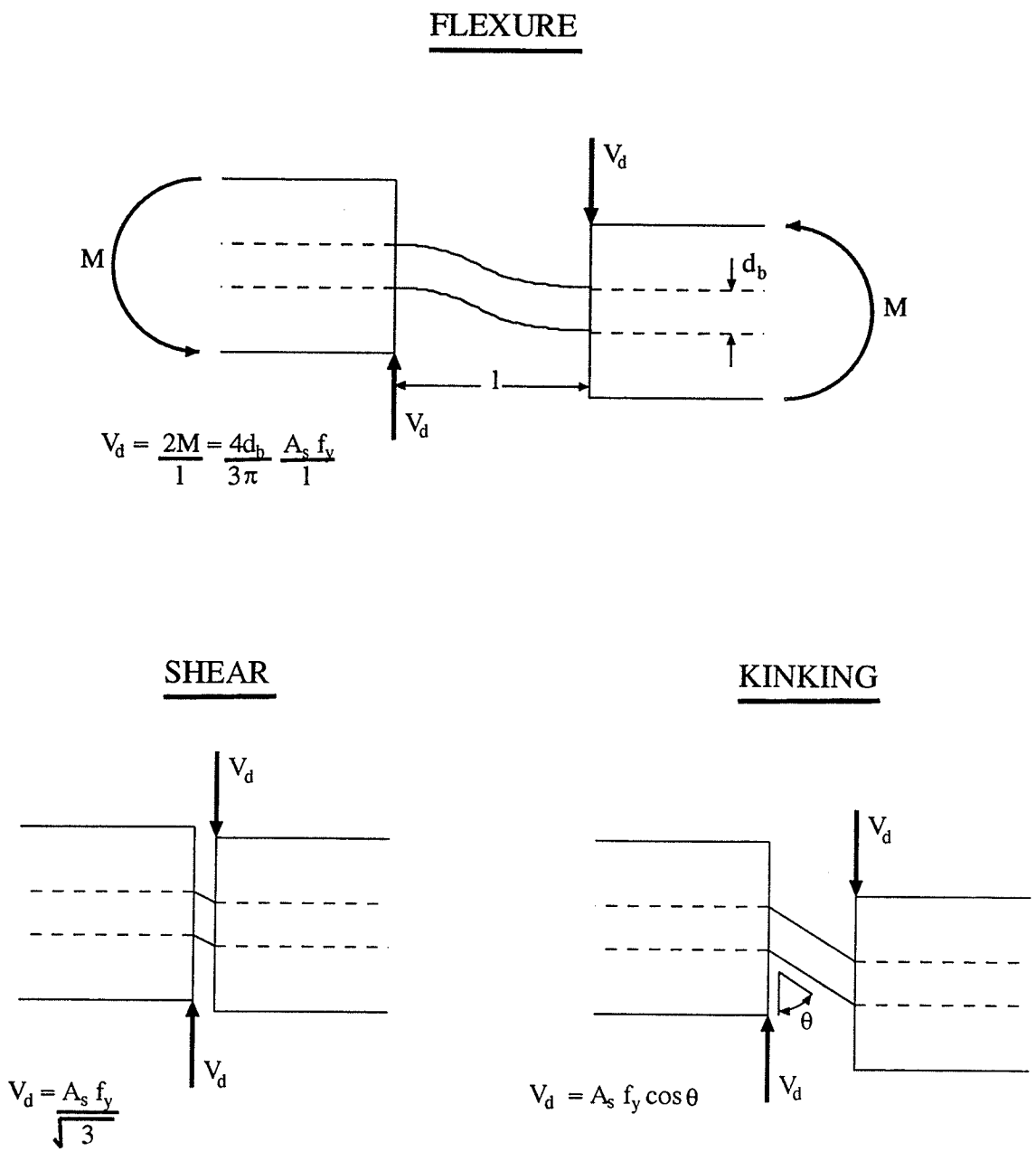

Figure 2.2: Dowel Action Mechanisms

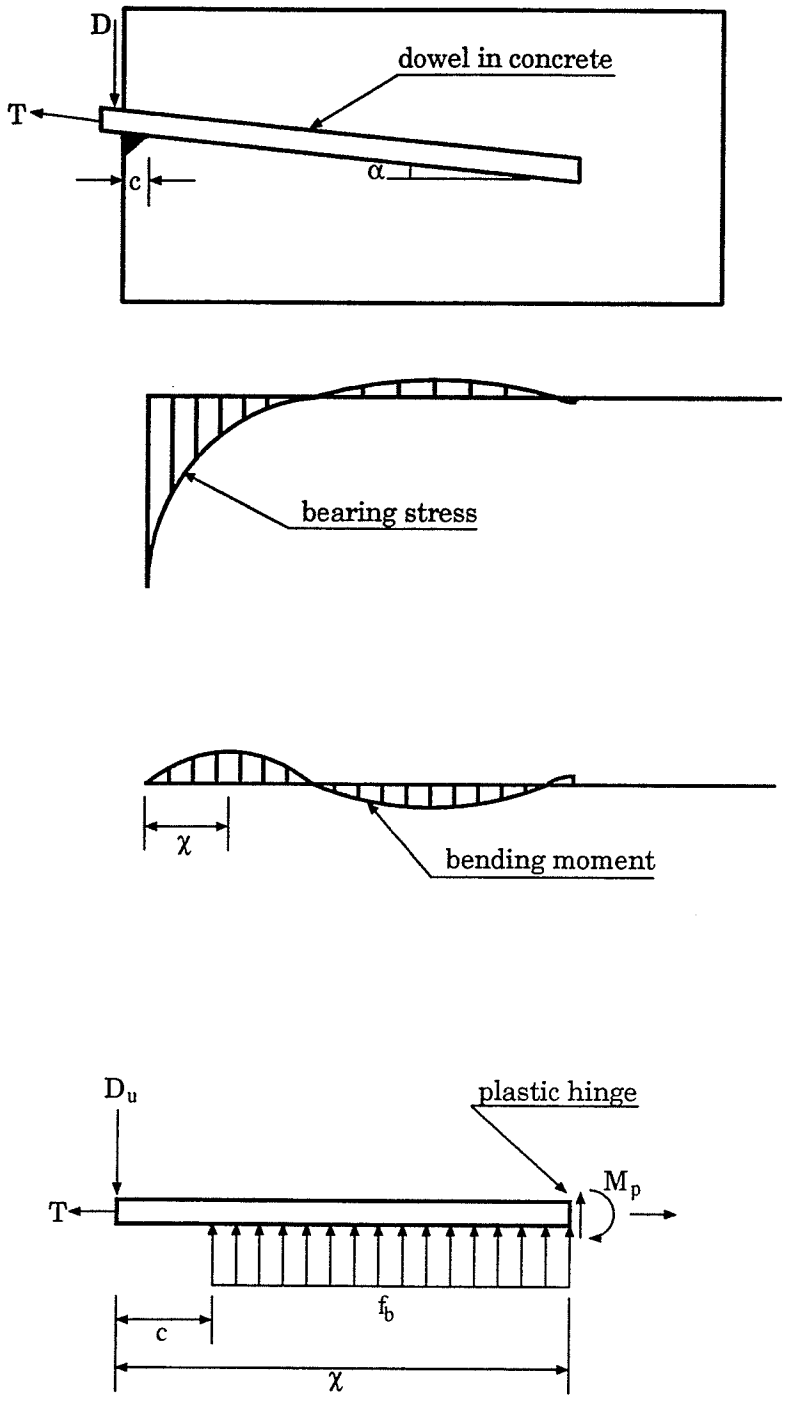

Figure 2.3: Beam on an Elastic Foundation Model

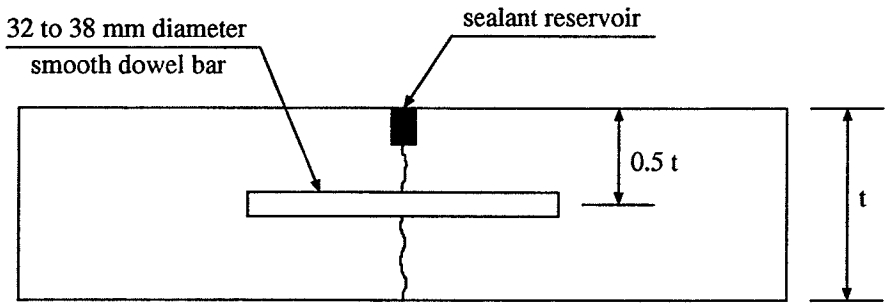

(a) Contraction Joint

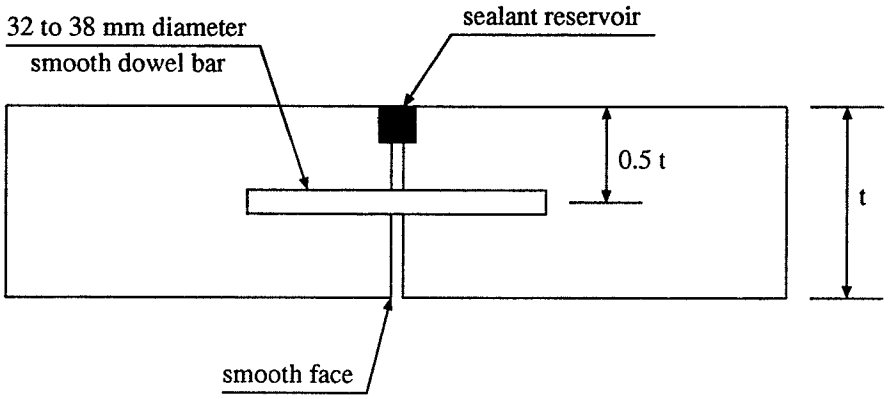

(b) Construction Joint

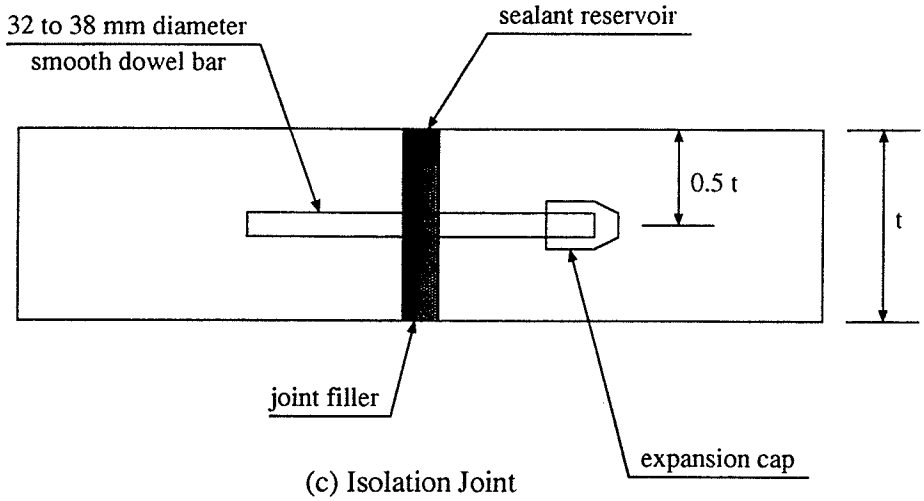

(c) Isolation Joint

Figure 2.4: Transverse Joint Types

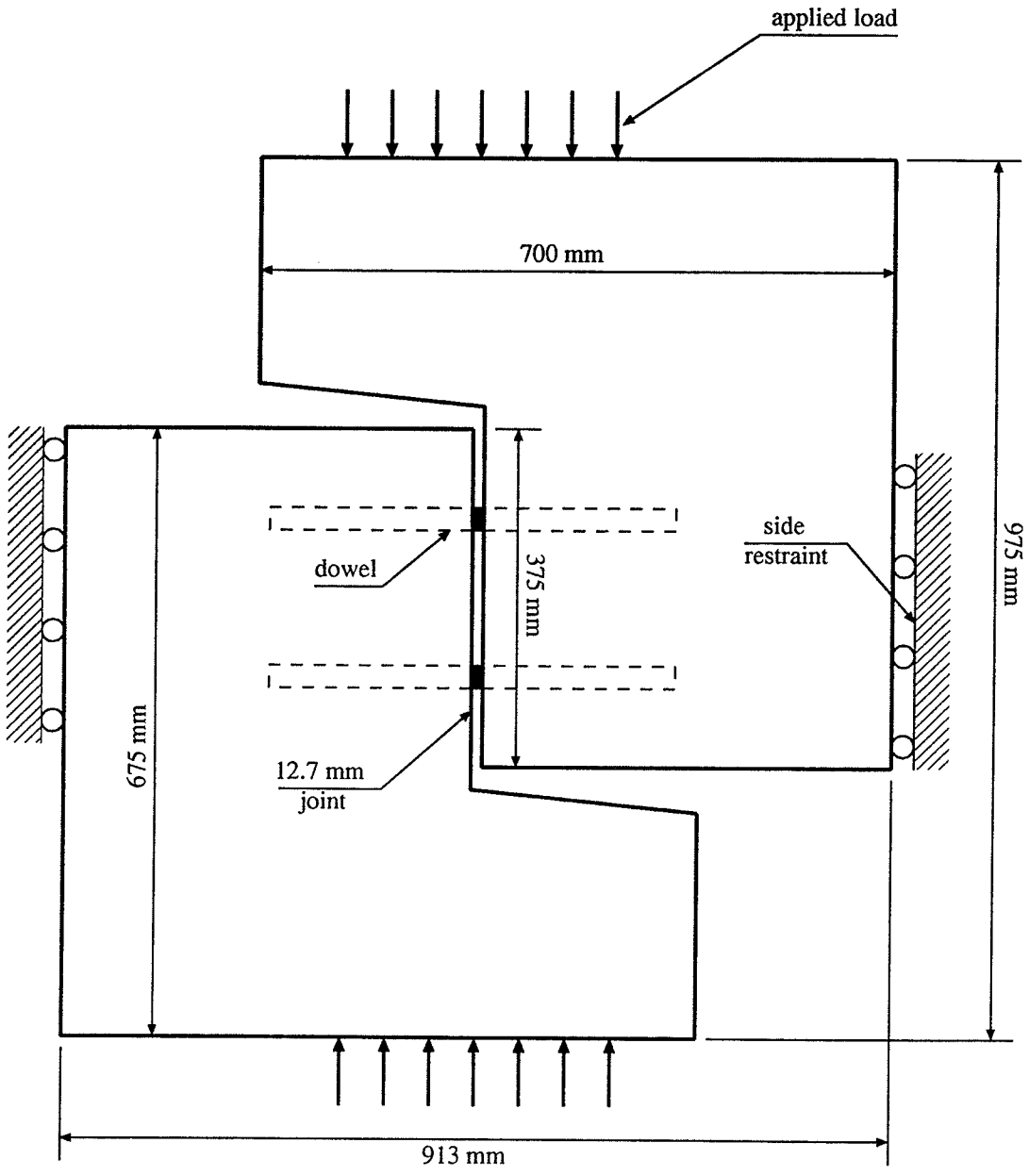

Note: Specimen thickness = 250 mm

Figure 3.1: Typical Push-off Test Specimen

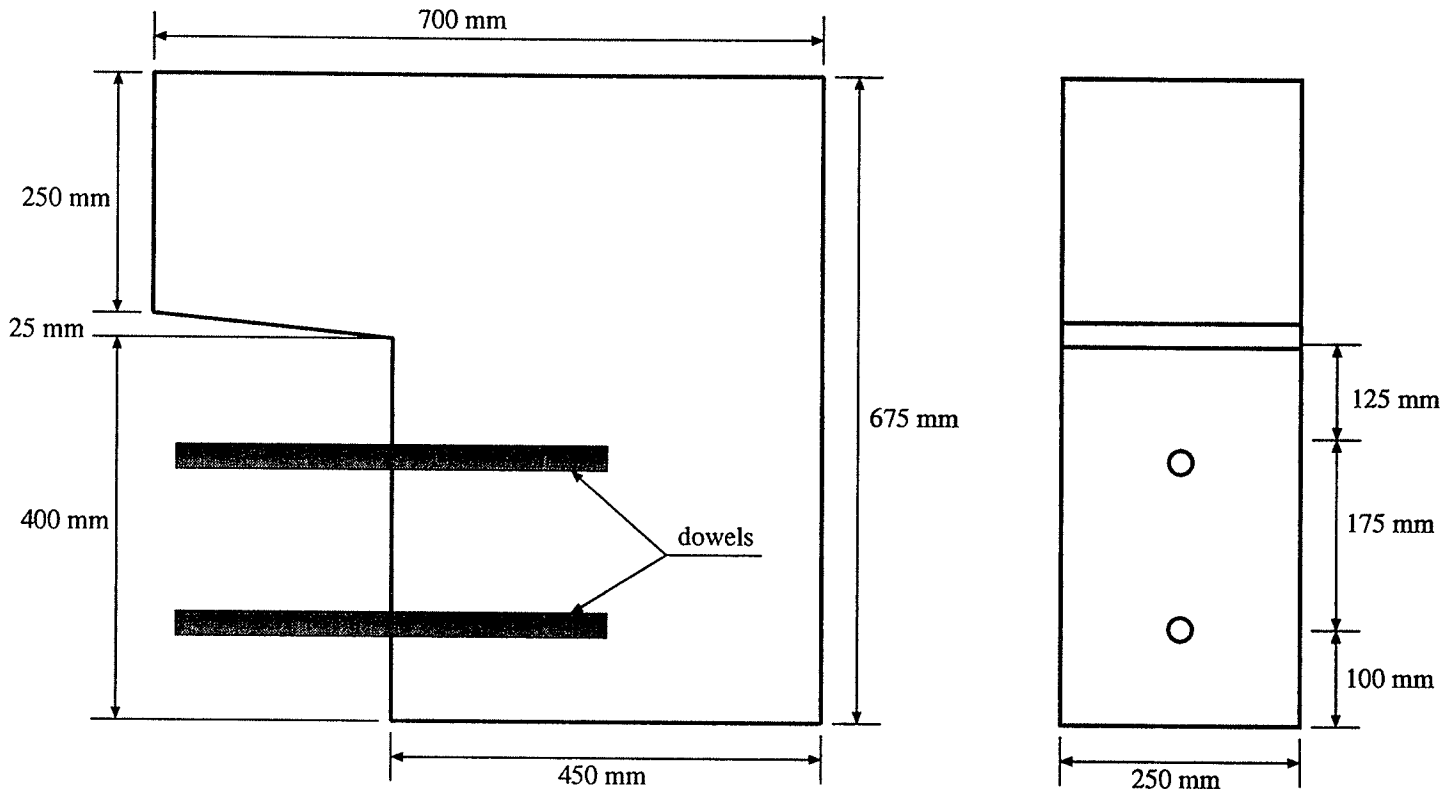

Figure 3.2: Dimensions of Typical Concrete Panel

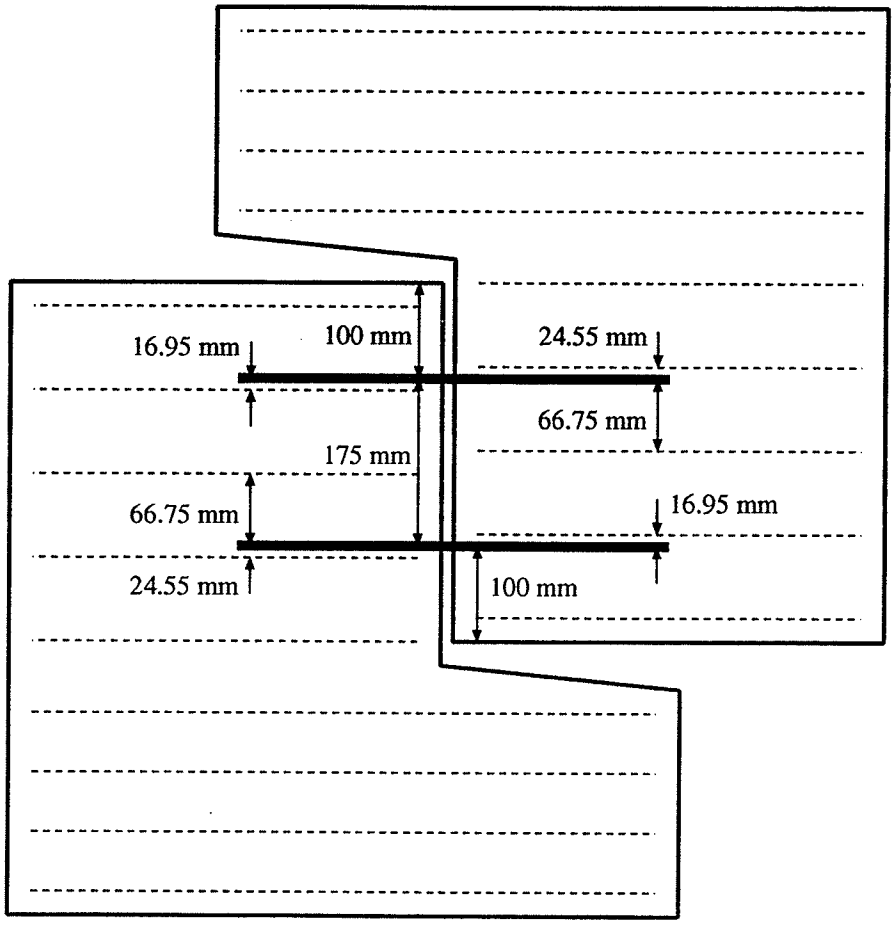

---- closed stirrup
450 mm long dowel bar

Note: All dimensions are to centreline of bars

Figure 3.3: Location of the Dowel Bars in Relation to the Reinforcement

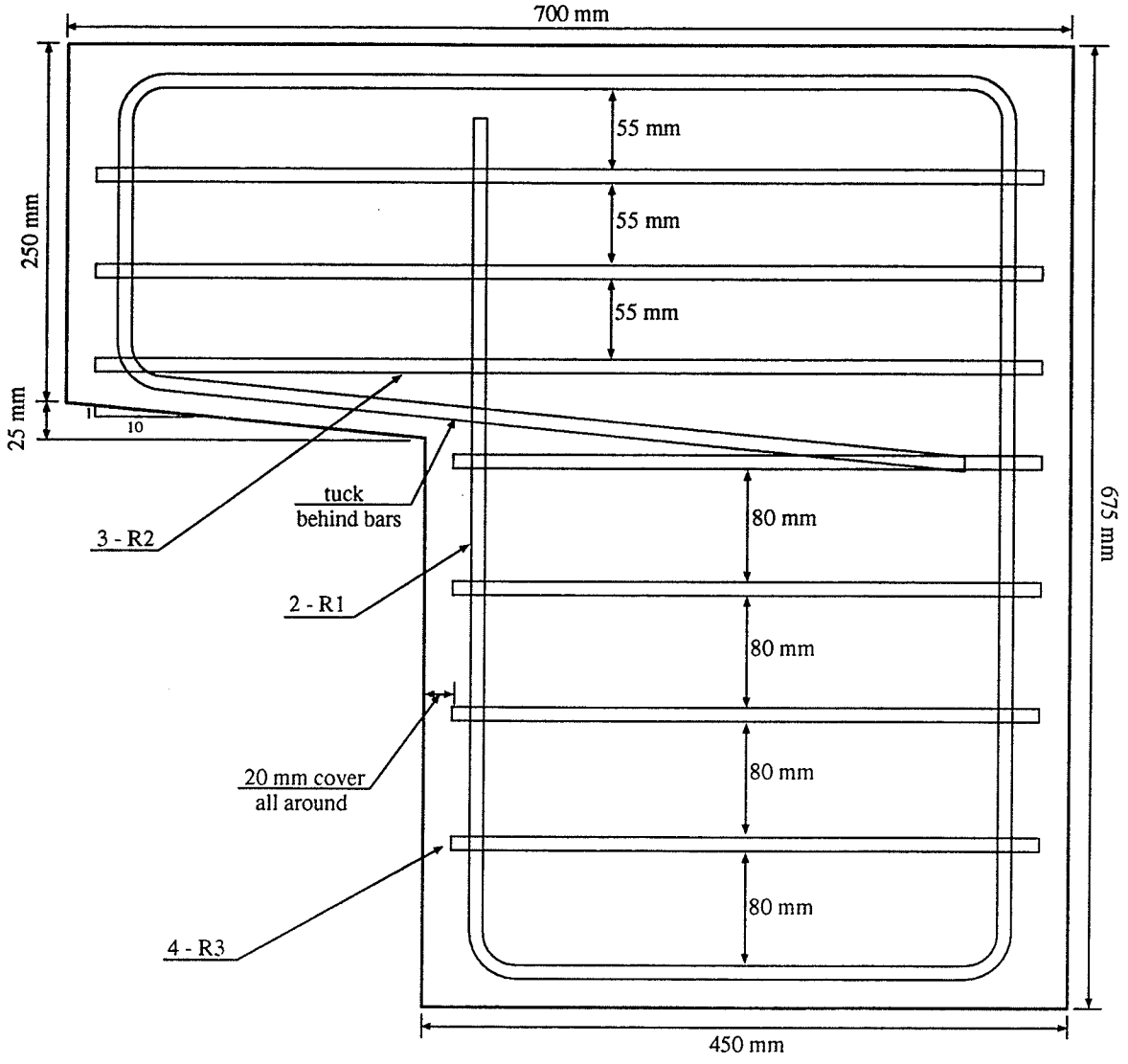

Notes: See Figures 3.5 and 3.6 for reinforcement dimensions and details
Specimen is 250 mm thick

Figure 3.4: Typical Reinforcement for a Concrete Panel

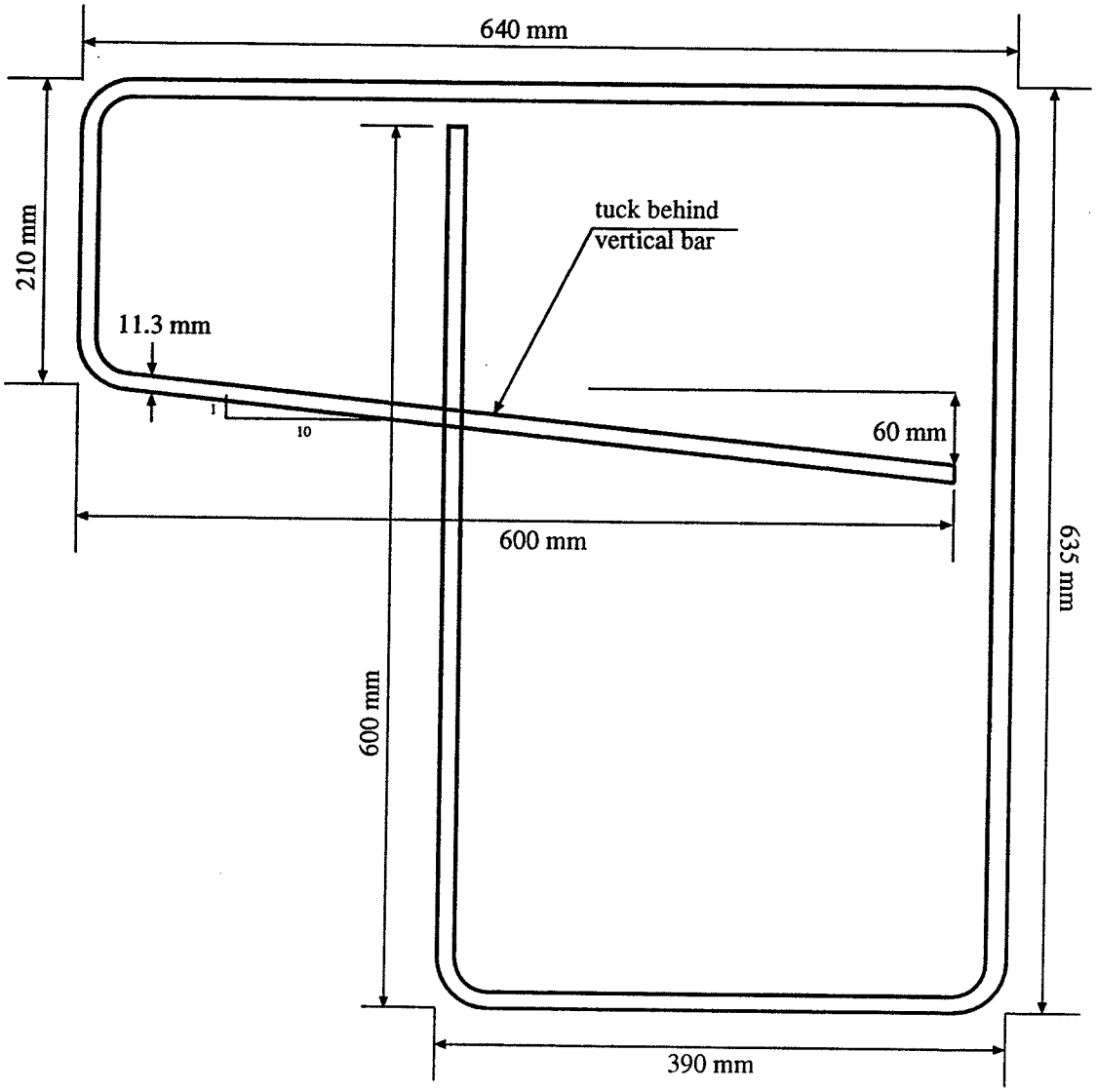

Notes: Use 10M reinforcing steel with yield strength of 400 MPa.
All bends have an interior diameter of 45 mm.
All dimensions measured to outside faces of bars.

Figure 3.5: Reinforcement Detail R-1

R-2

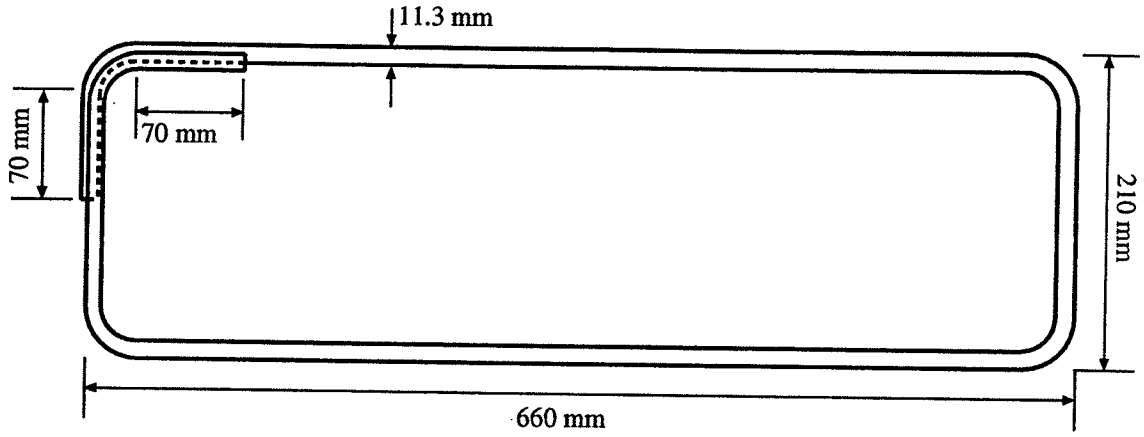

R-3

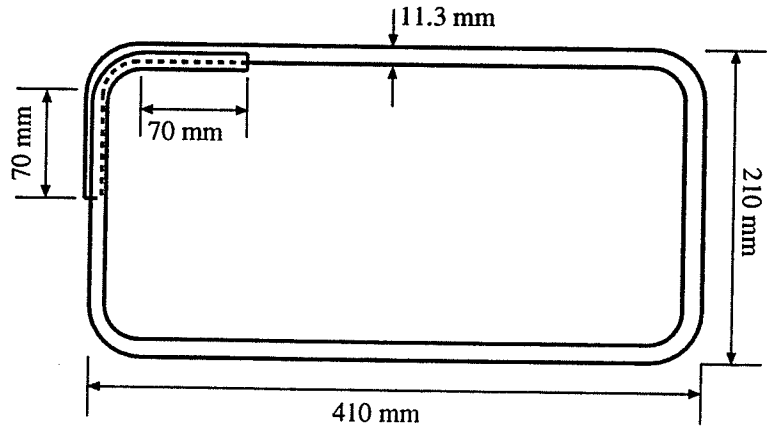

Top View

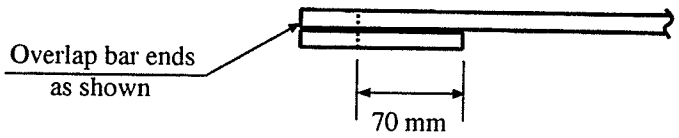

Notes: Use 10M reinforcing steel with yield strength of 400 MPa.
All bends have an internal diameter of 45 mm.
All dimensions measured to outside faces of bars.

Figure 3.6: Reinforcement Detail R-2 and R-3

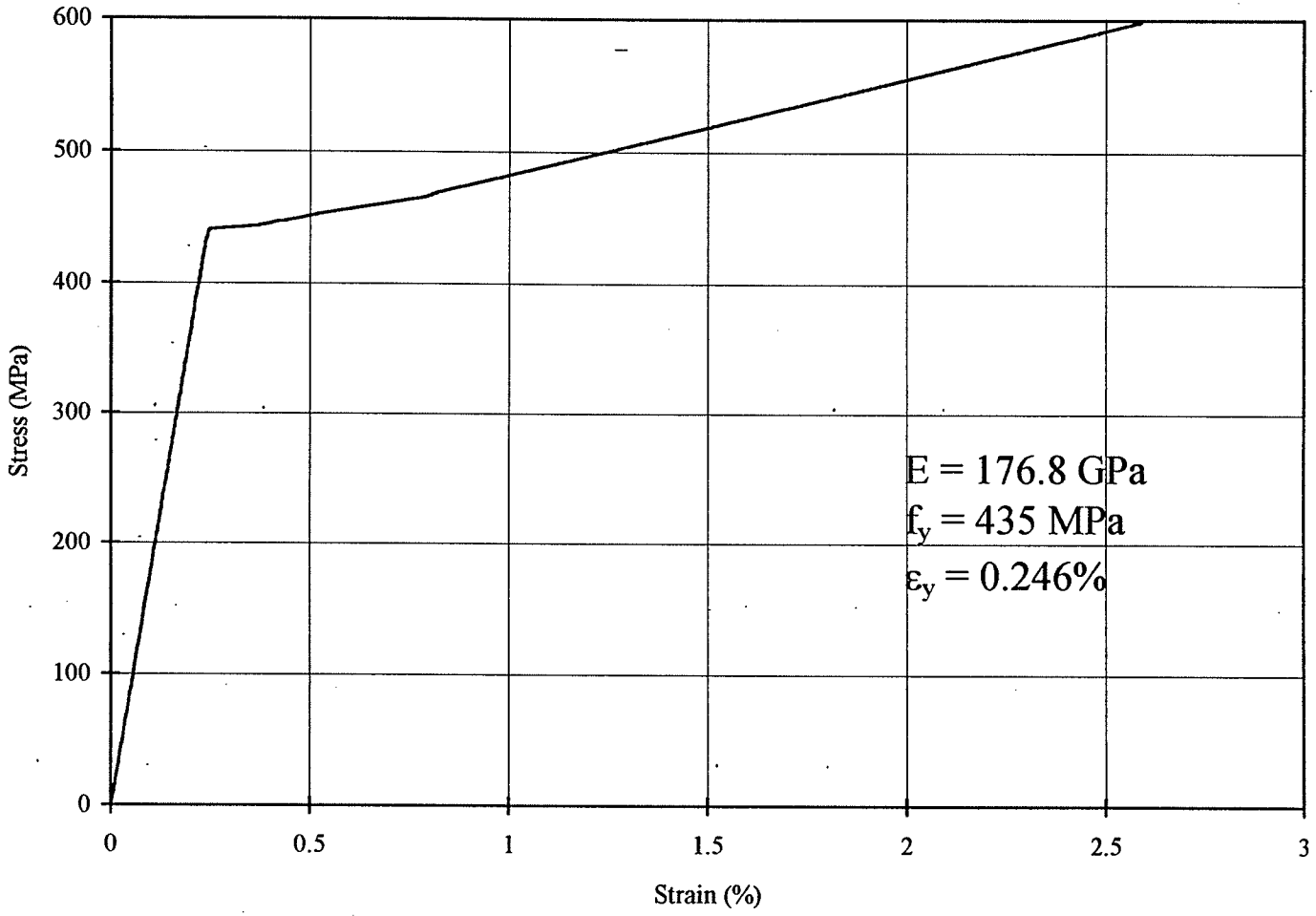

Figure 3.7: Stress-Strain Behaviour of Reinforcing Steel

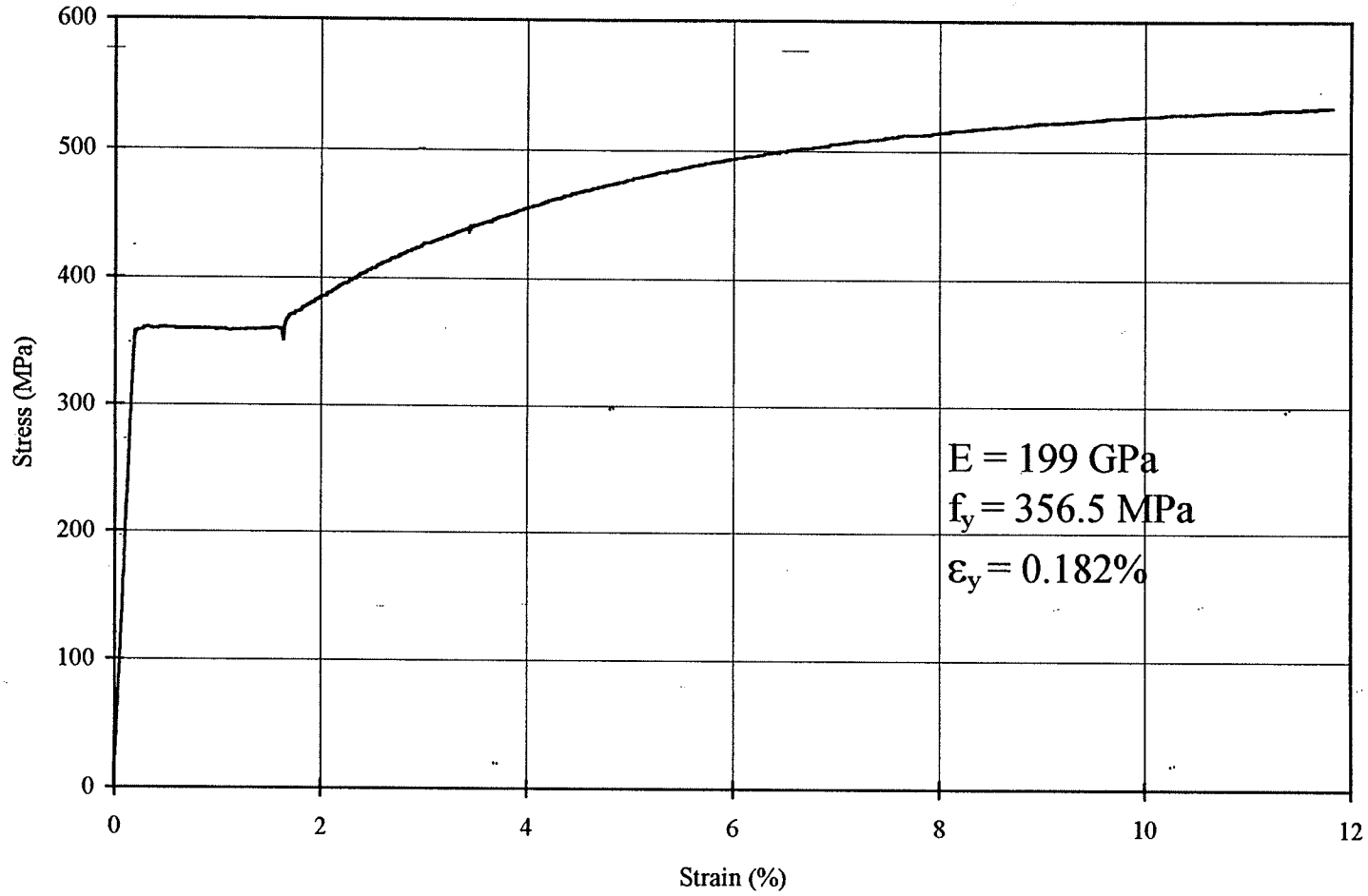

Figure 3.8: Stress-Strain Behaviour of Dowel Steel

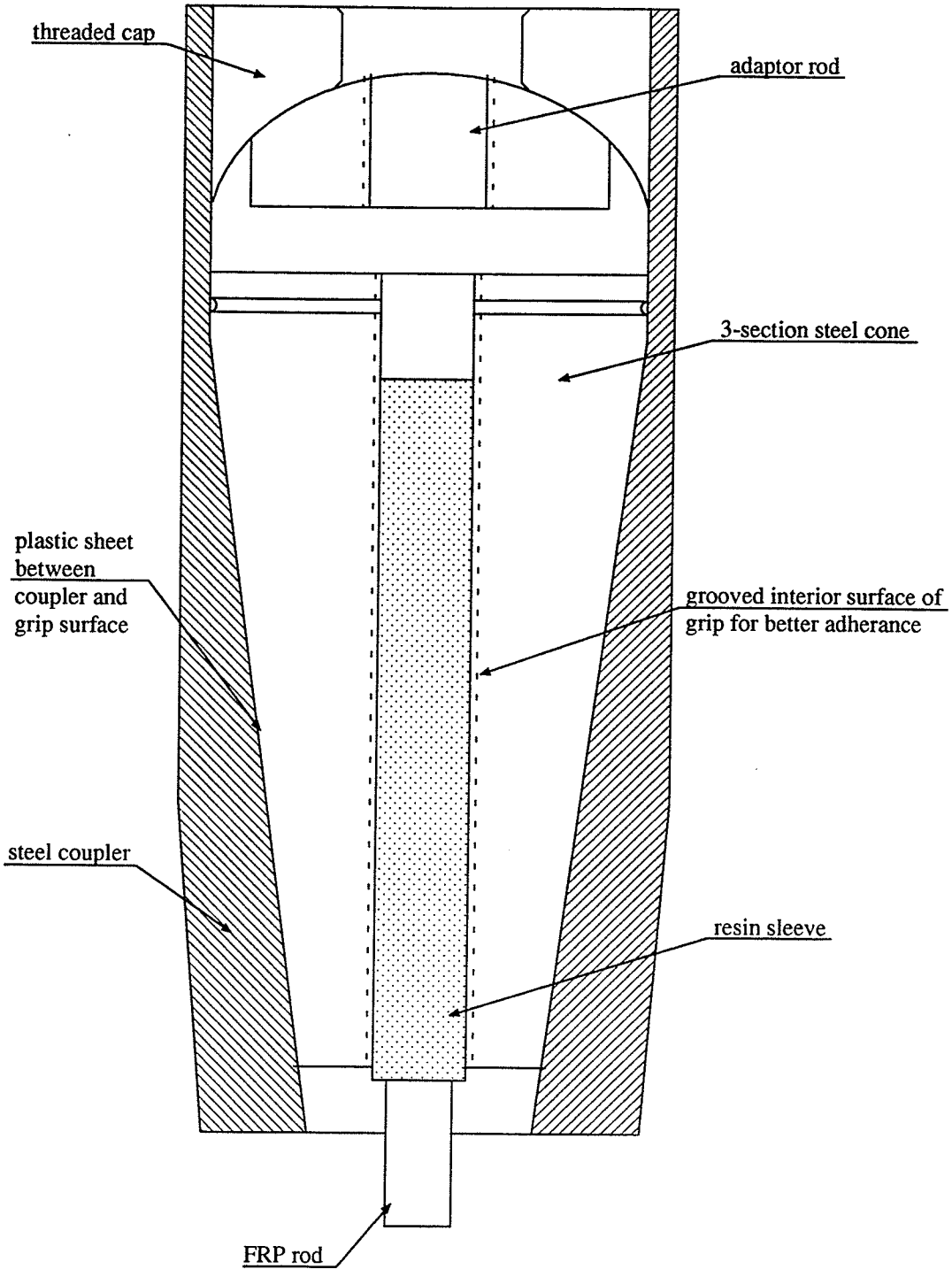

Figure 3.9: Coupler for Isorod Tension Test

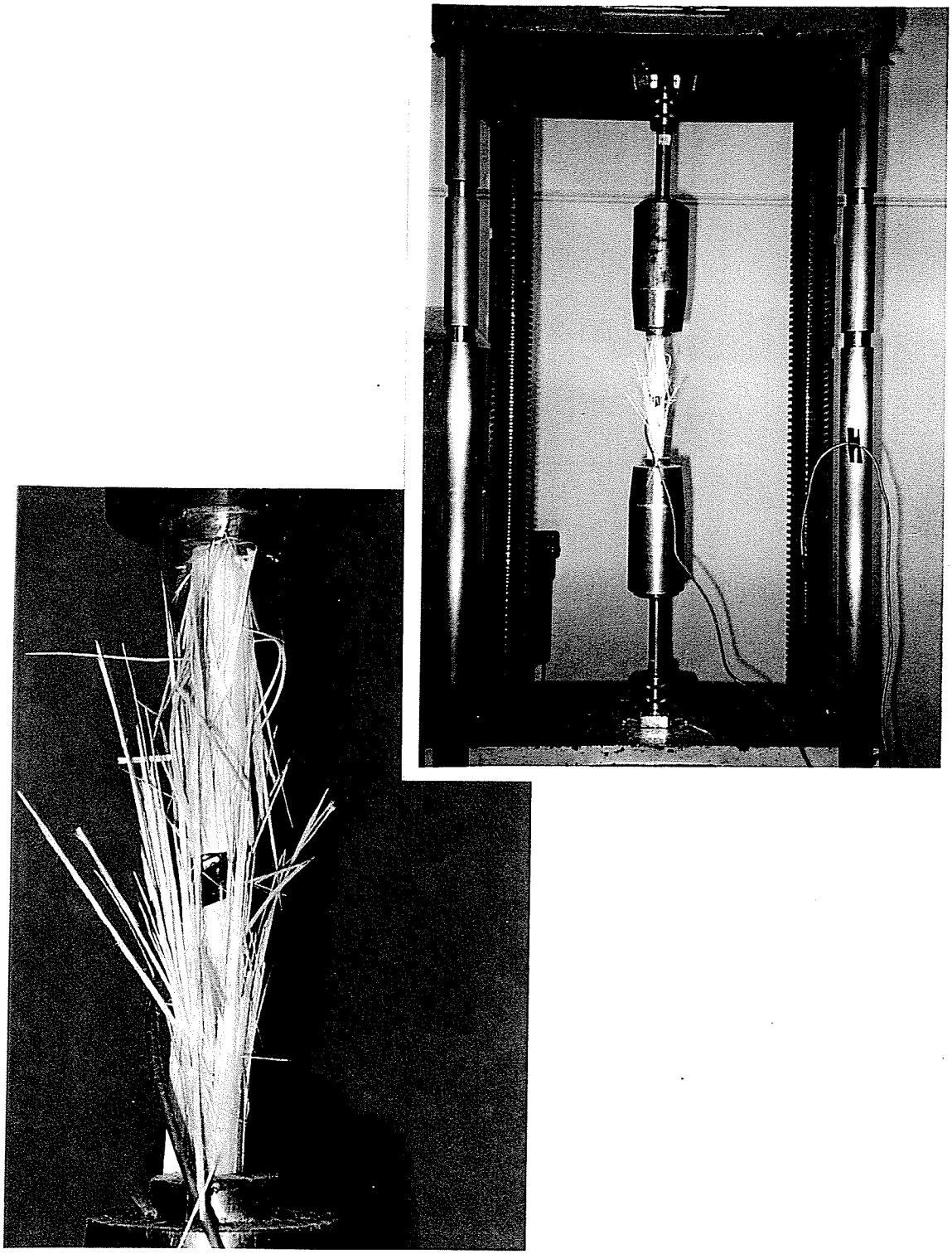

Figure 3.10: Tension Failure of Isorod

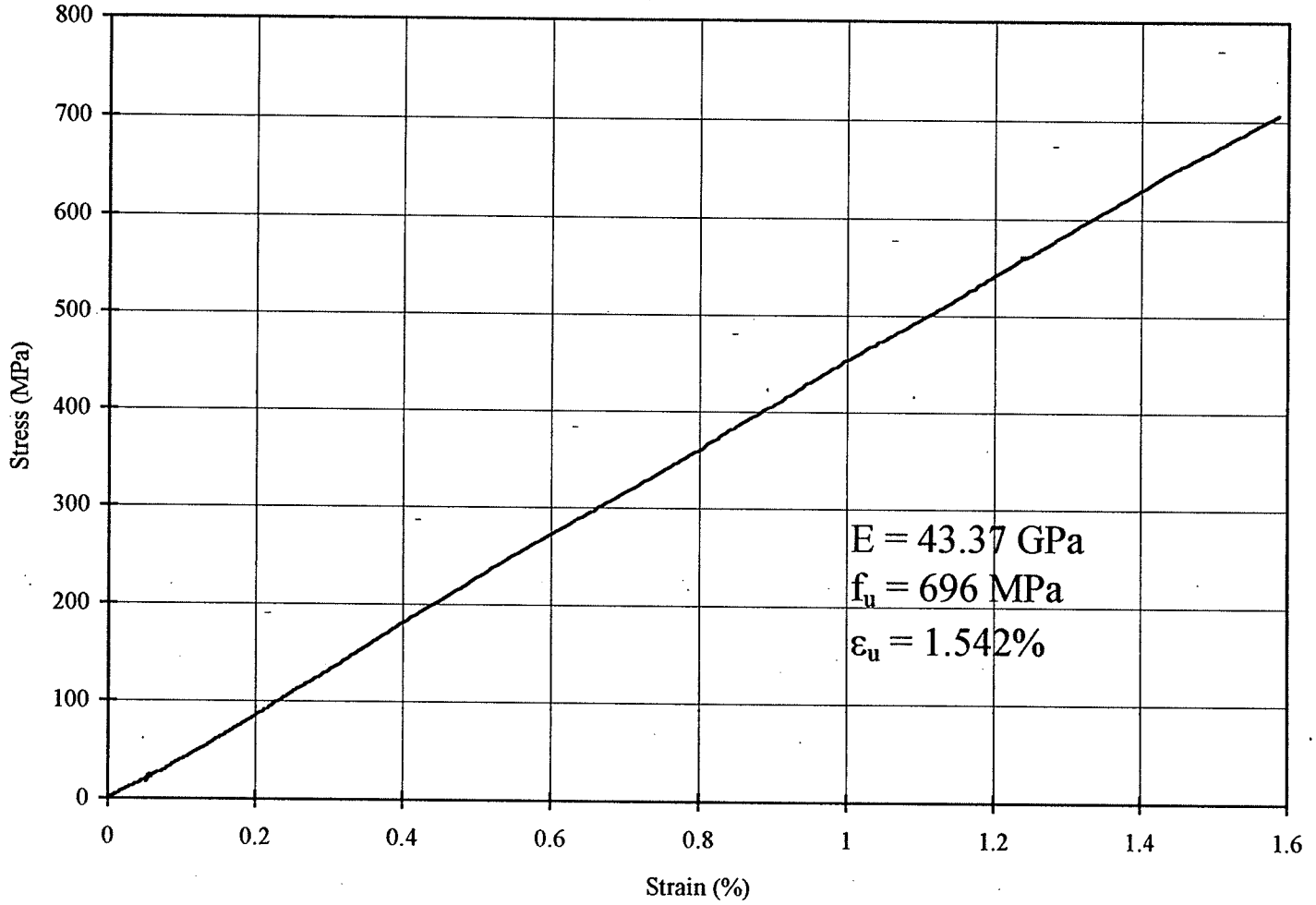

Figure 3.11: Stress-Strain Behaviour of Isorod

Figure 3.12: Formwork and First Specimen Cast

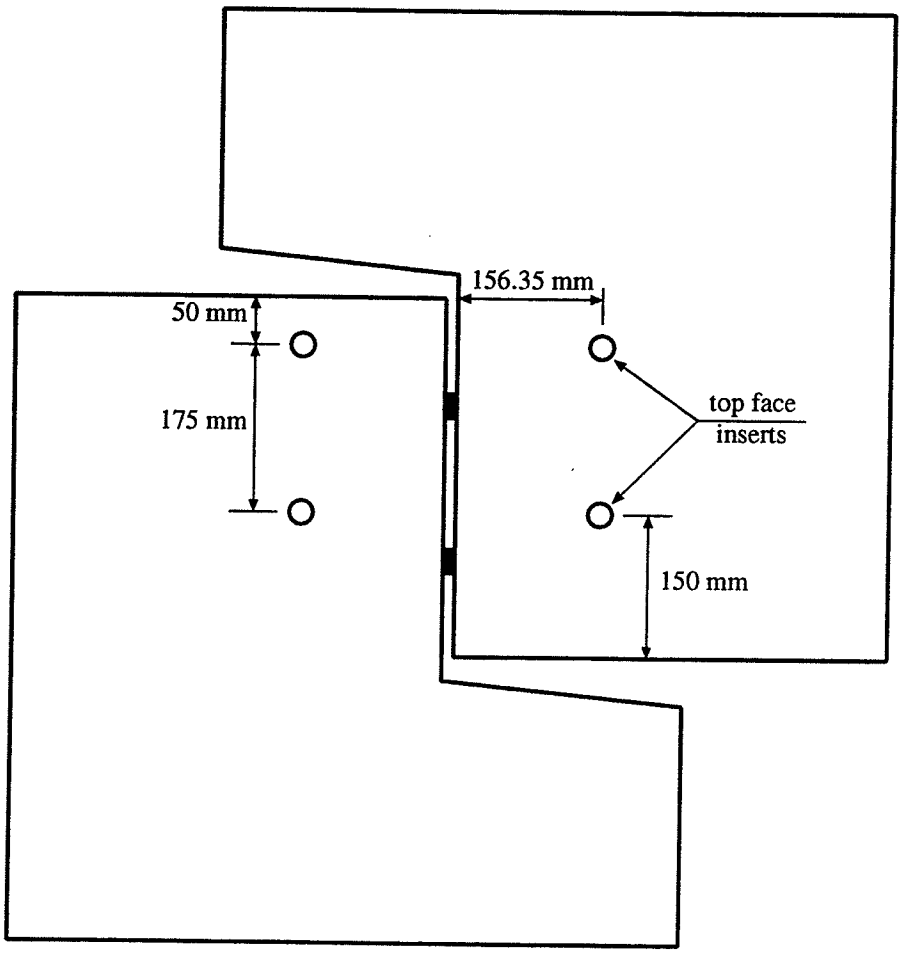

Note: 3/4" bolt diameter loop inserts are used.

Figure 3.13: Location of Lifting Inserts

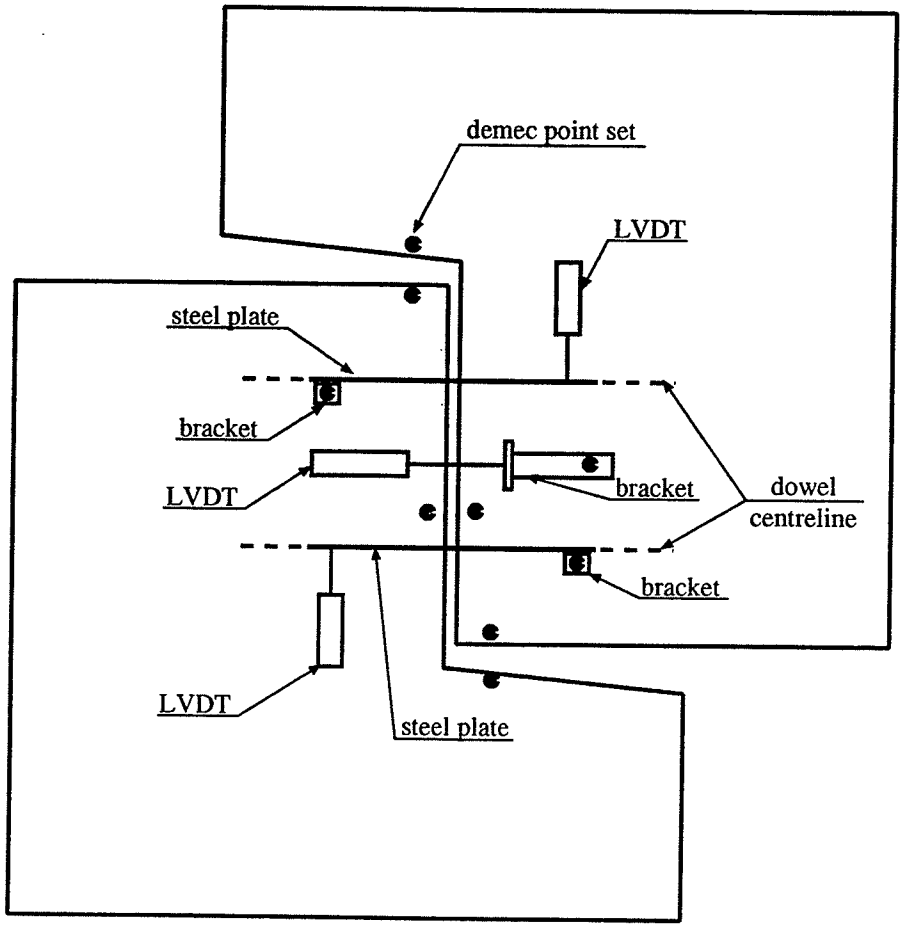

Figure 3.14: LVDT and Demec Point Locations

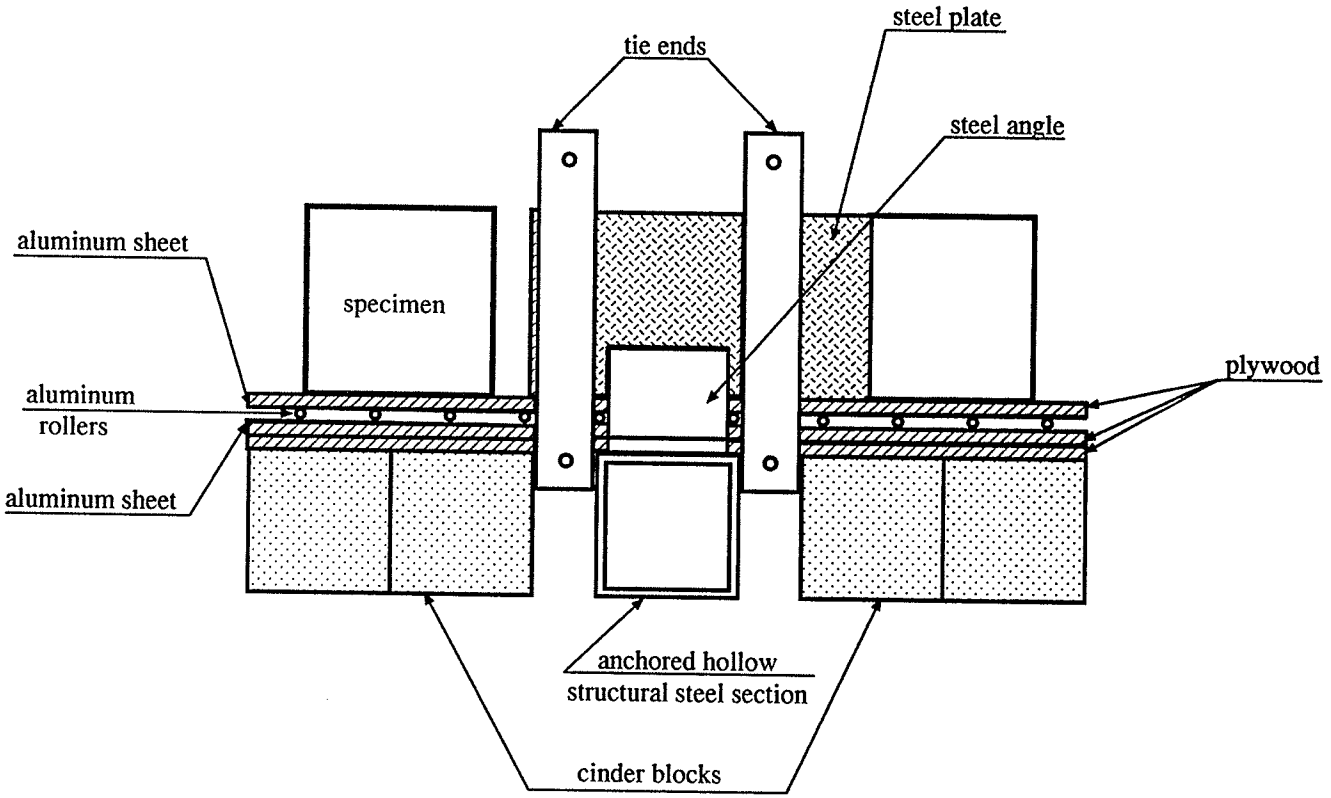

Figure 3.15: Side View of Setup for Push-off Specimen

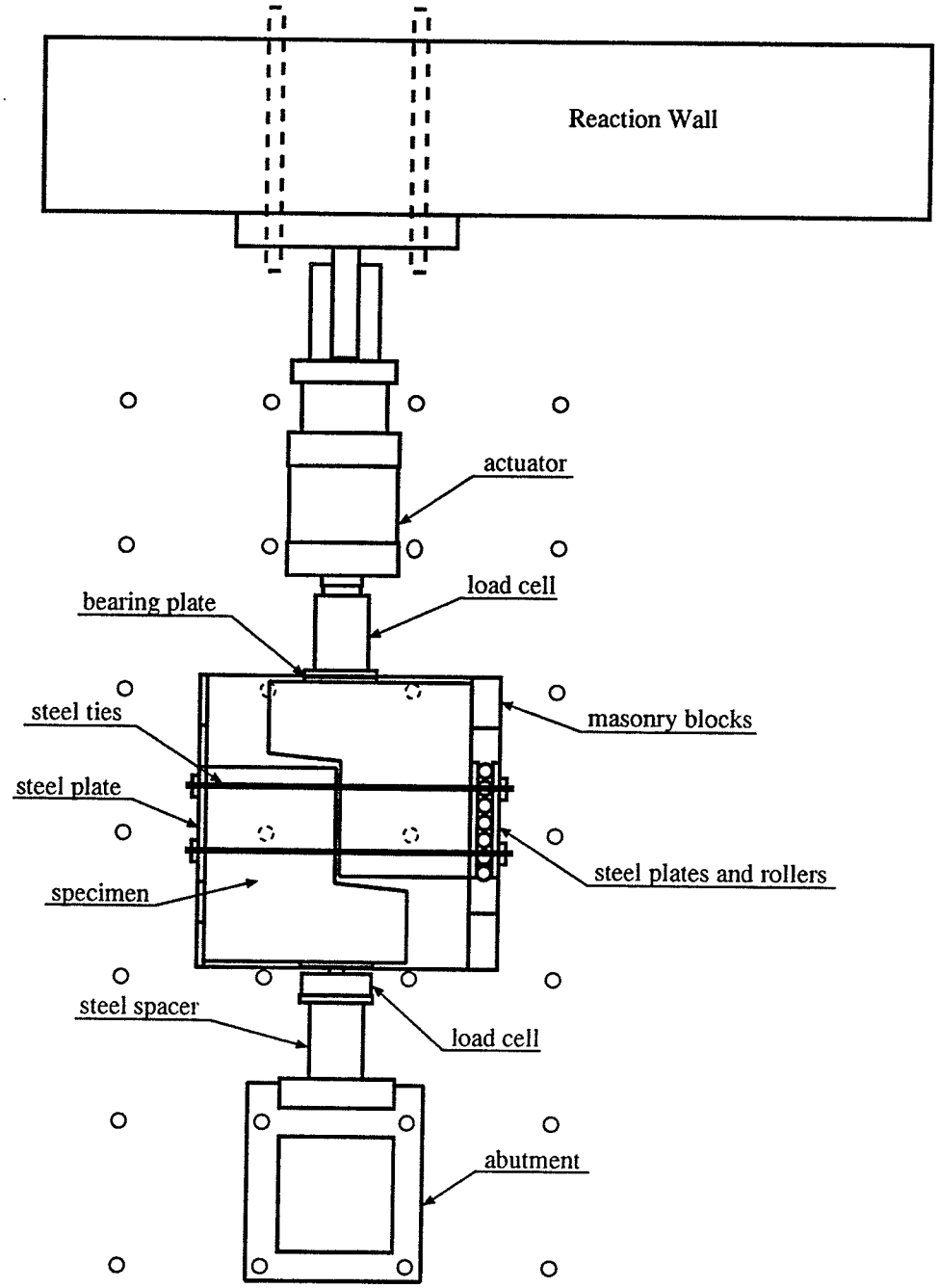

Figure 3.16: Test Setup for Push-off Specimens

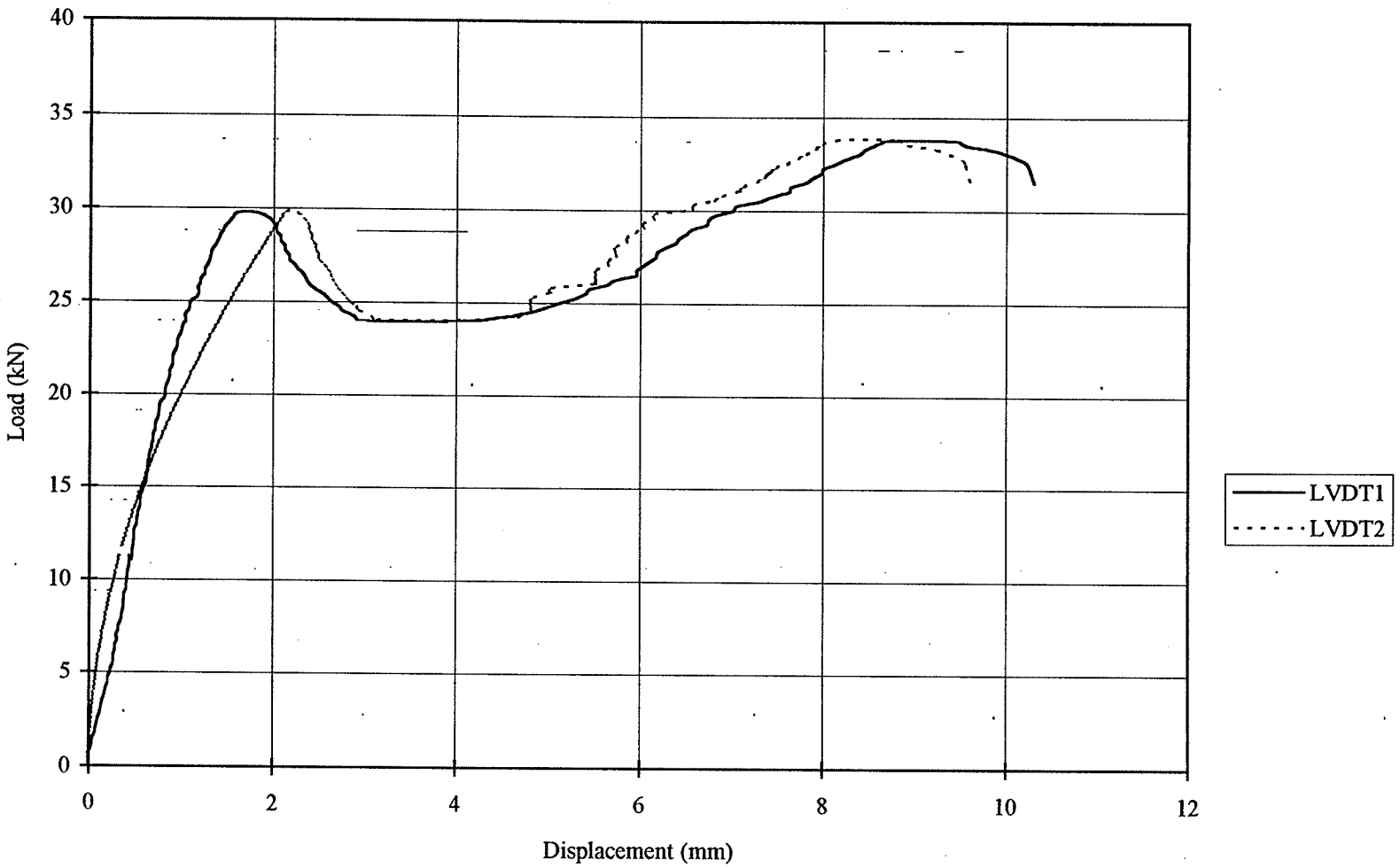

Figure 4.1: Load Versus Displacement from LVDT Readings for Specimen IS-N-1

Figure 4.2: Load versus Displacement from Demec Readings for Specimen IS-N-1

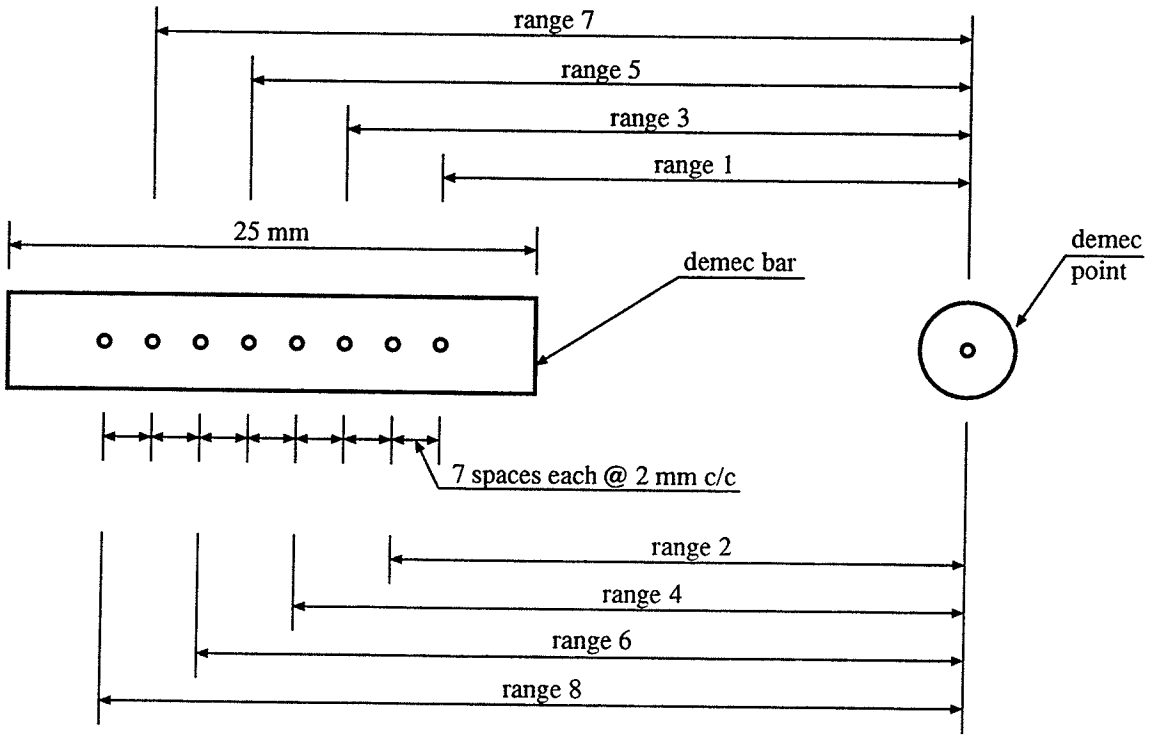

Figure 4.3: Multiple Ranges of Demec Bar

Figure 4.4: Specimen IS-N-1 After Failure

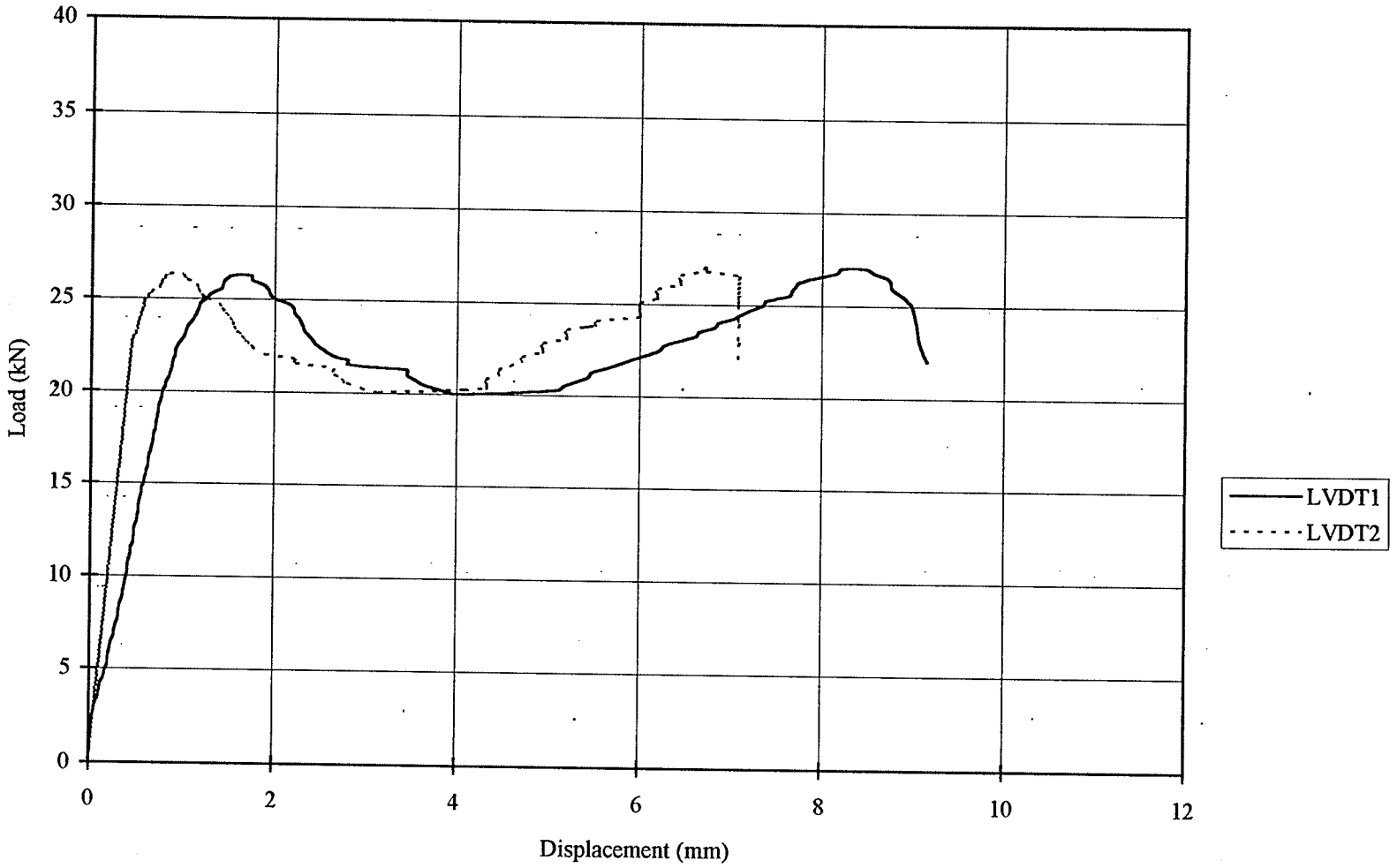

Figure 4.5: Load Versus Displacement from LVDT Readings for Specimen IS-N-2

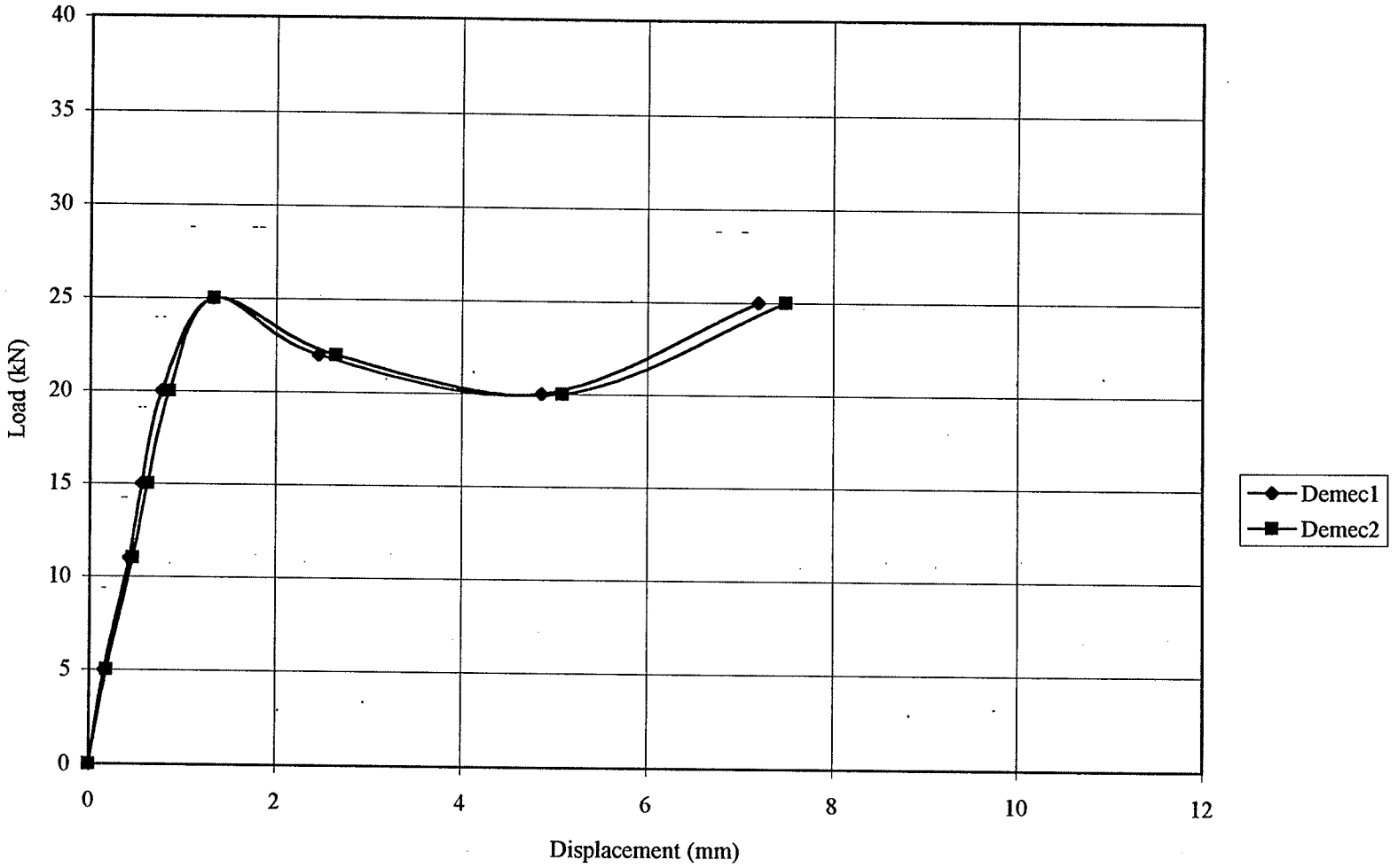

Figure 4.6: Load versus Displacement from Demec Readings for Specimen IS-N-2

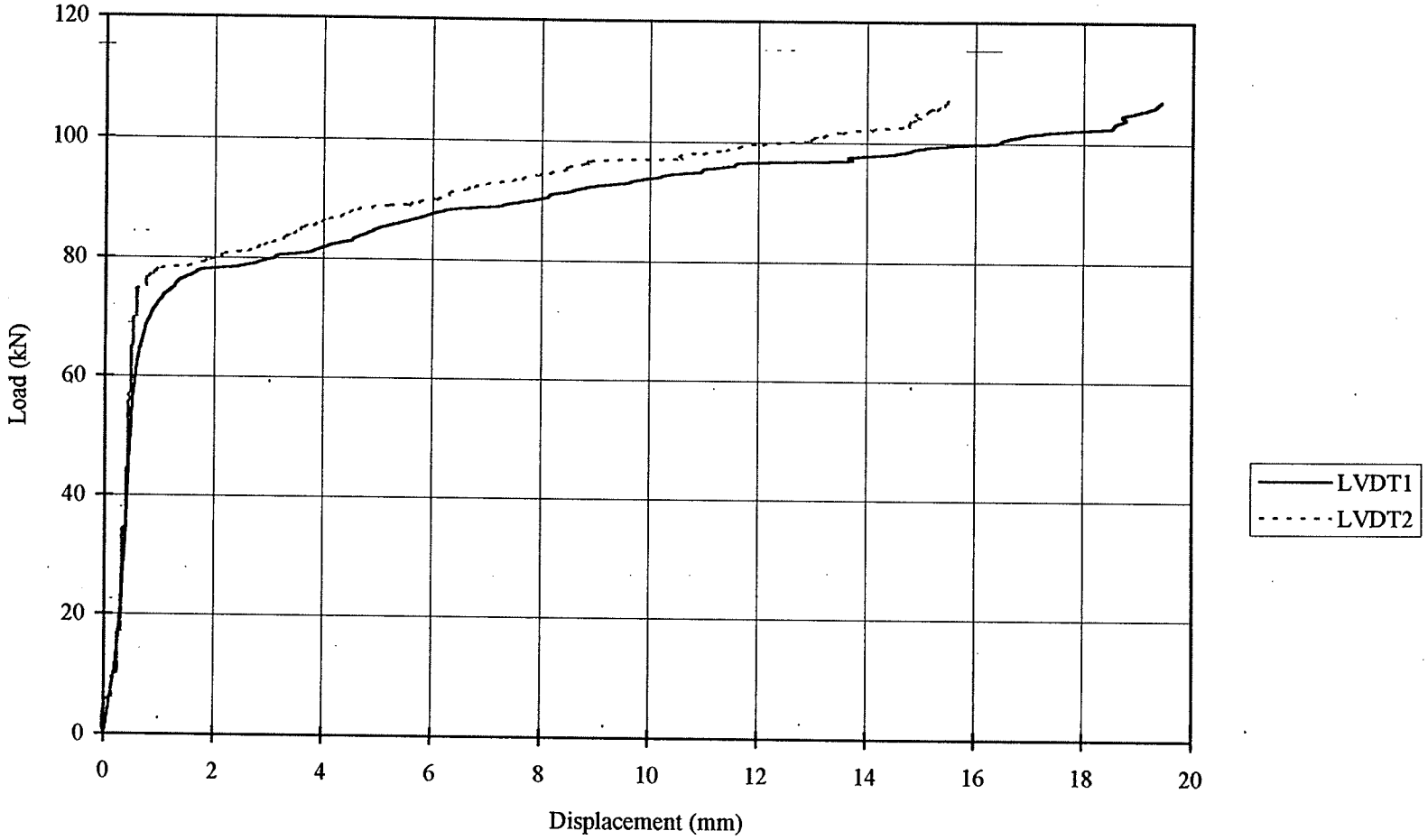

Figure 4.7: Load Versus Displacement from LVDT Readings for Specimen ST-N-1

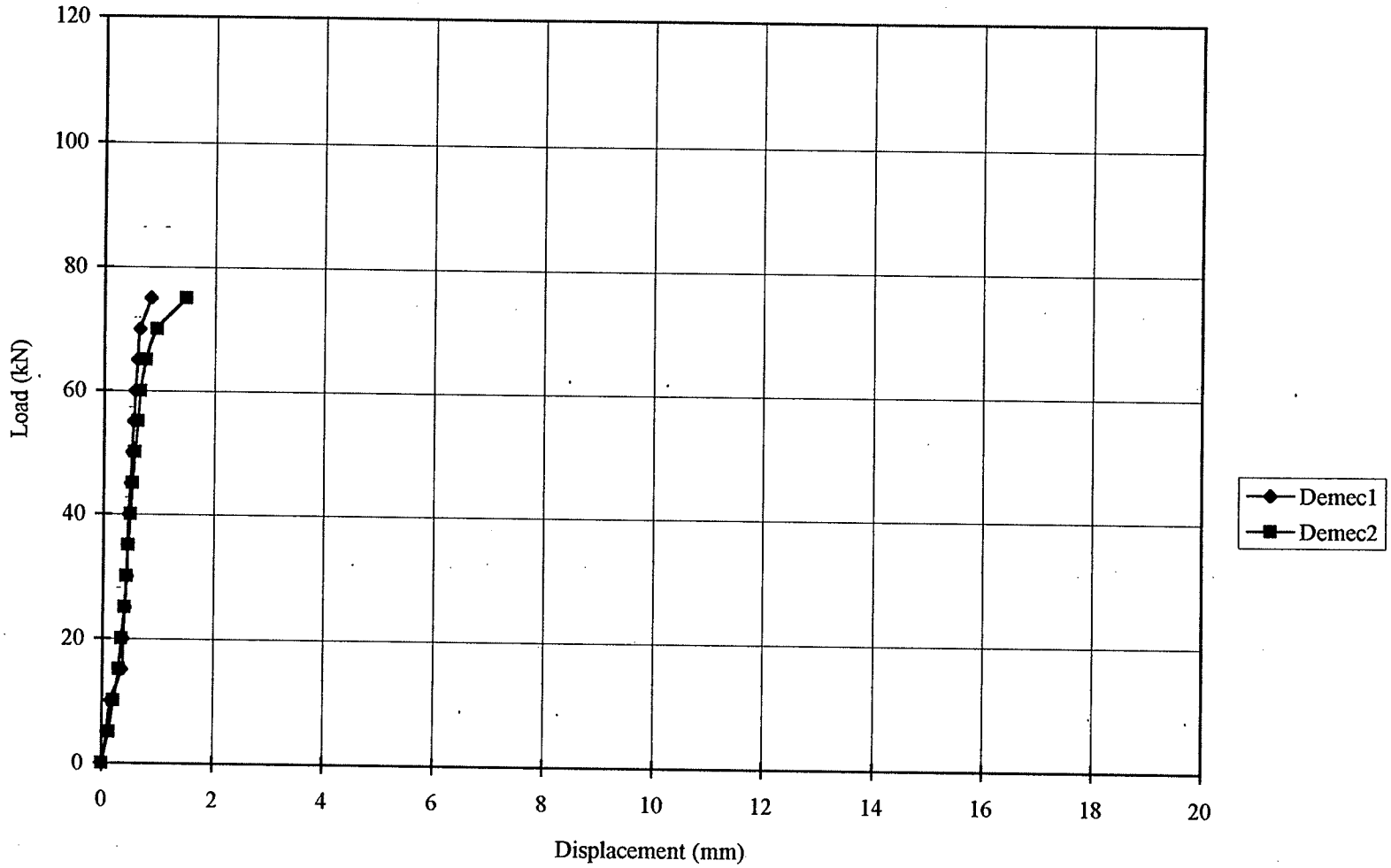

Figure 4.8: Load Versus Displacement from Demec Readings for Specimen ST-N-1

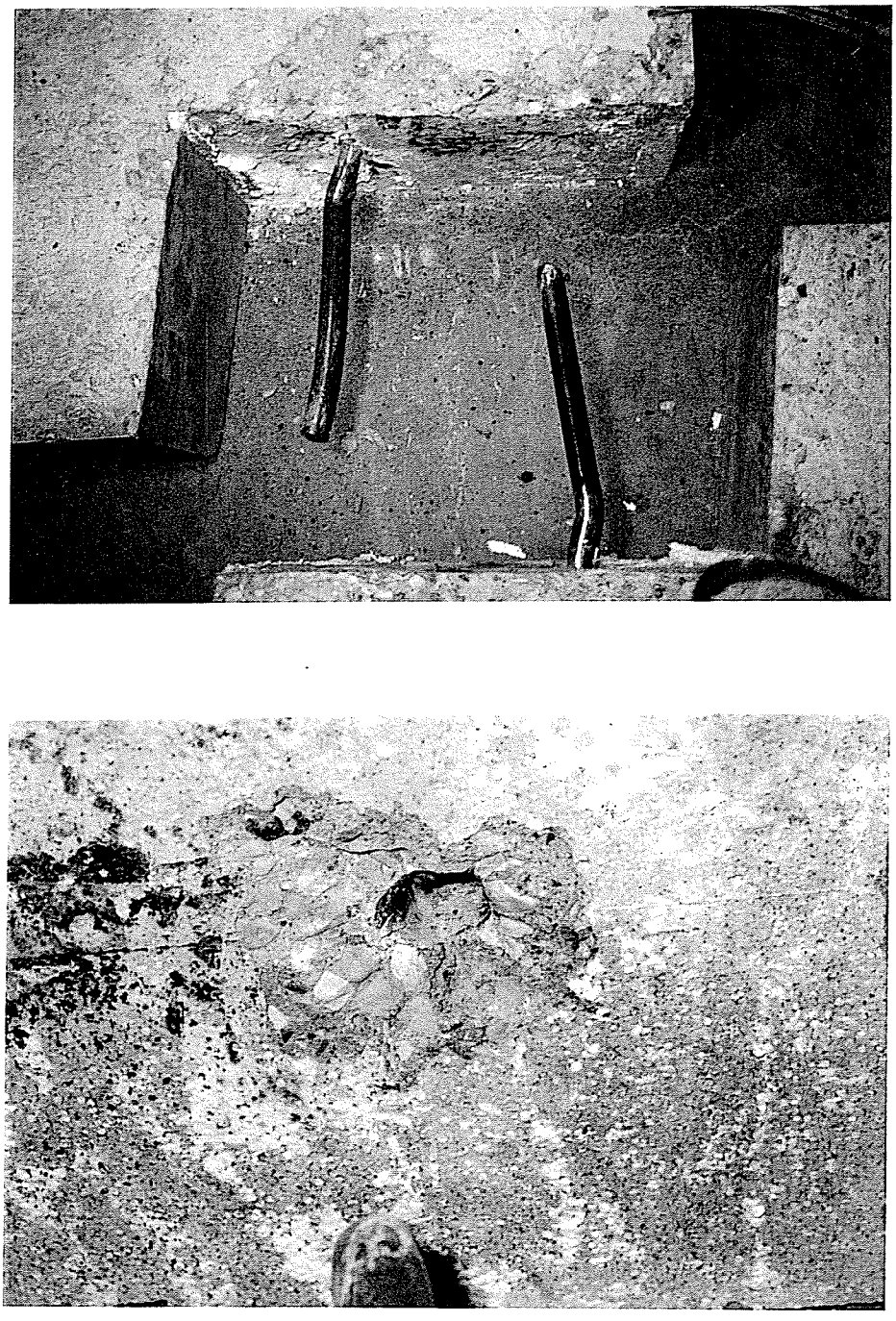

Figure 4.9: Specimen ST-N-1 After Failure

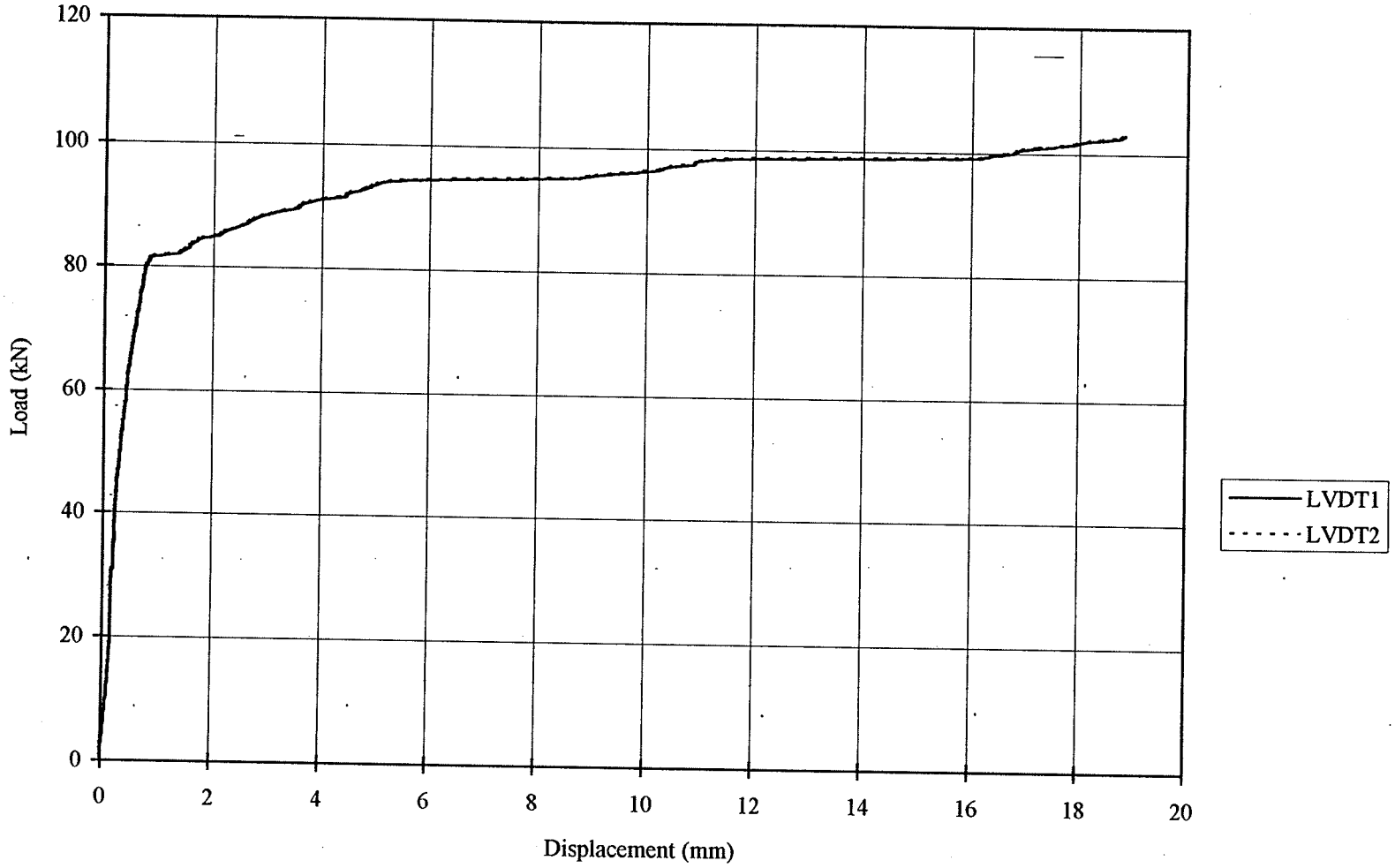

Figure 4.10: Load Versus Displacement from LVDT Readings for Specimen ST-N-2

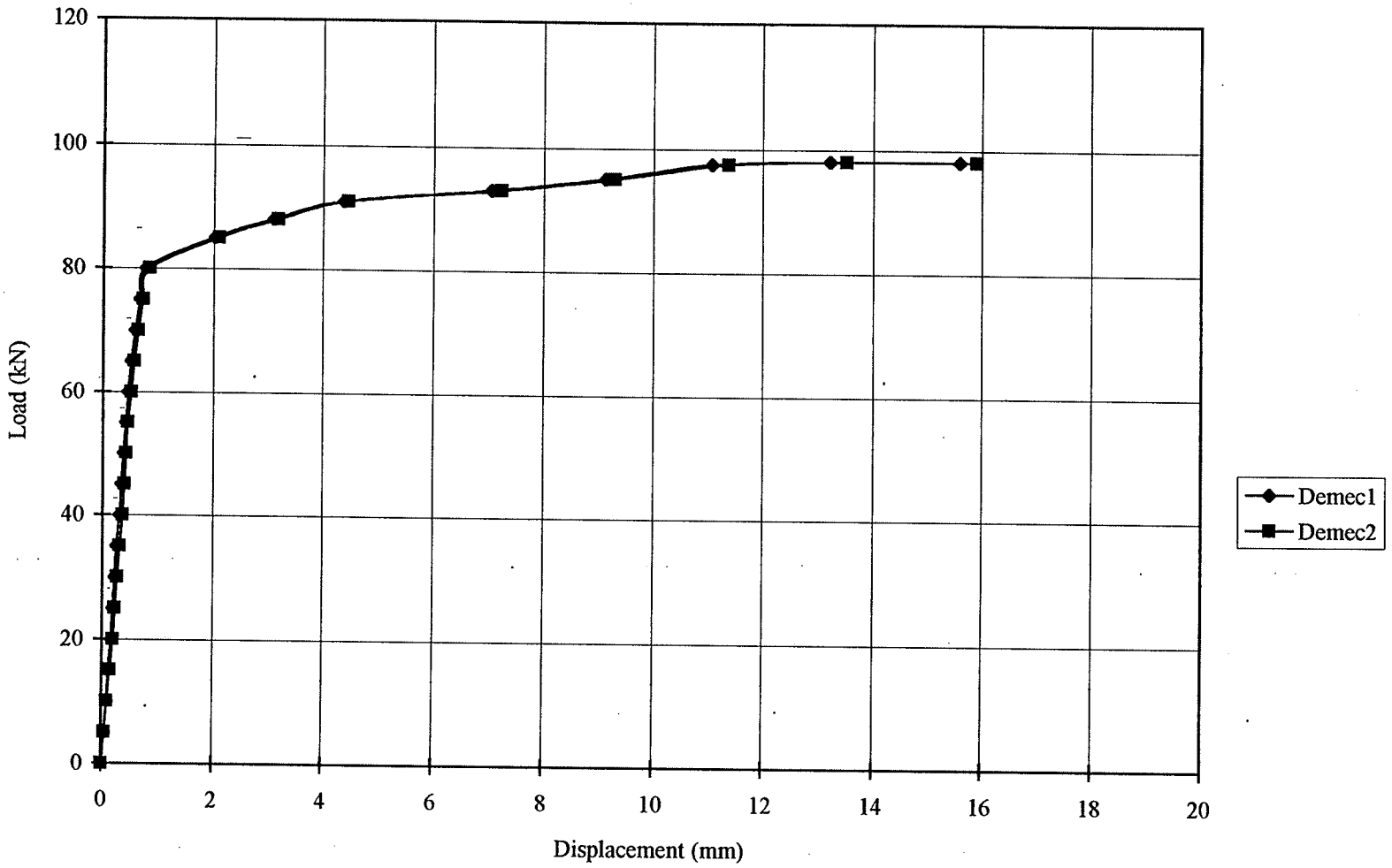

Figure 4.11: Load Versus Displacement from Demec Readings for Specimen ST-N-2

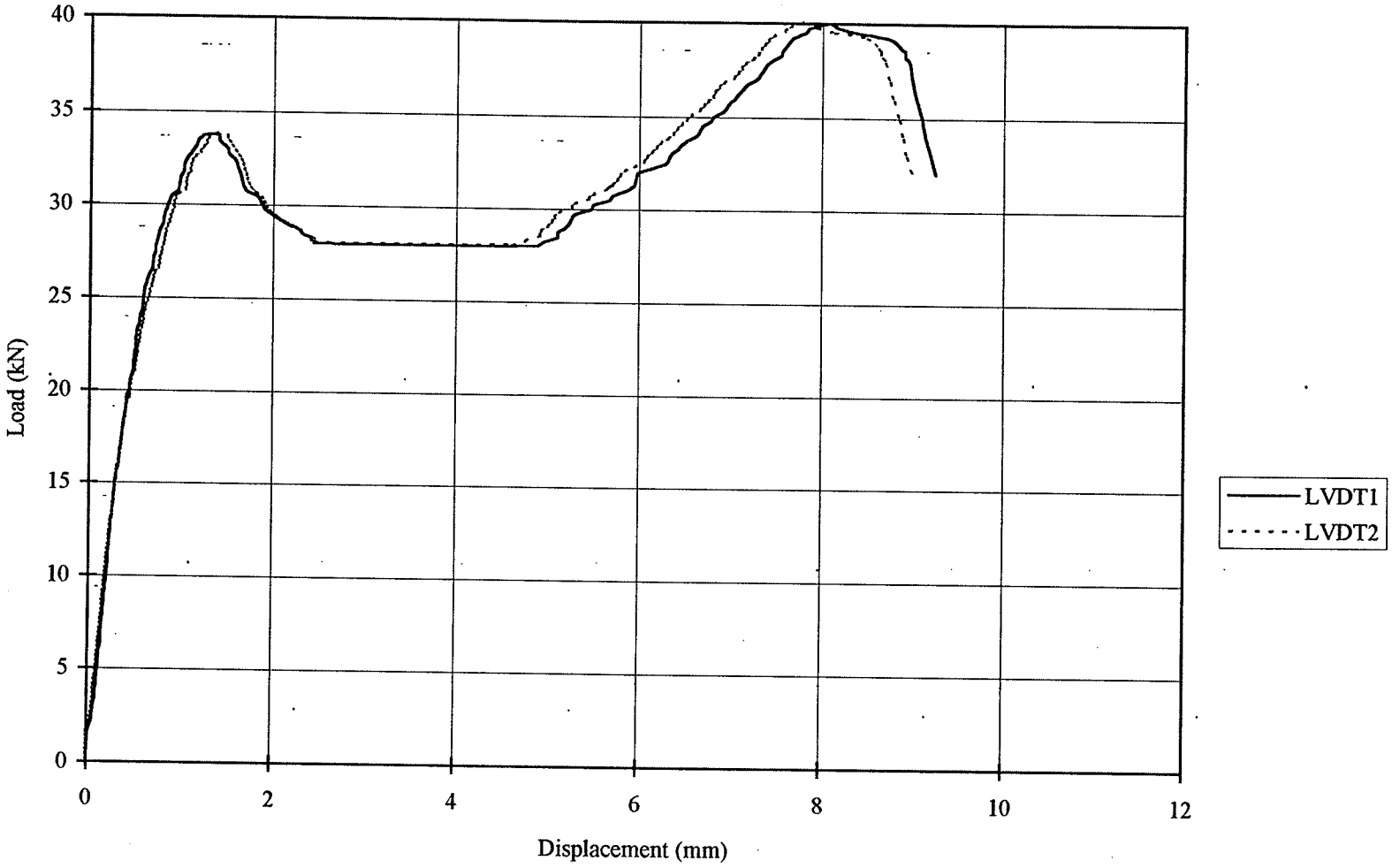

Figure 4.12: Load Versus Displacement from LVDT Readings for Specimen IS-P-1

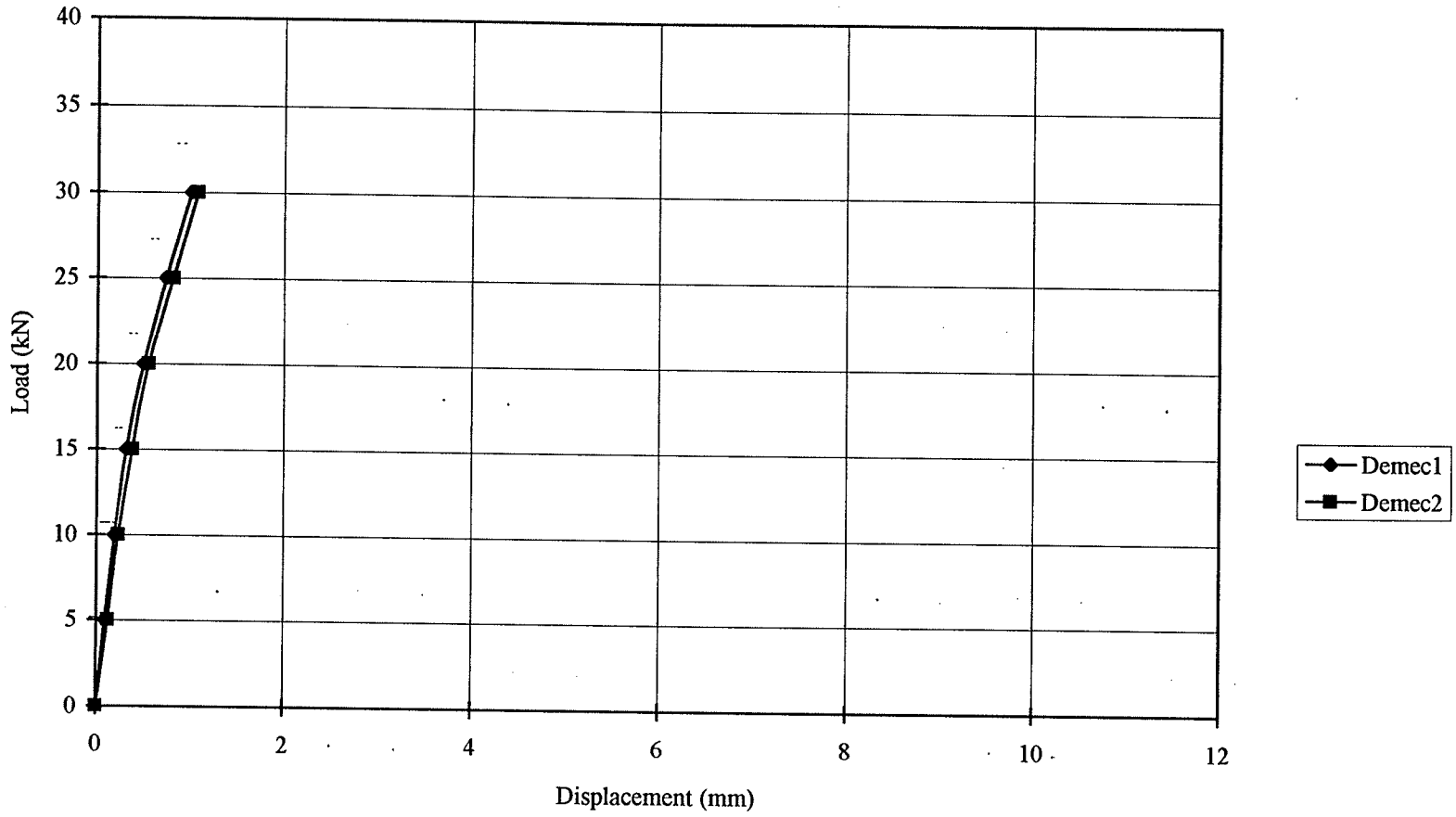

Figure 4.13: Load Versus Displacement from Demec Readings for Specimen IS-P-1

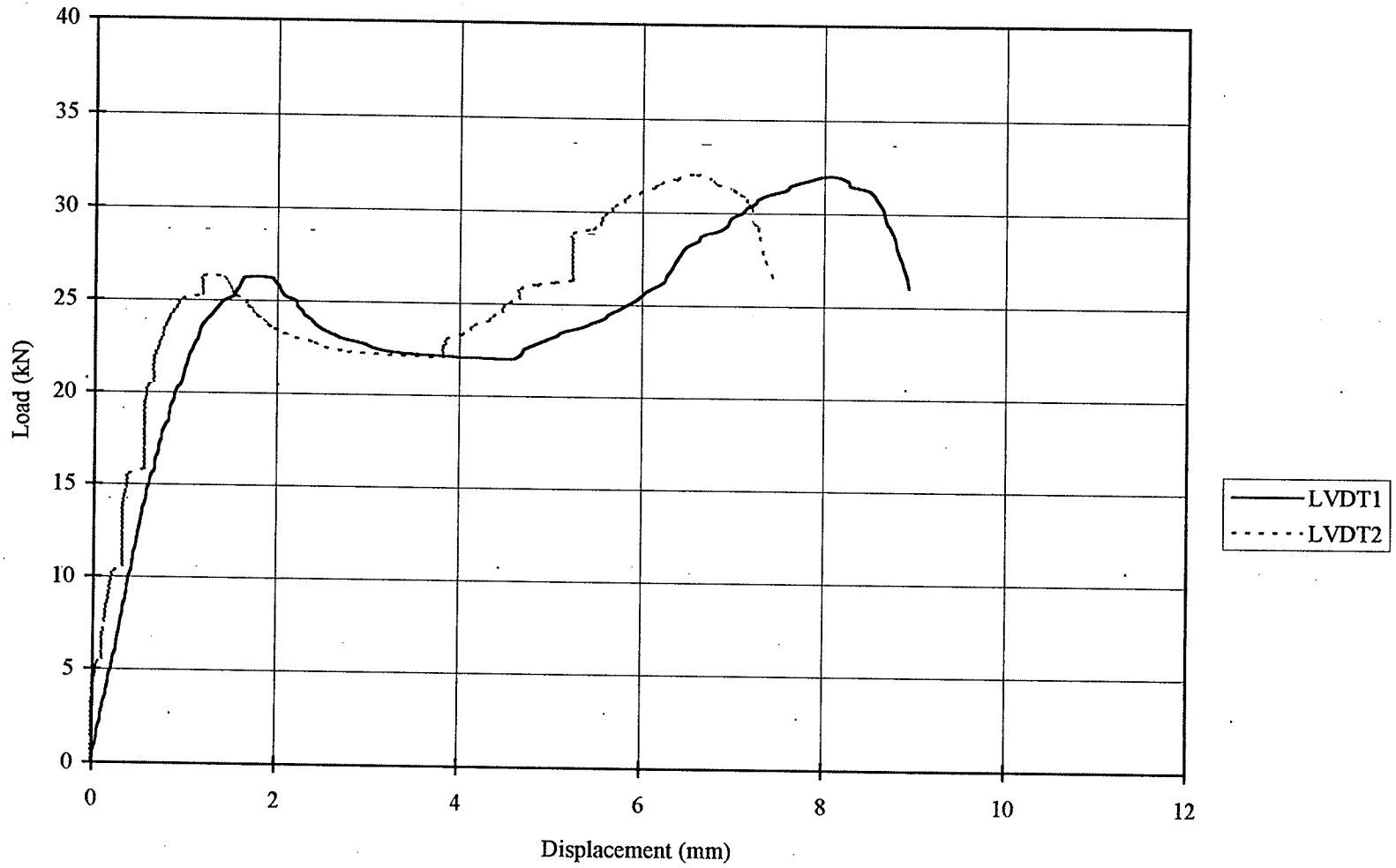

Figure 4.14: Load Versus Displacement from LVDT Readings for Specimen IS-P-2

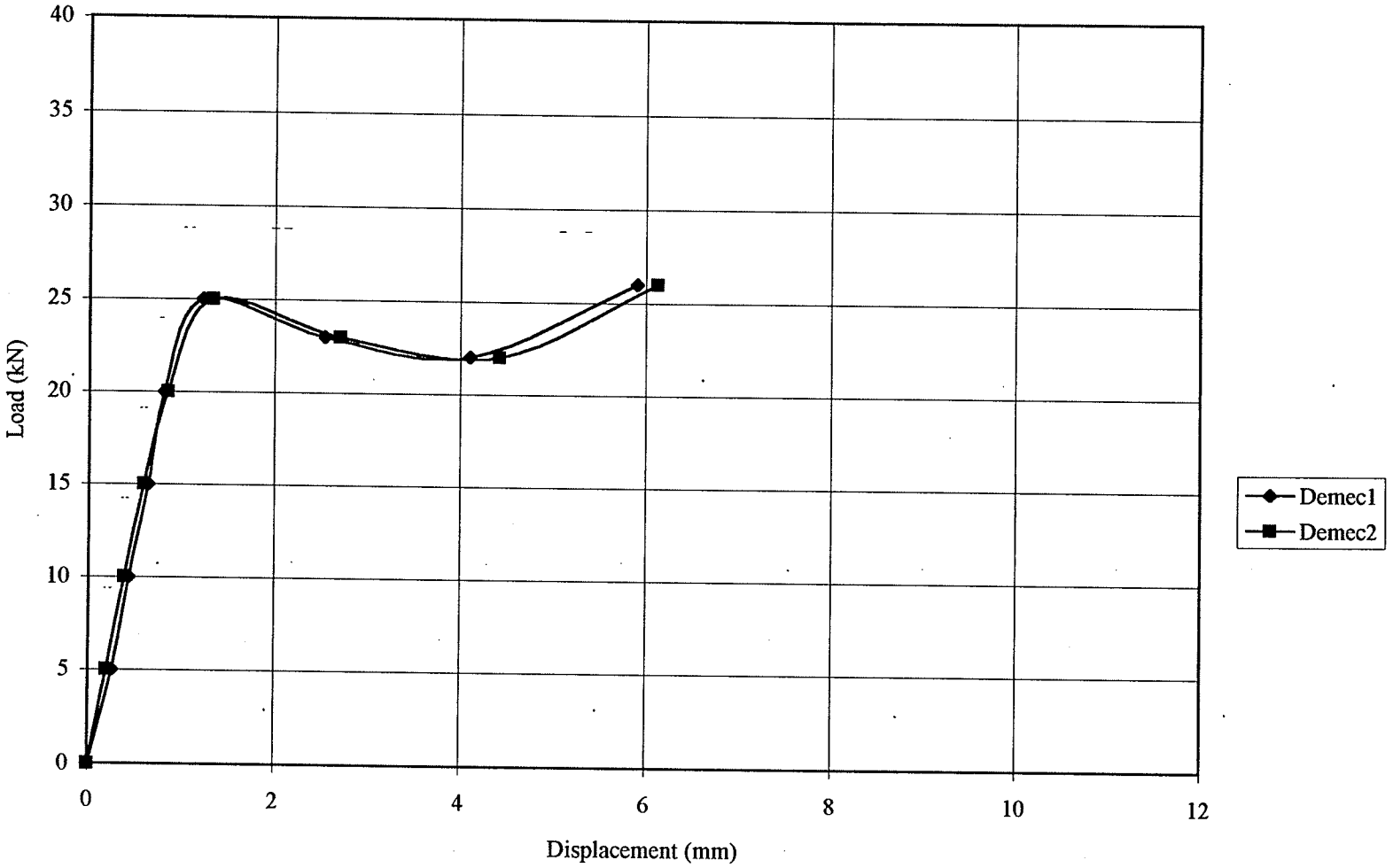

Figure 4.15: Load versus Displacement from Demec Readings for Specimen IS-P-2

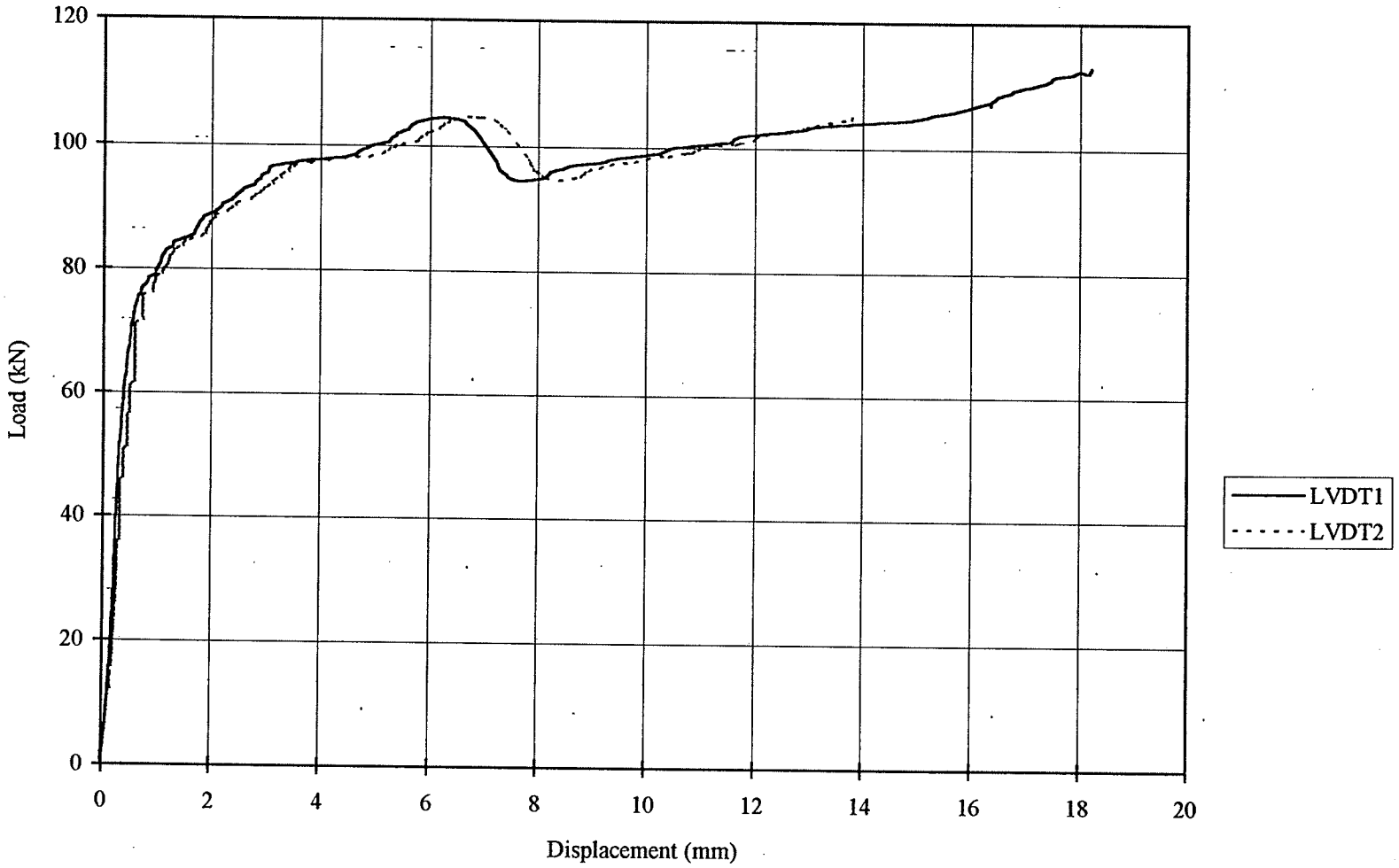

FIgure 4.16: Load Versus Displacement from LVDT Readings for Specimen ST-P-1

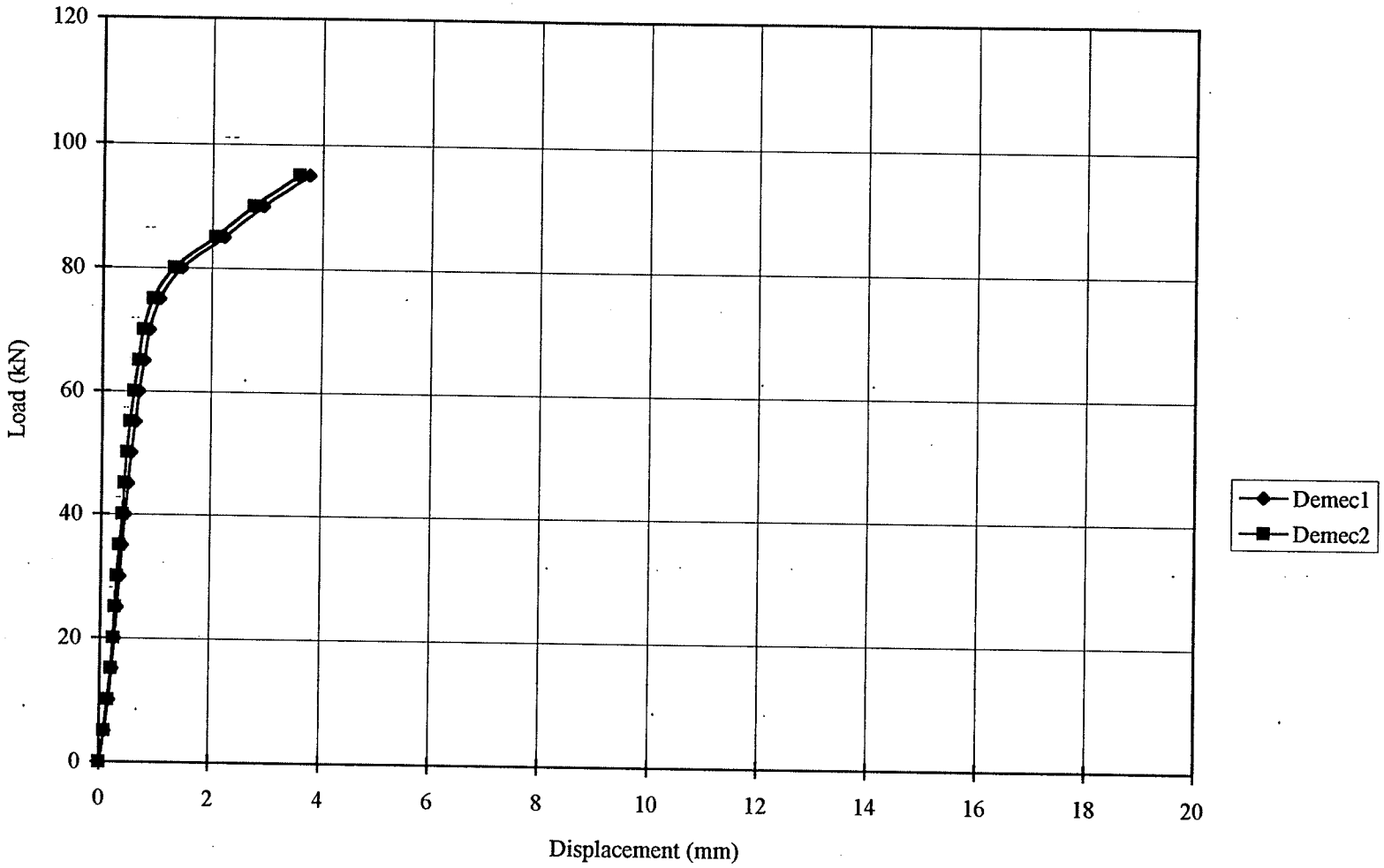

Figure 4.17: Load Versus Displacement from Demec Readings for Specimen ST-P-1

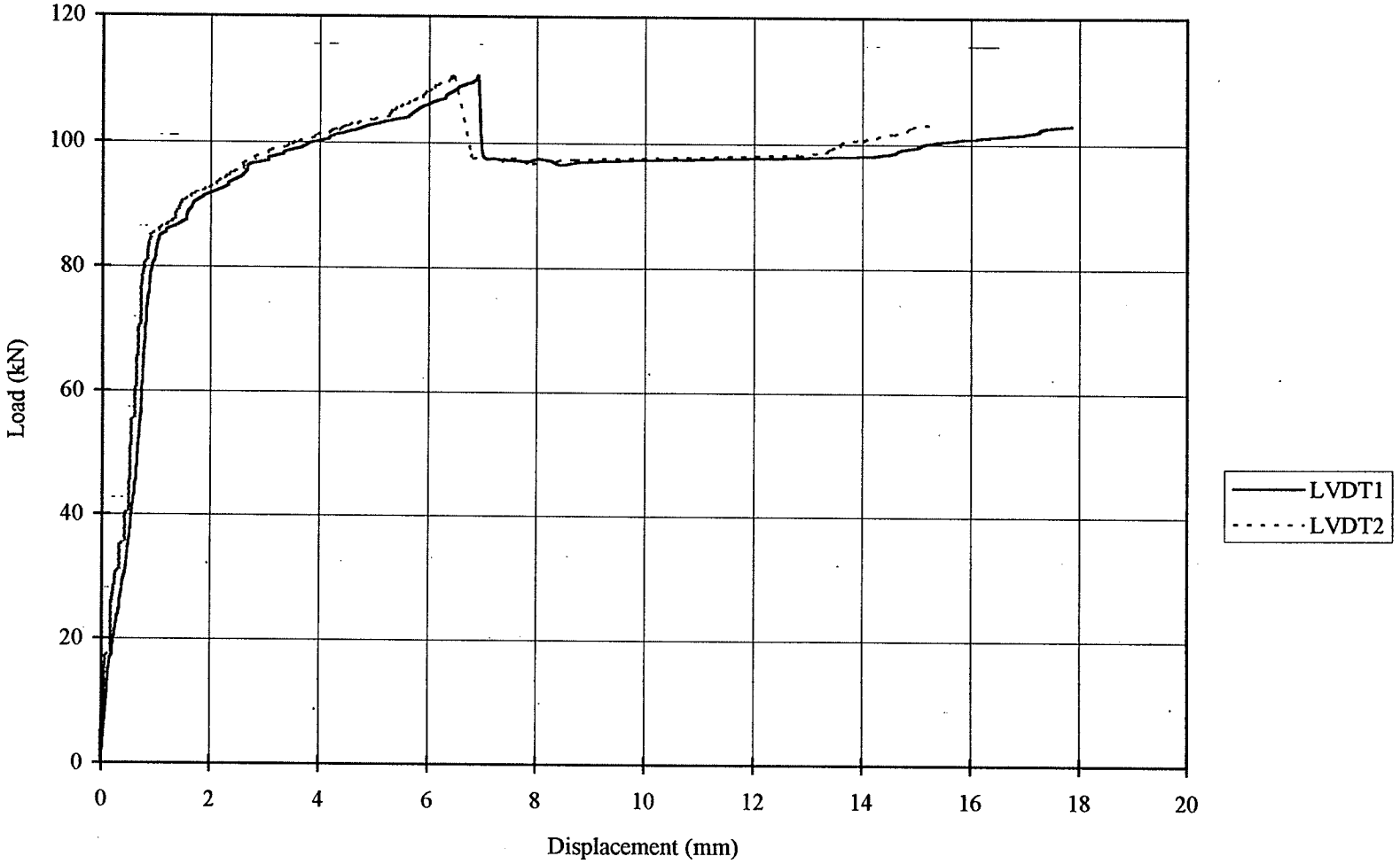

Figure 4.18: Load Versus Displacement from LVDT Readings for Specimen ST-P-2

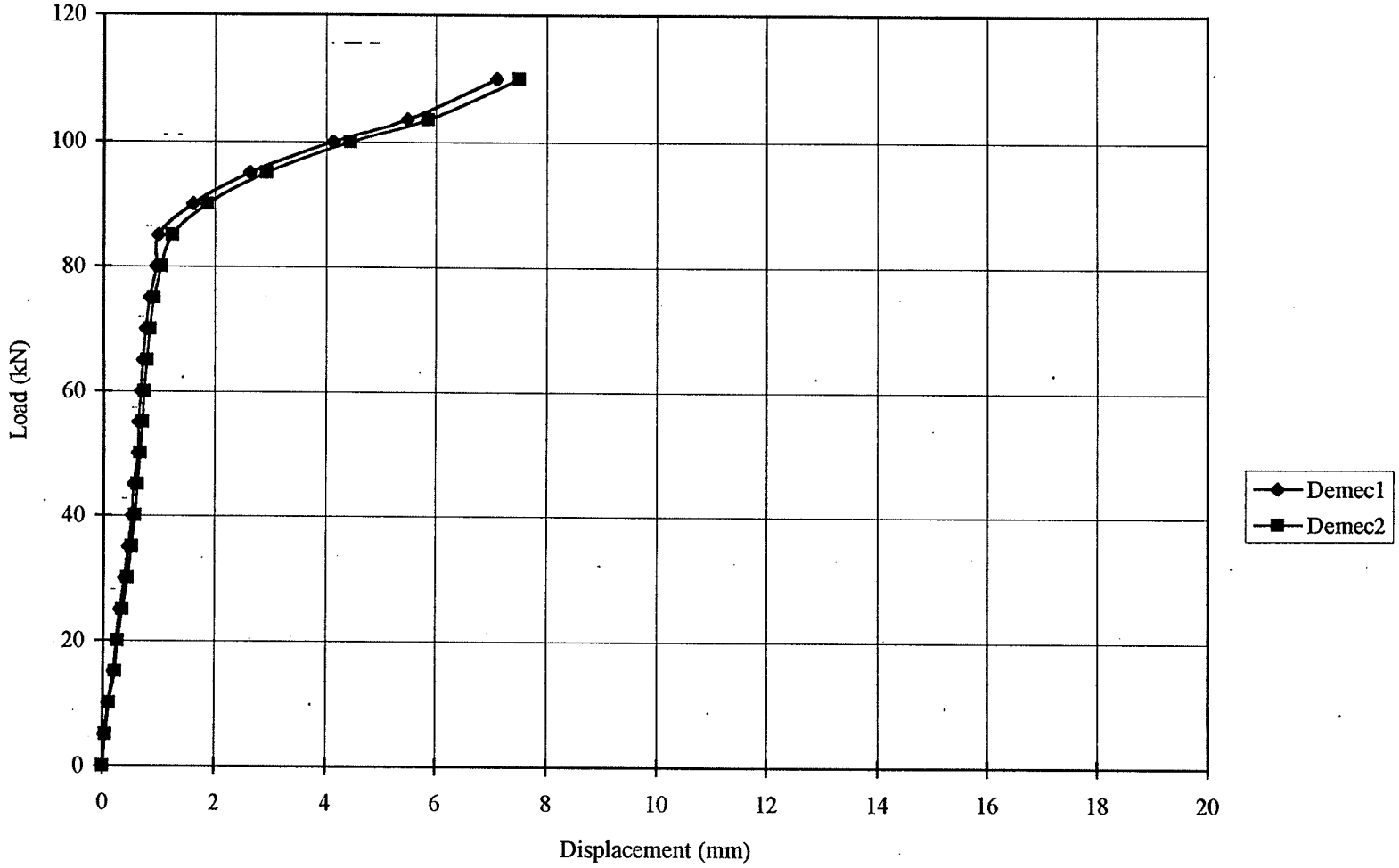

Figure 4.19: Load Versus Displacement from Demec Readings for Specimen ST-P-2

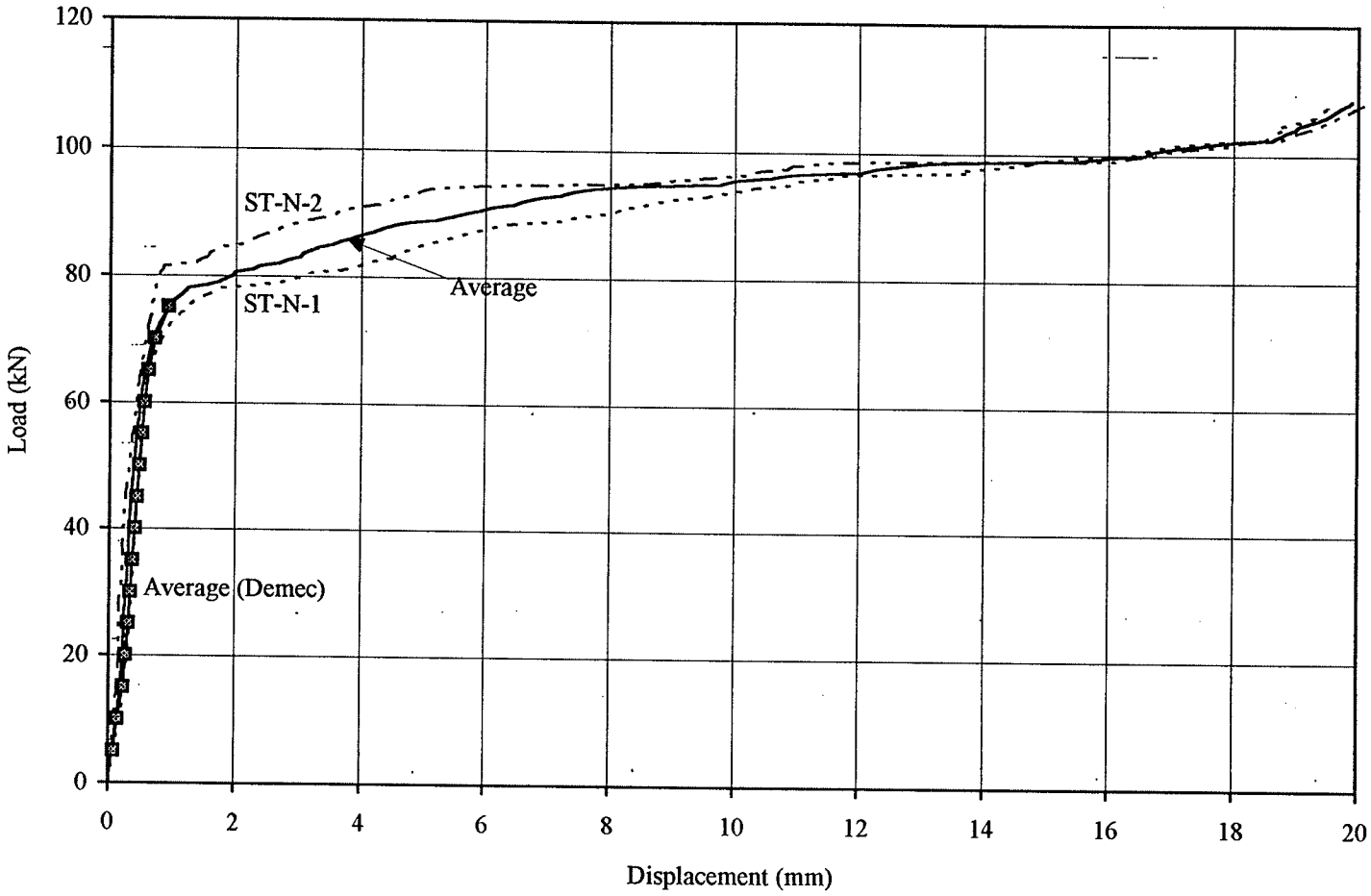

Figure 5.1: Load-Displacement Comparison of Unbonded Steel Specimens

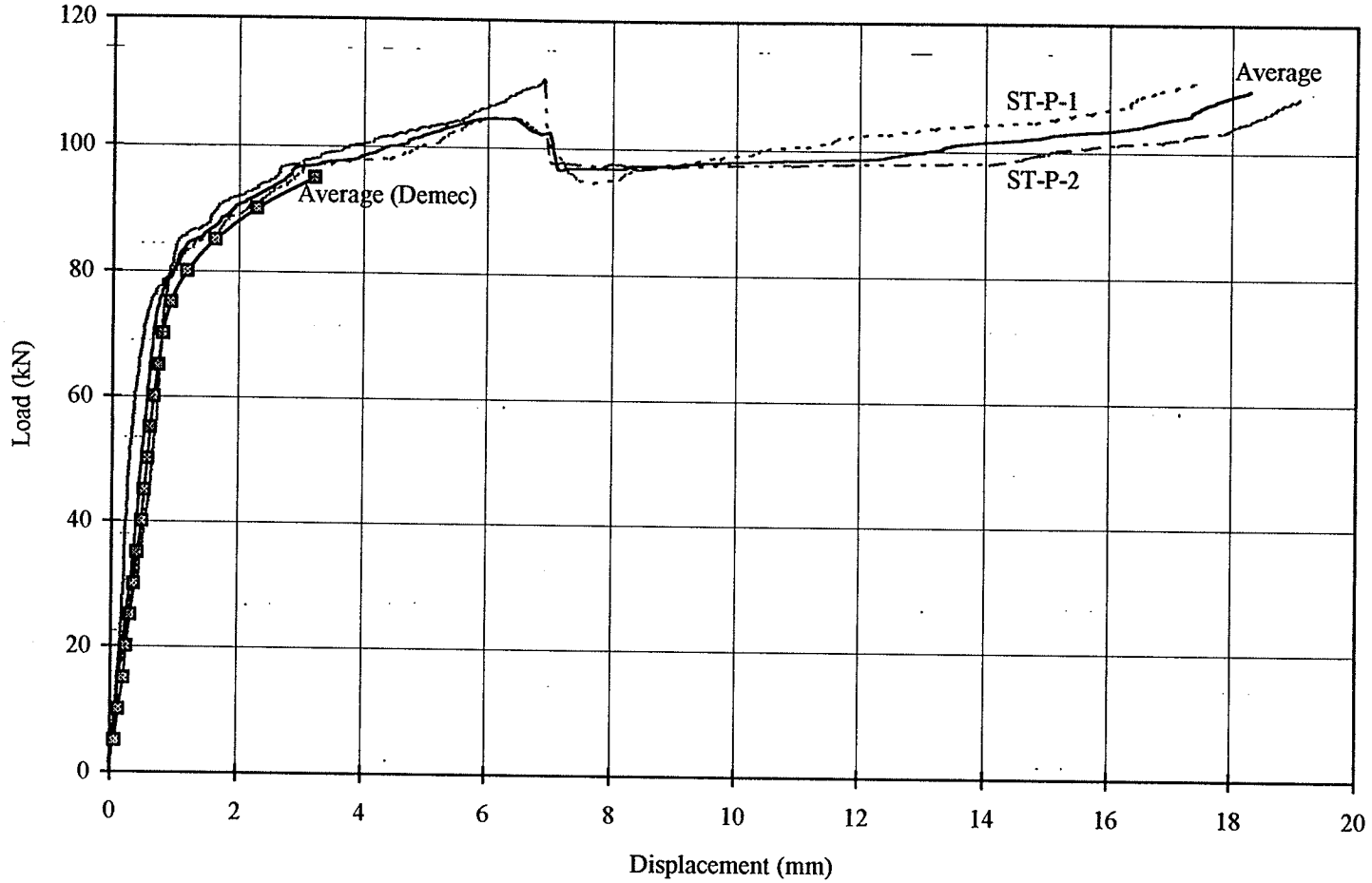

Figure 5.2: Load-Displacement Comparison of Partially Bonded Steel Specimens

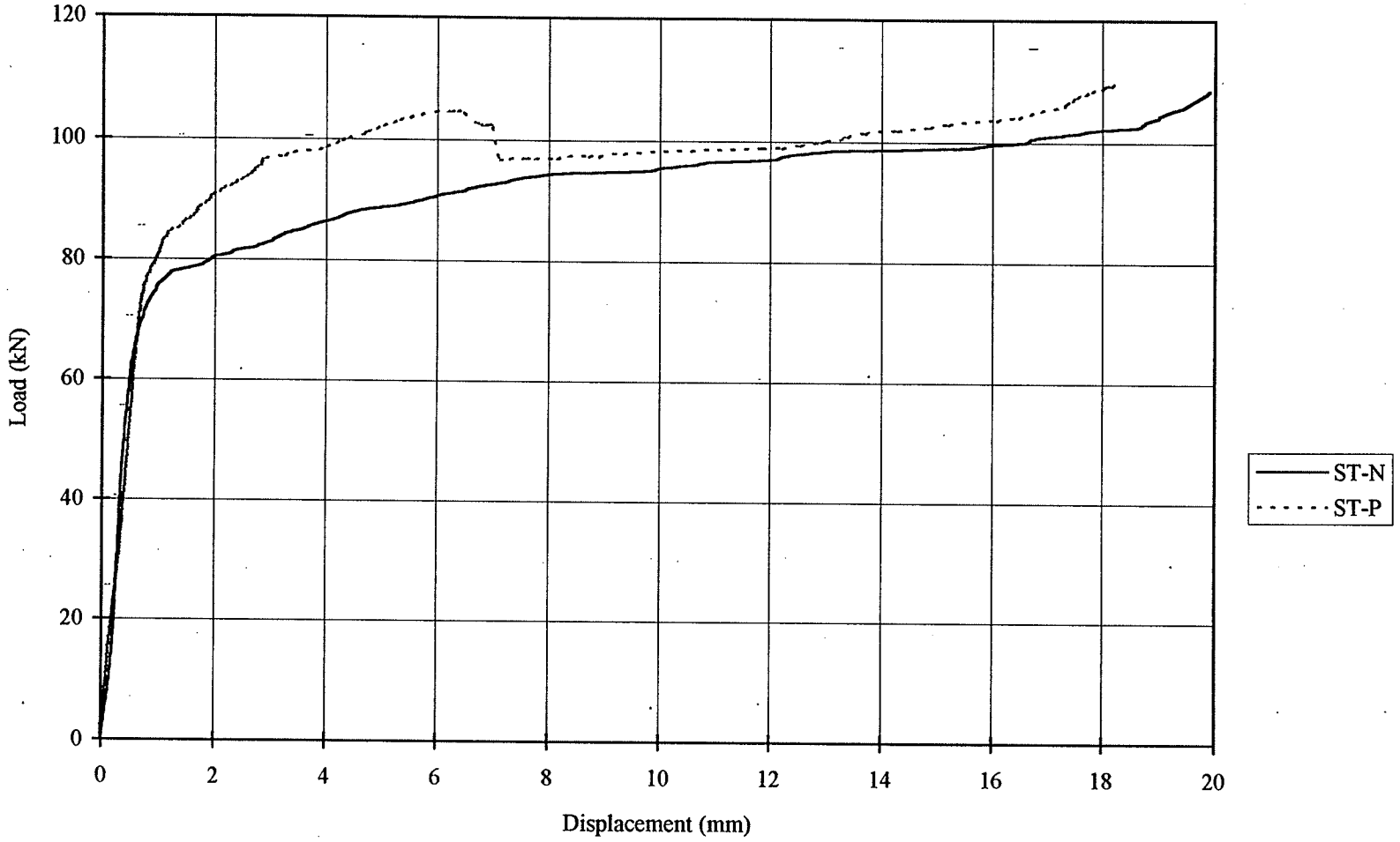

Figure 5.3: Comparison of Average ST-N and ST-P Behaviour

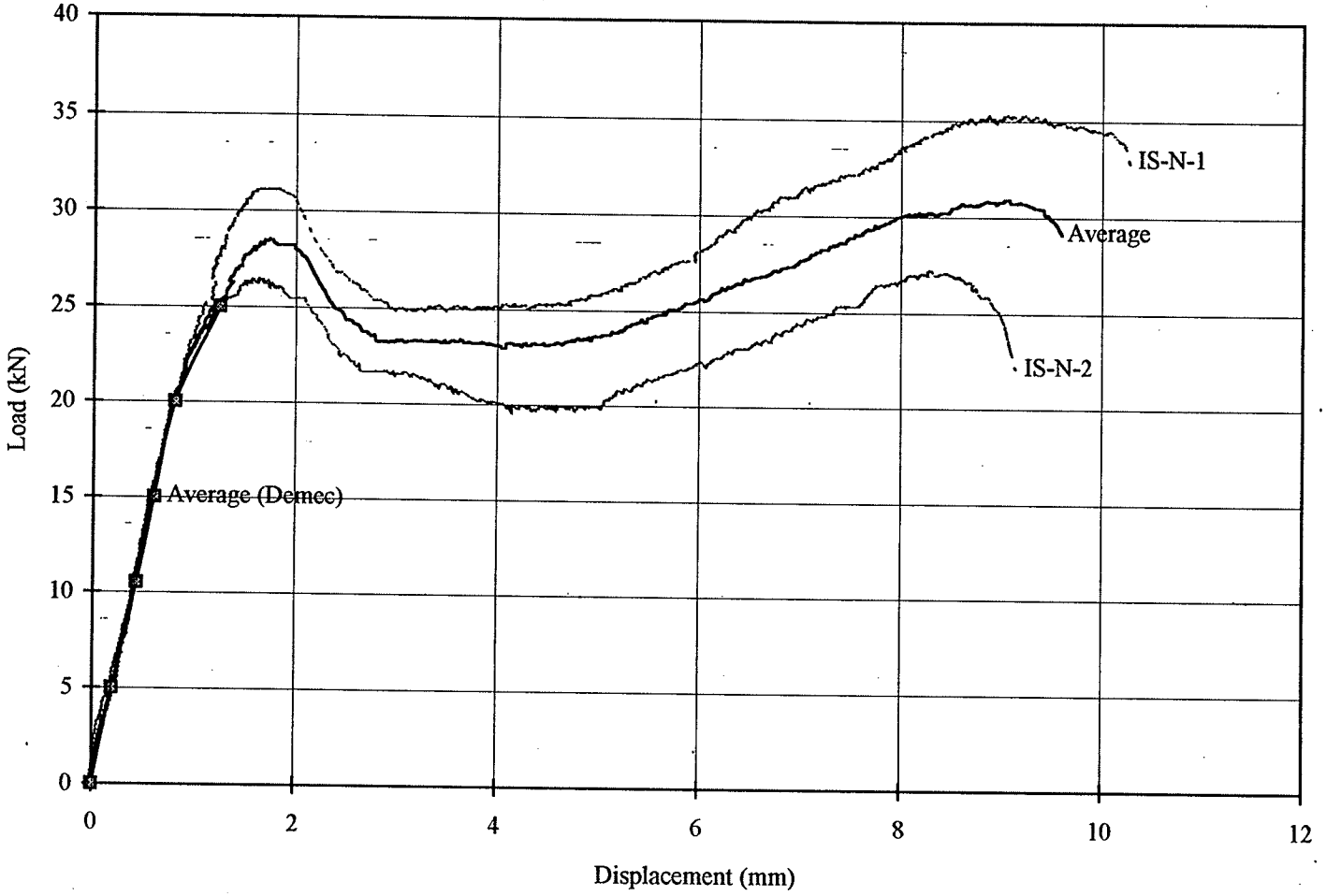

Figure 5.4: Load-Displacement Comparison of Unbonded Isorod Specimens

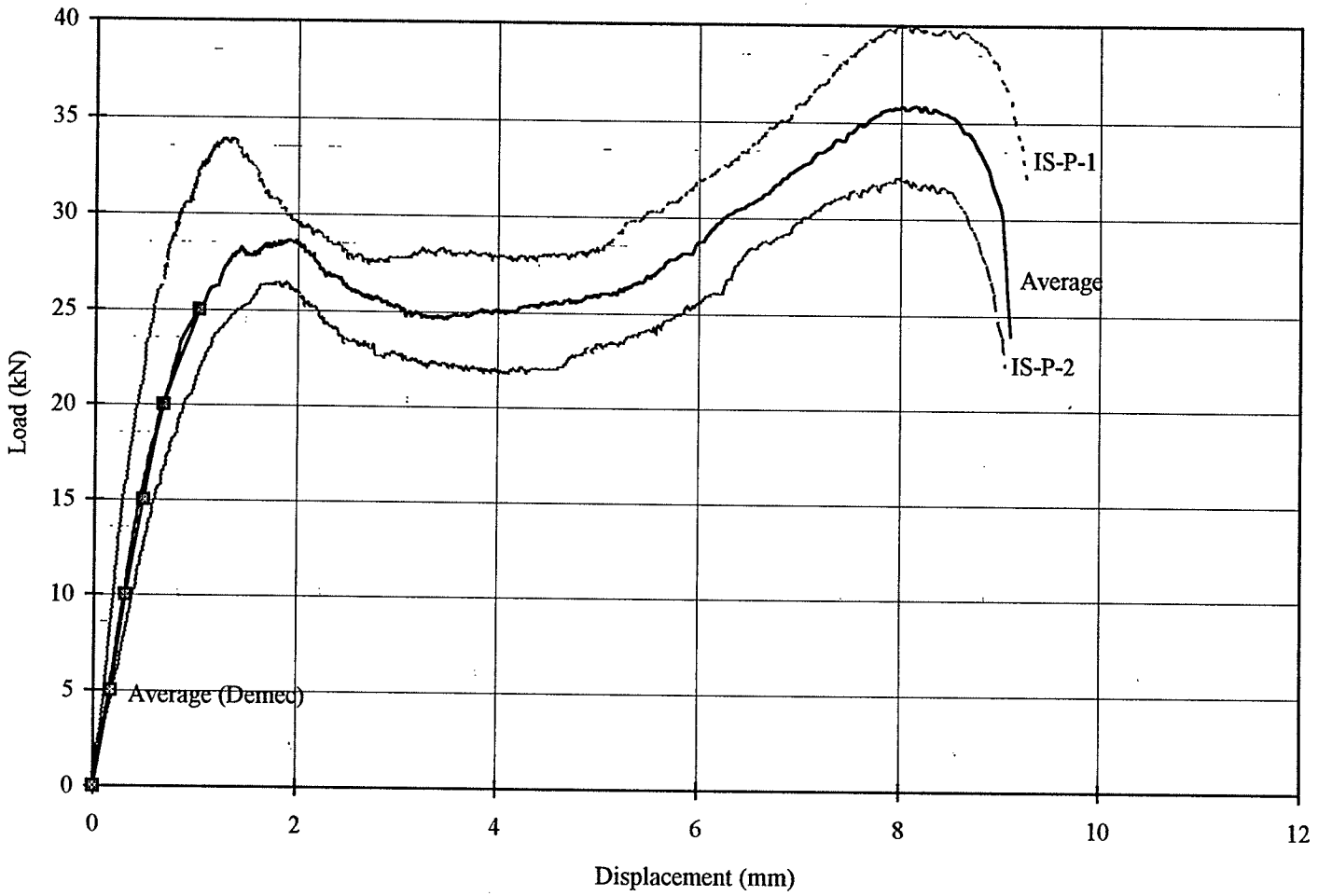

Figure 5.5: Load-Displacement Comparison of Partially Bonded Isorod Specimens

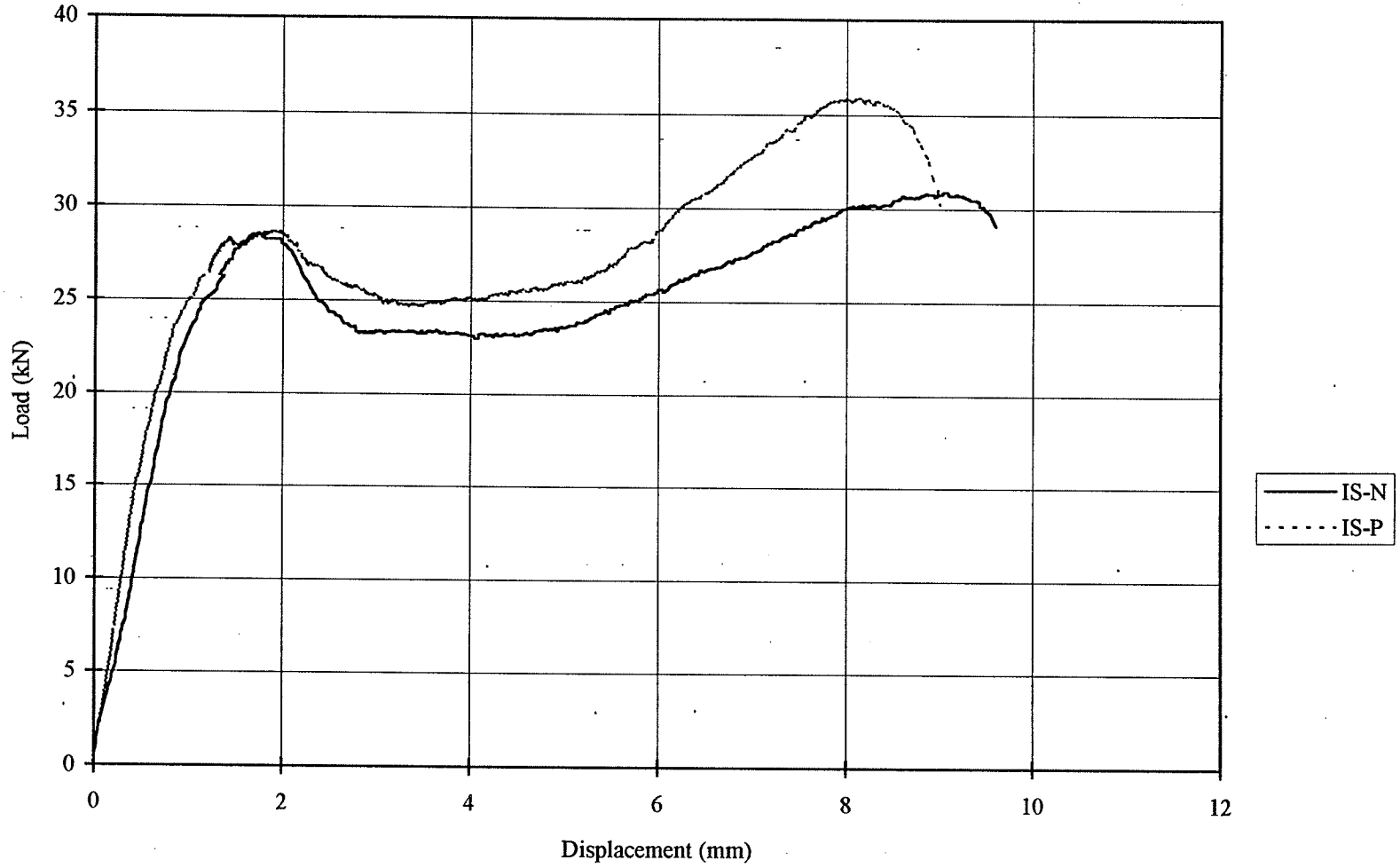

Figure 5.6: Comparison of Average IS-N and IS-P Behaviour

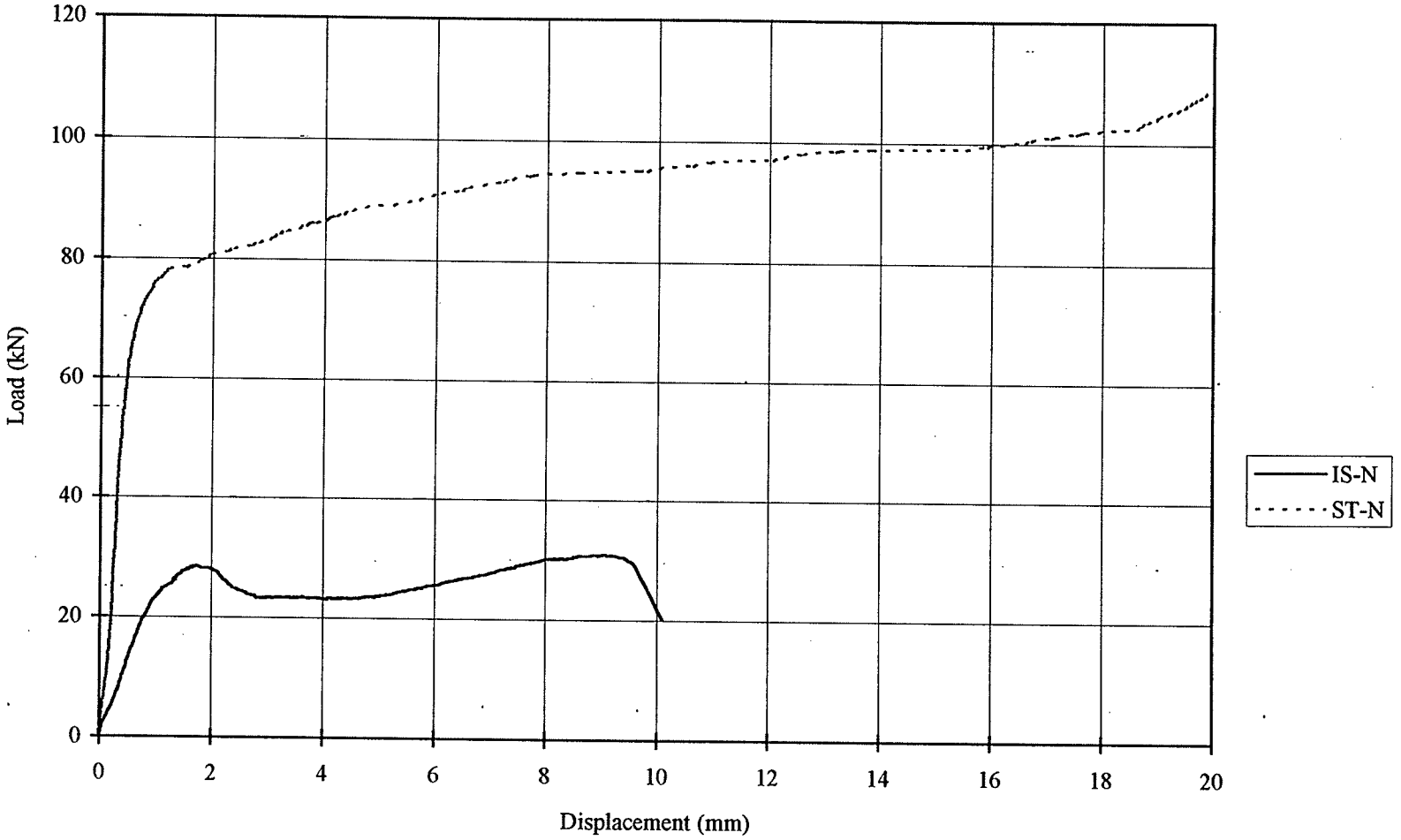

Figure 5.7: Comparison of Average ST-N and IS-N Behaviour

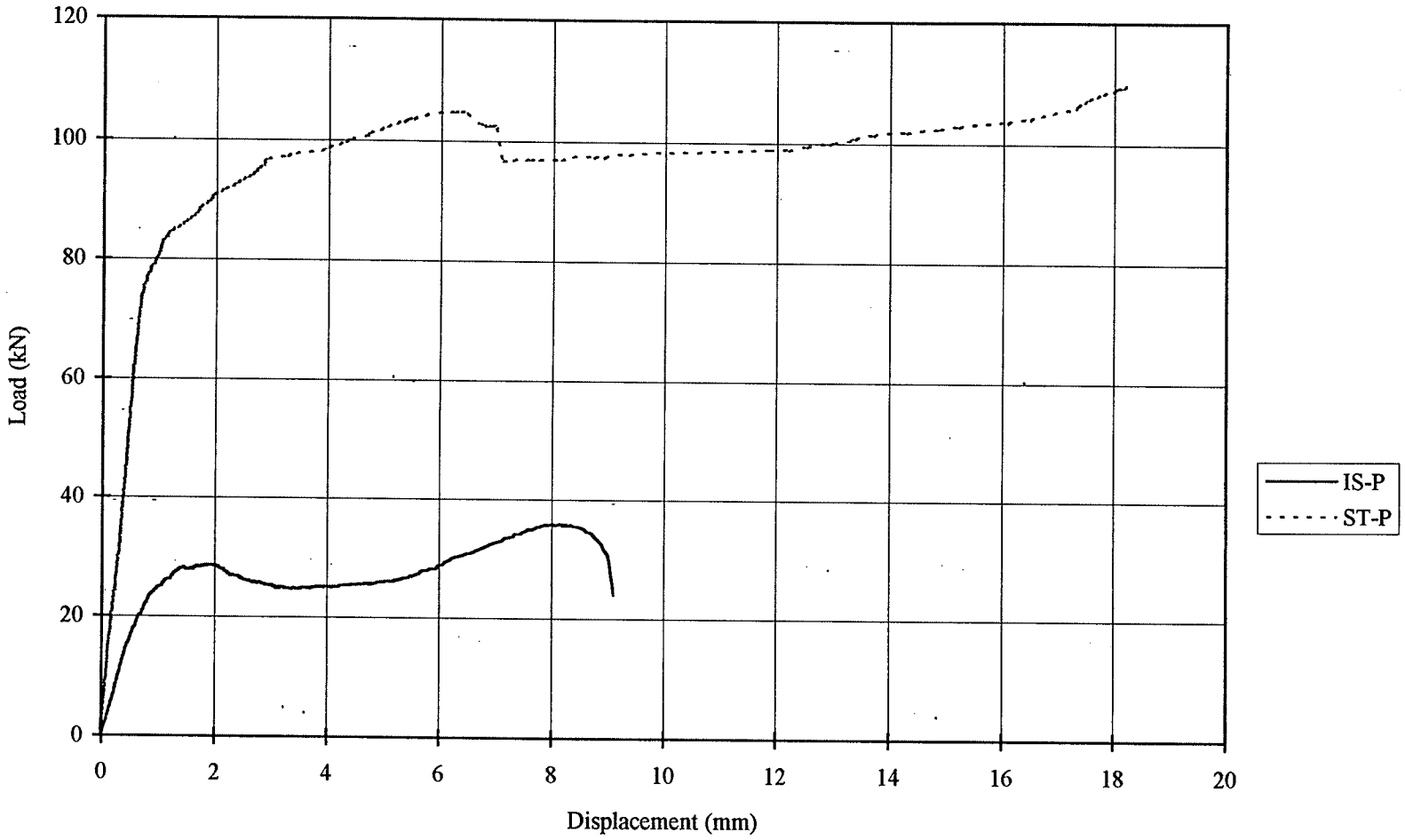

Figure 5.8: Comparison of Average ST-P and IS-P Behaviour

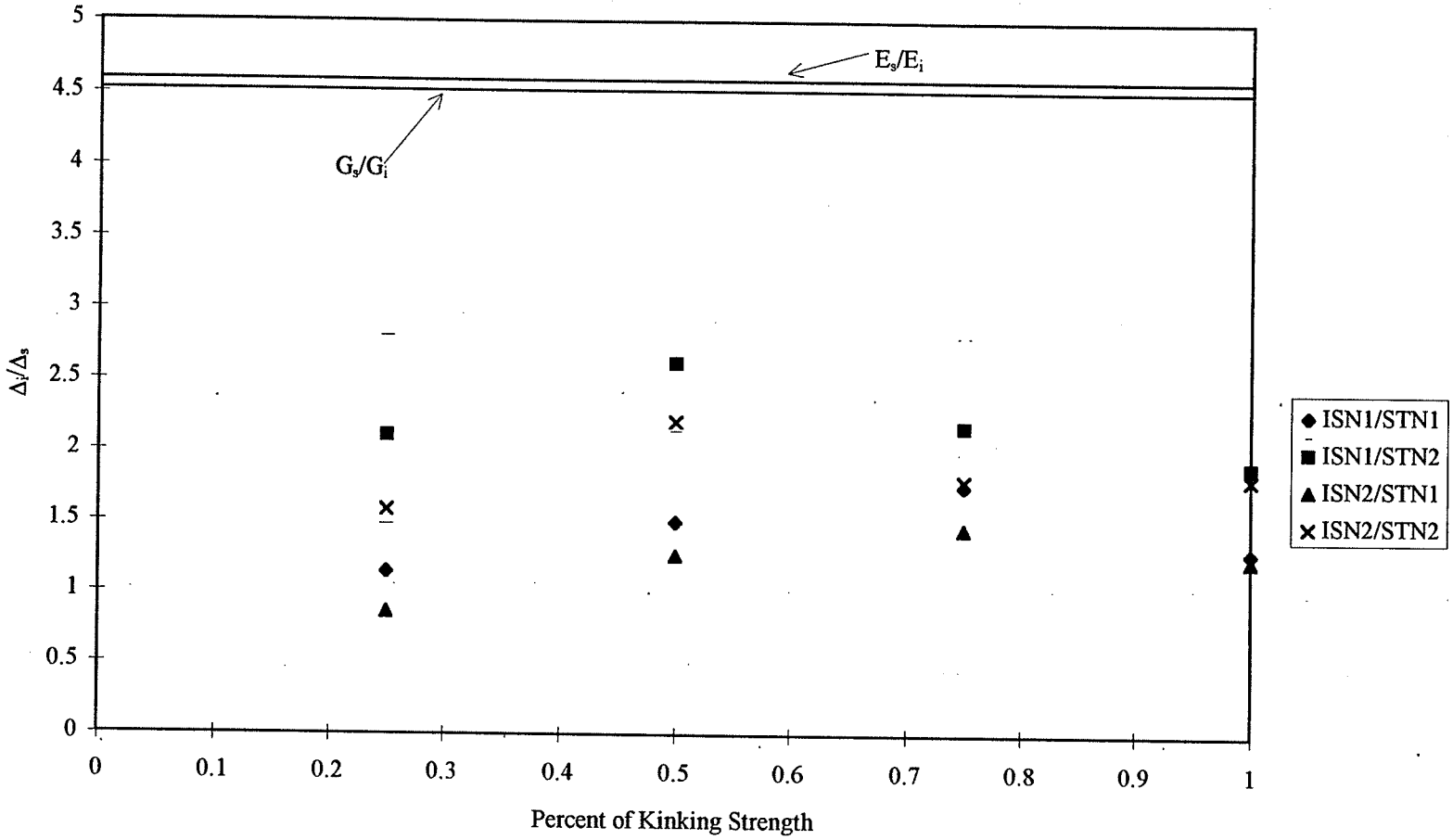

Figure 6.1: Ratio of Δ_i/Δ_s for Unbonded Specimens

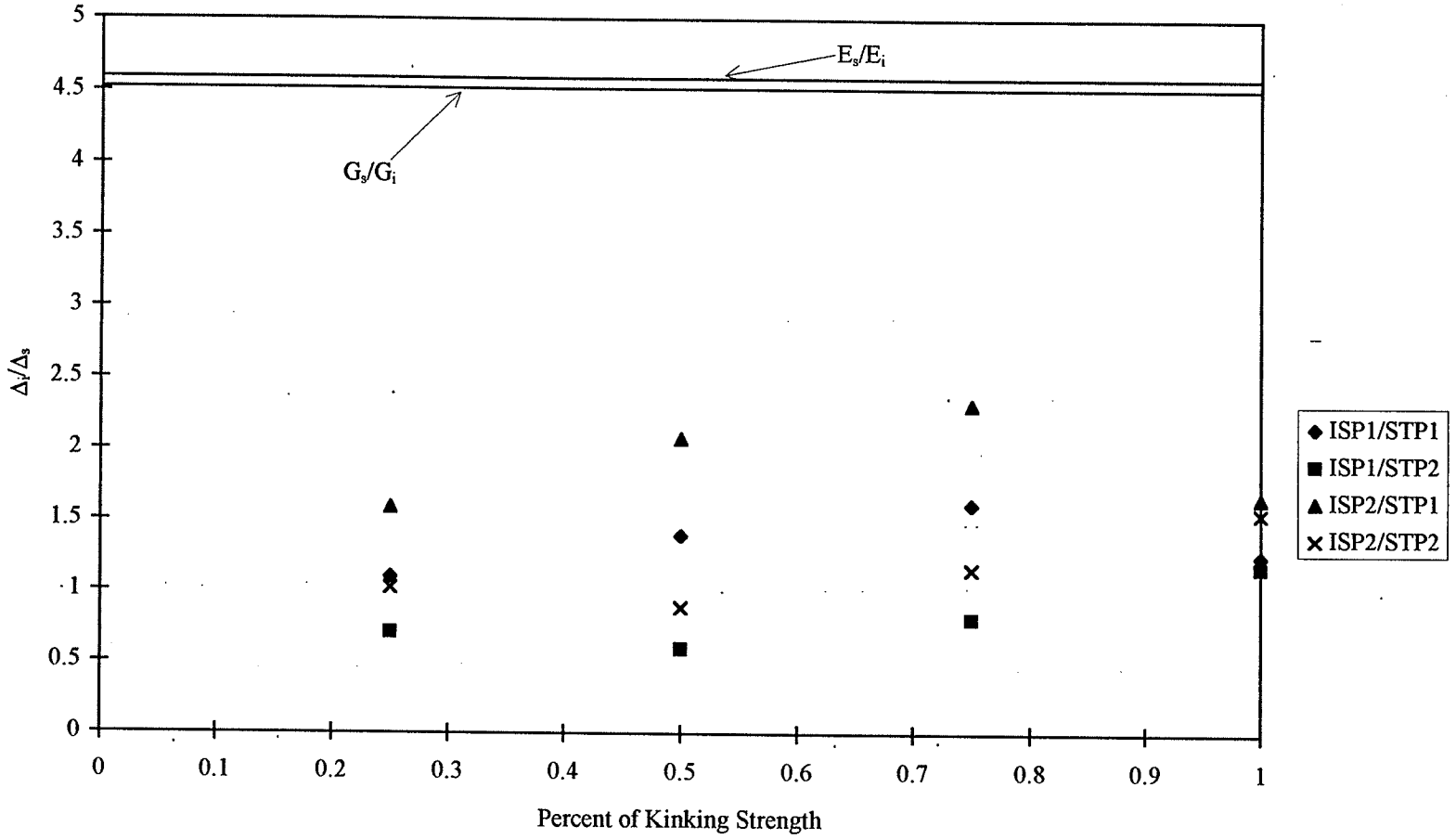

Figure 6.2: Ratio of Δ_i/Δ_s for Partially Bonded Specimens

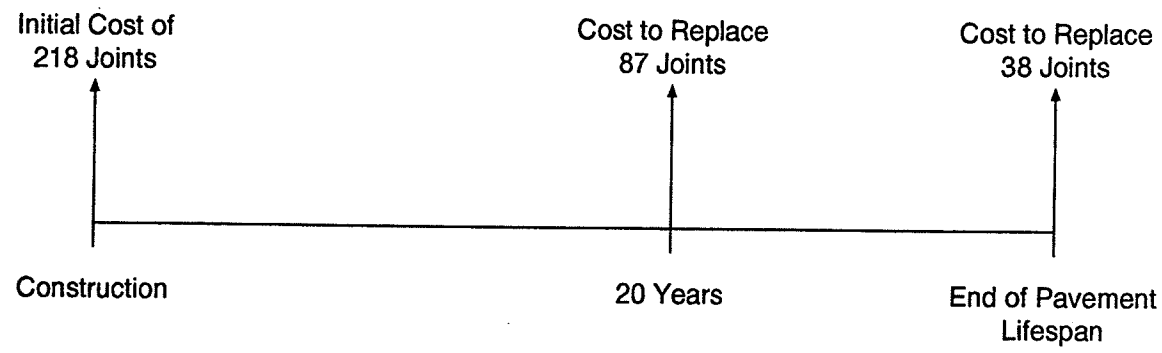

Plain and Epoxy-Coated Steel Dowels

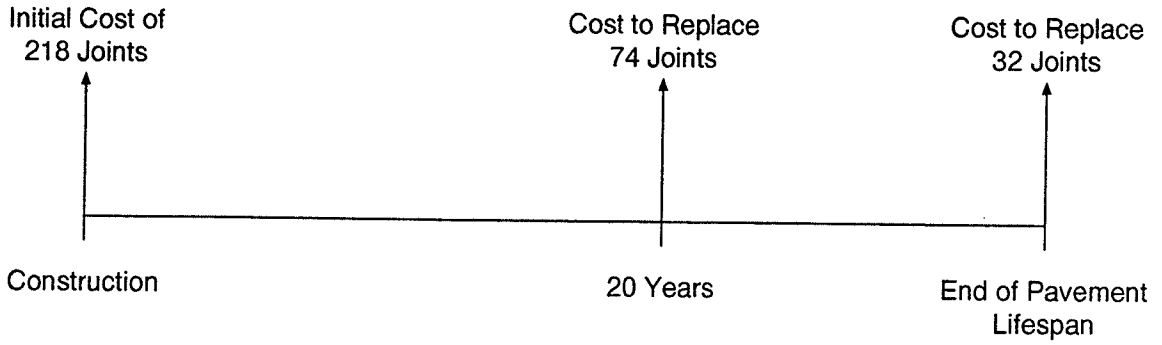

Stainless Steel and GFRP Dowels

Figure 7.1: Timelines of Construction and Repair Costs for the Five Alternative Dowel Materials

APPENDIX A

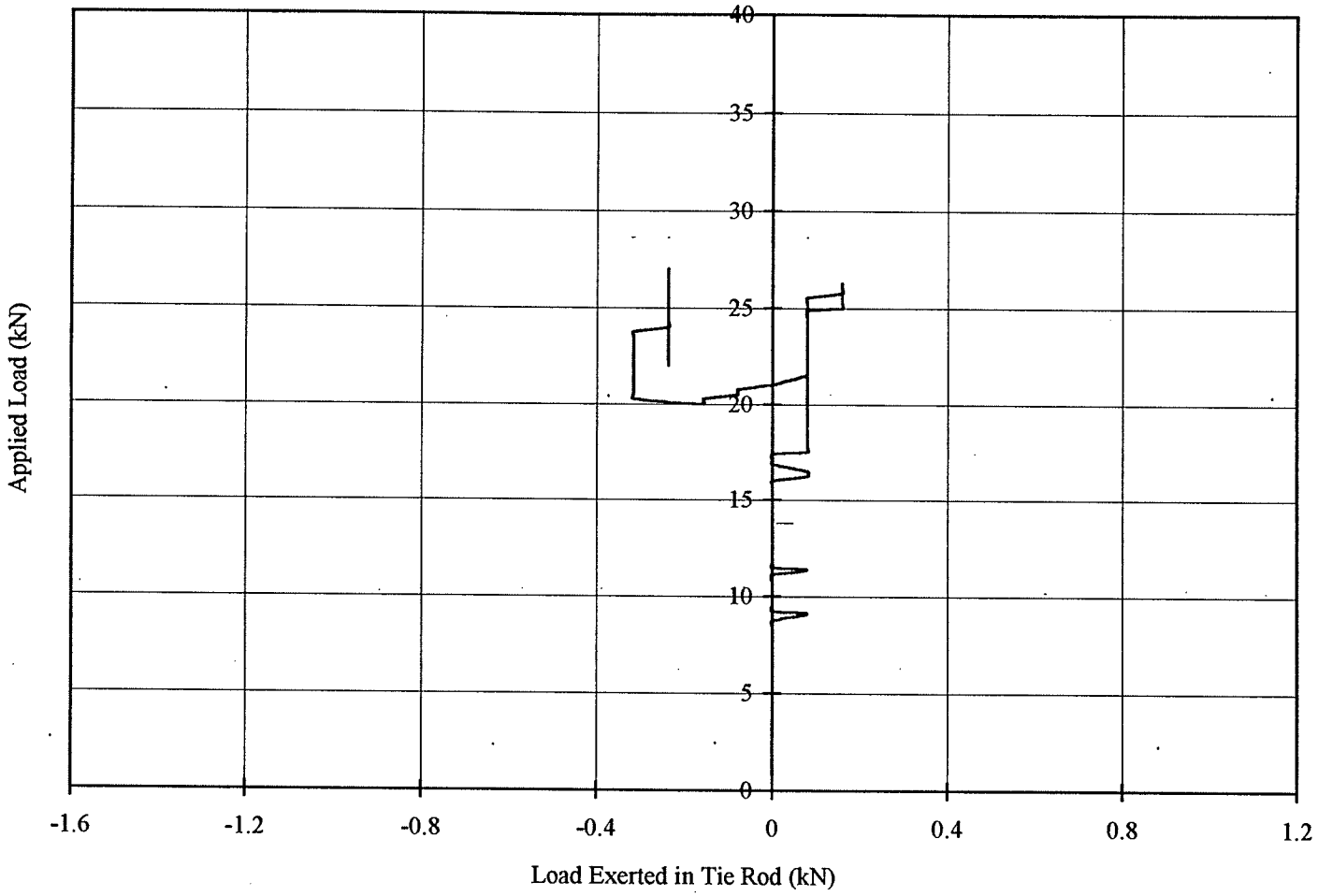

Figure A1: Applied Load Versus Load Exerted in Tie Rod for Specimen IS-N-2

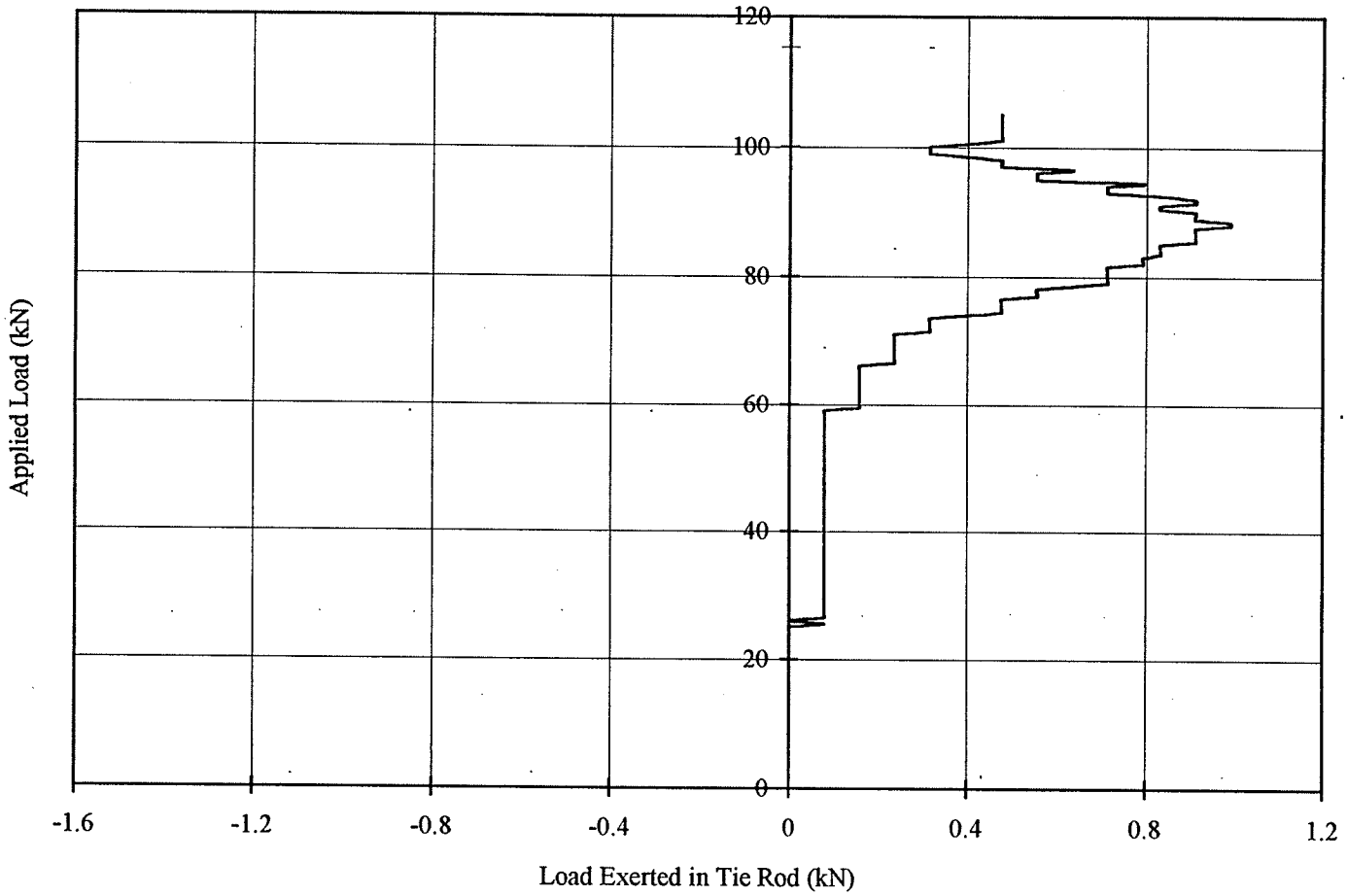

Figure A2: Applied Load Versus Load Exerted in Tie Rod for Specimen ST-N-1

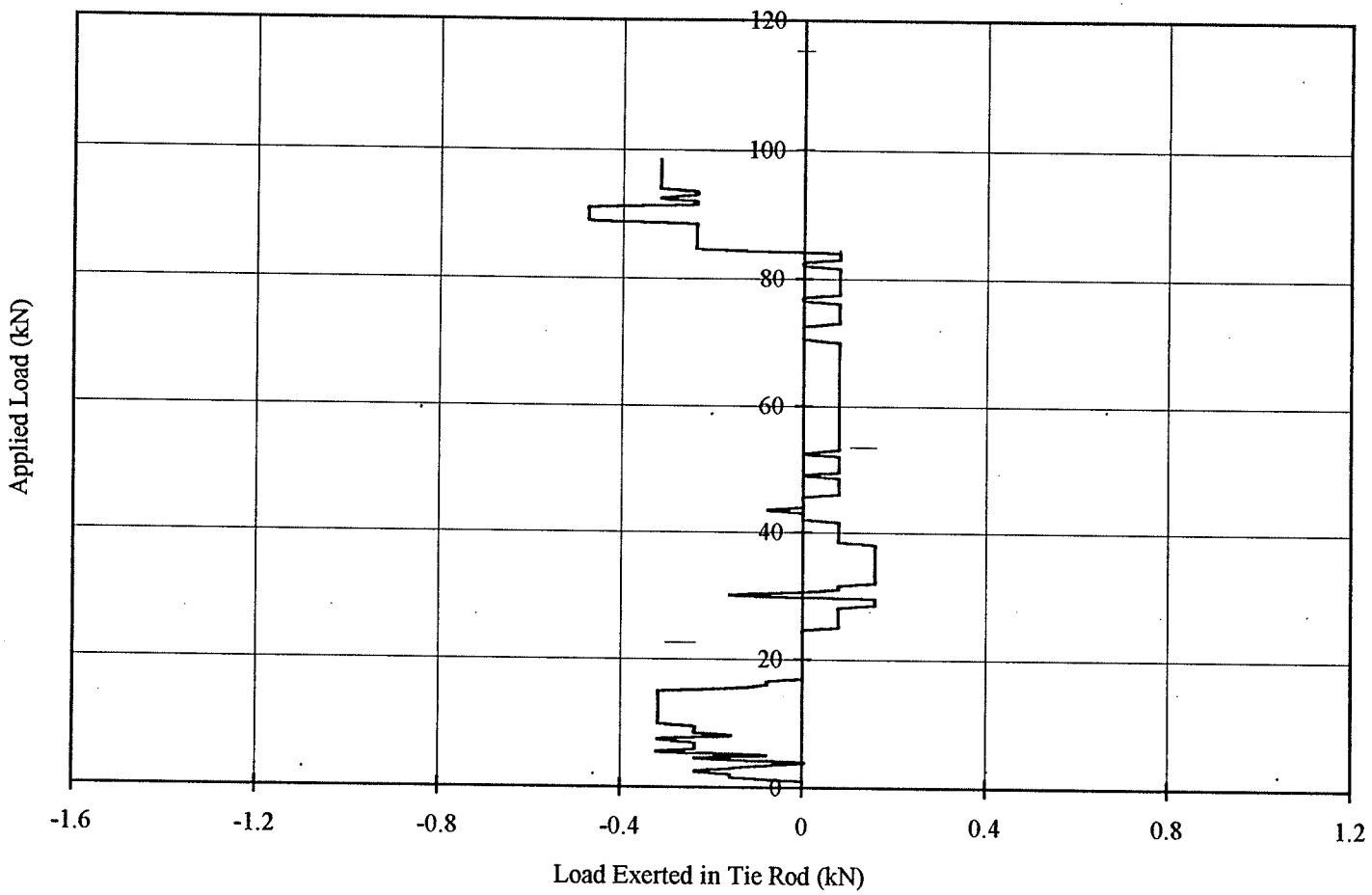

Figure A3: Applied Load Versus Load Exerted in Tie Rod for Specimen ST-N-2

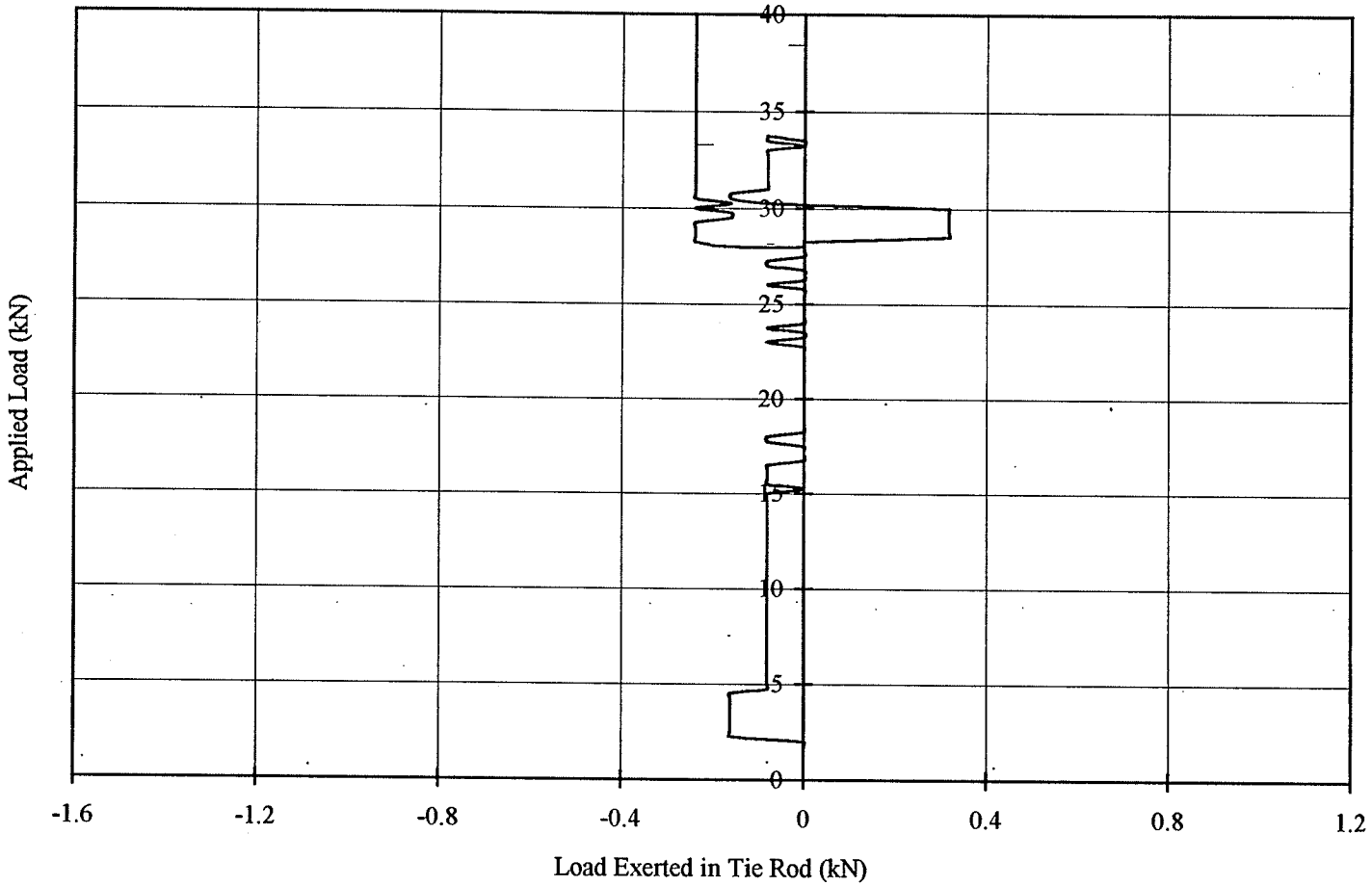

Figure A4: Applied Load Versus Load Exerted in Tie Rod for Specimen IS-P-1

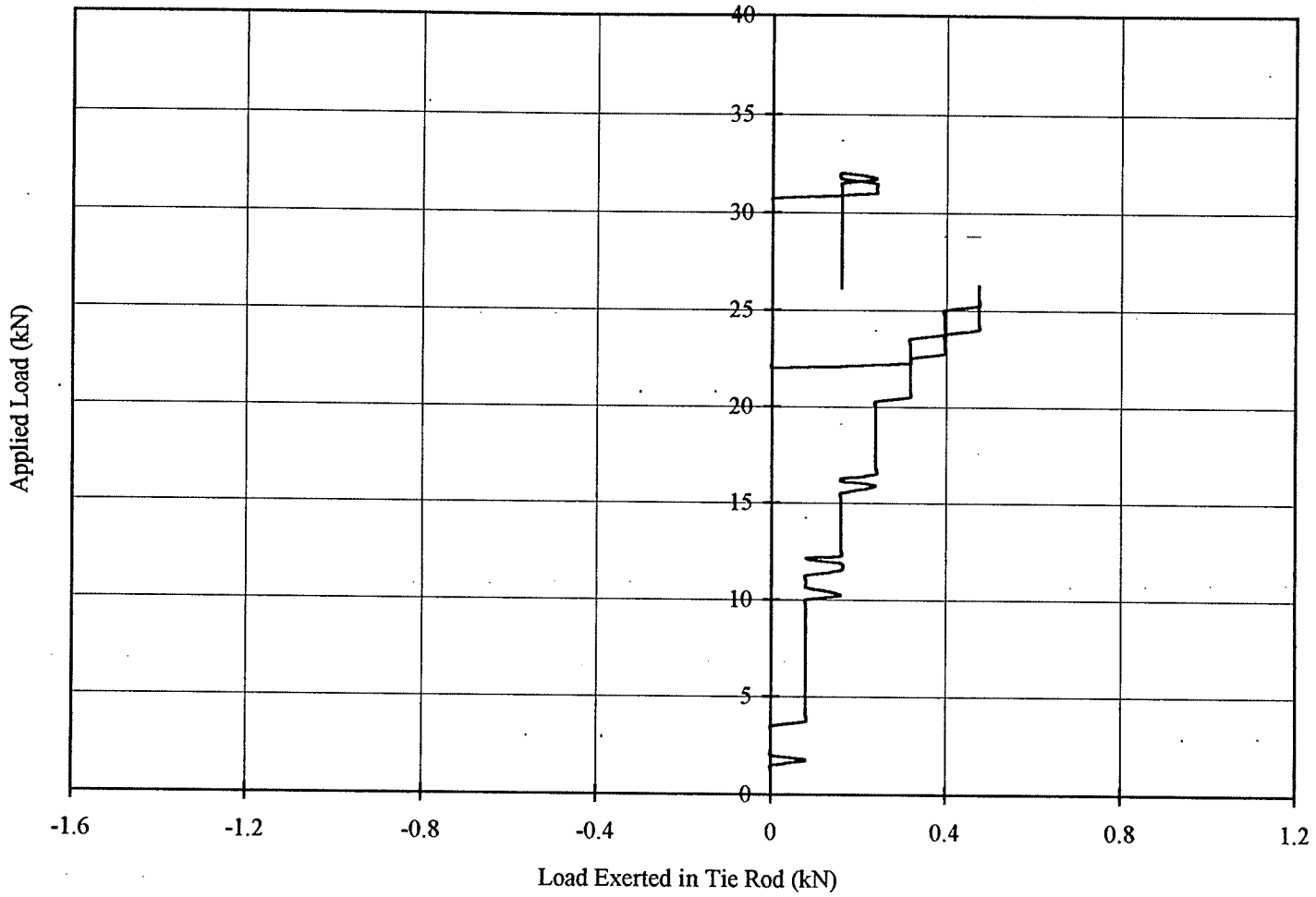

Figure A5: Applied Load Versus Load Exerted in Tie Rod for Specimen IS-P-2

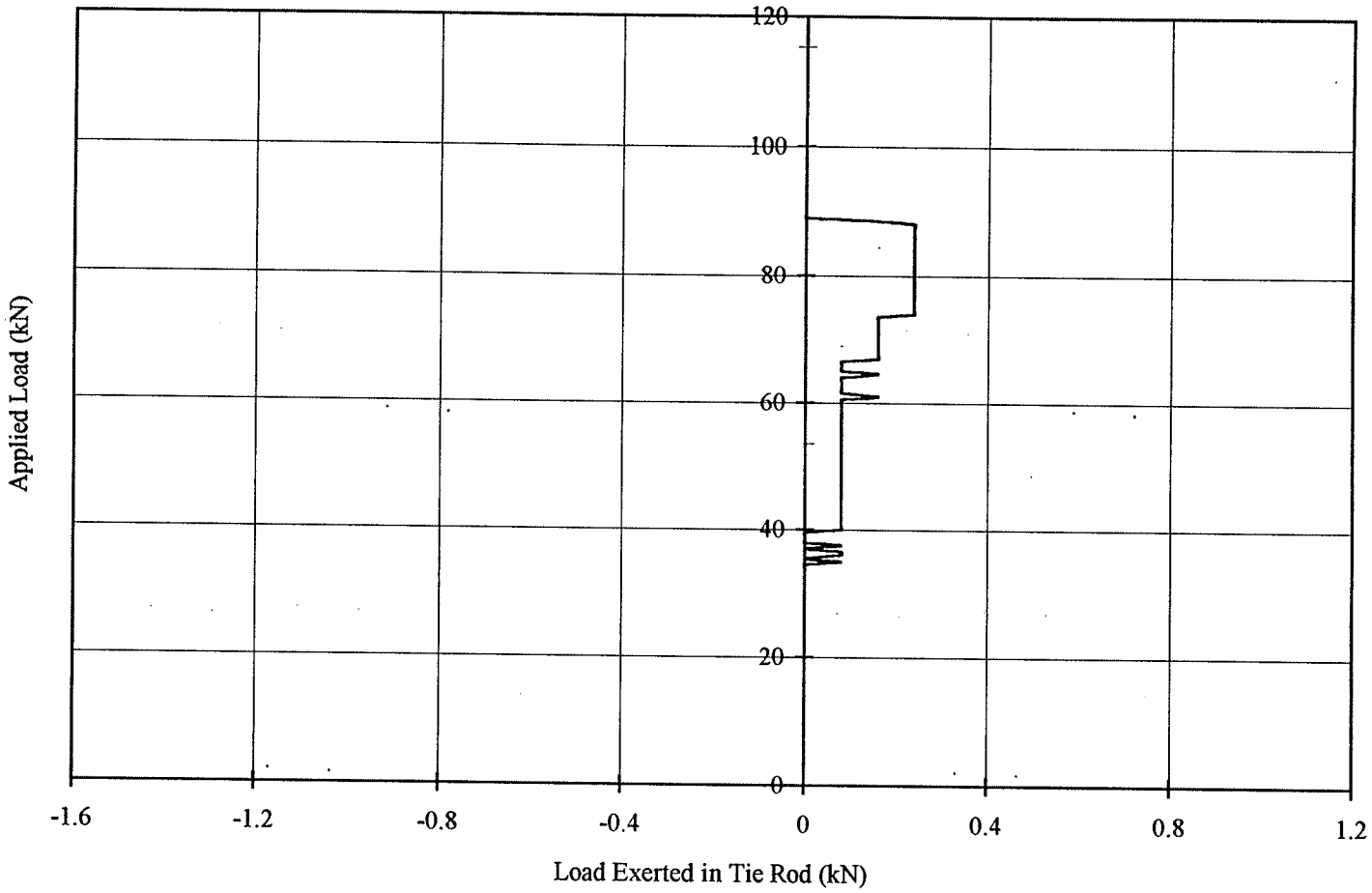

Figure A6: Applied Load Versus Load Exerted in Tie Rod for Specimen ST-P-1

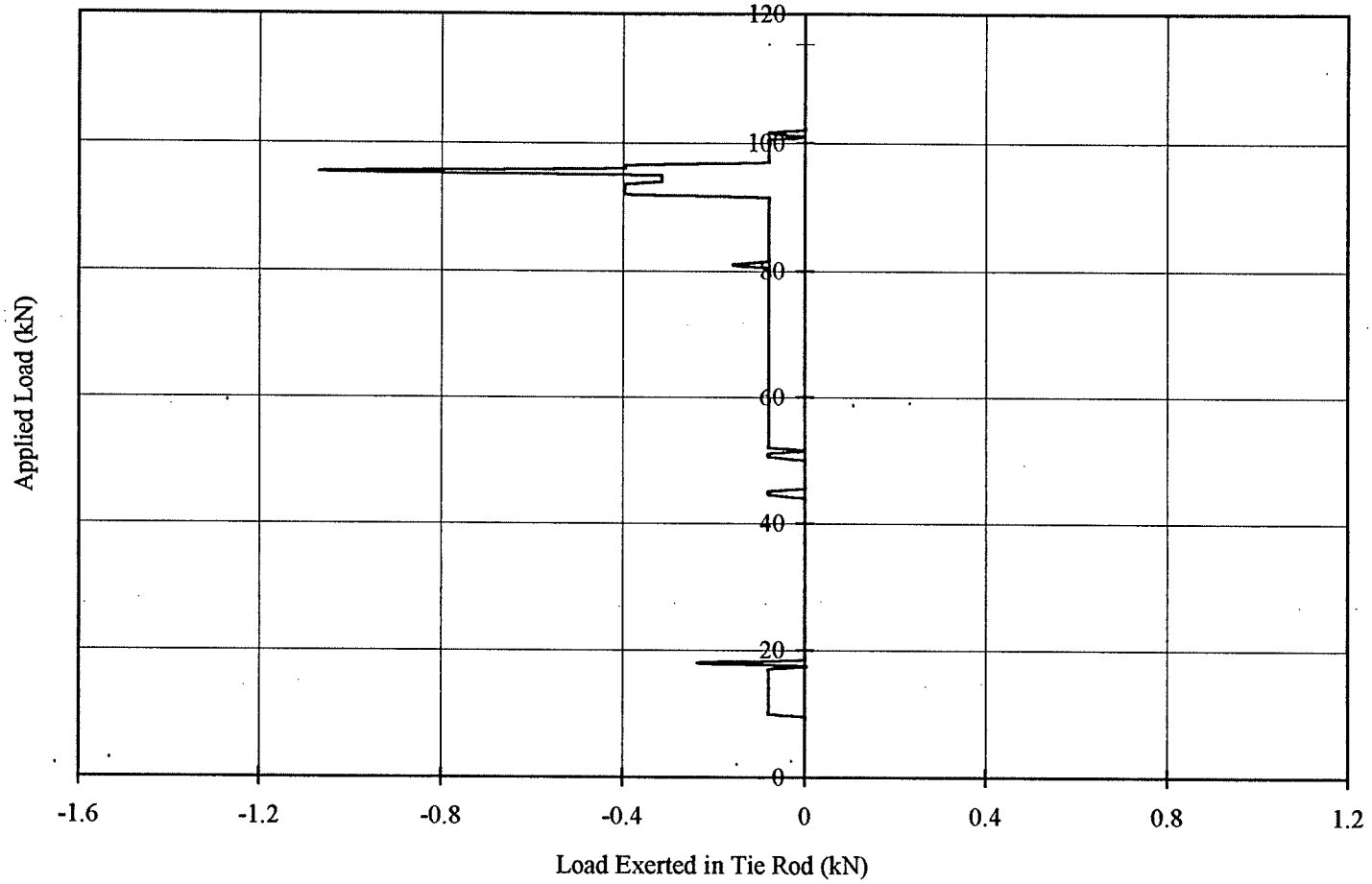

Figure A7: Applied Load Versus Load Exerted in Tie Rod for Specimen ST-P-2

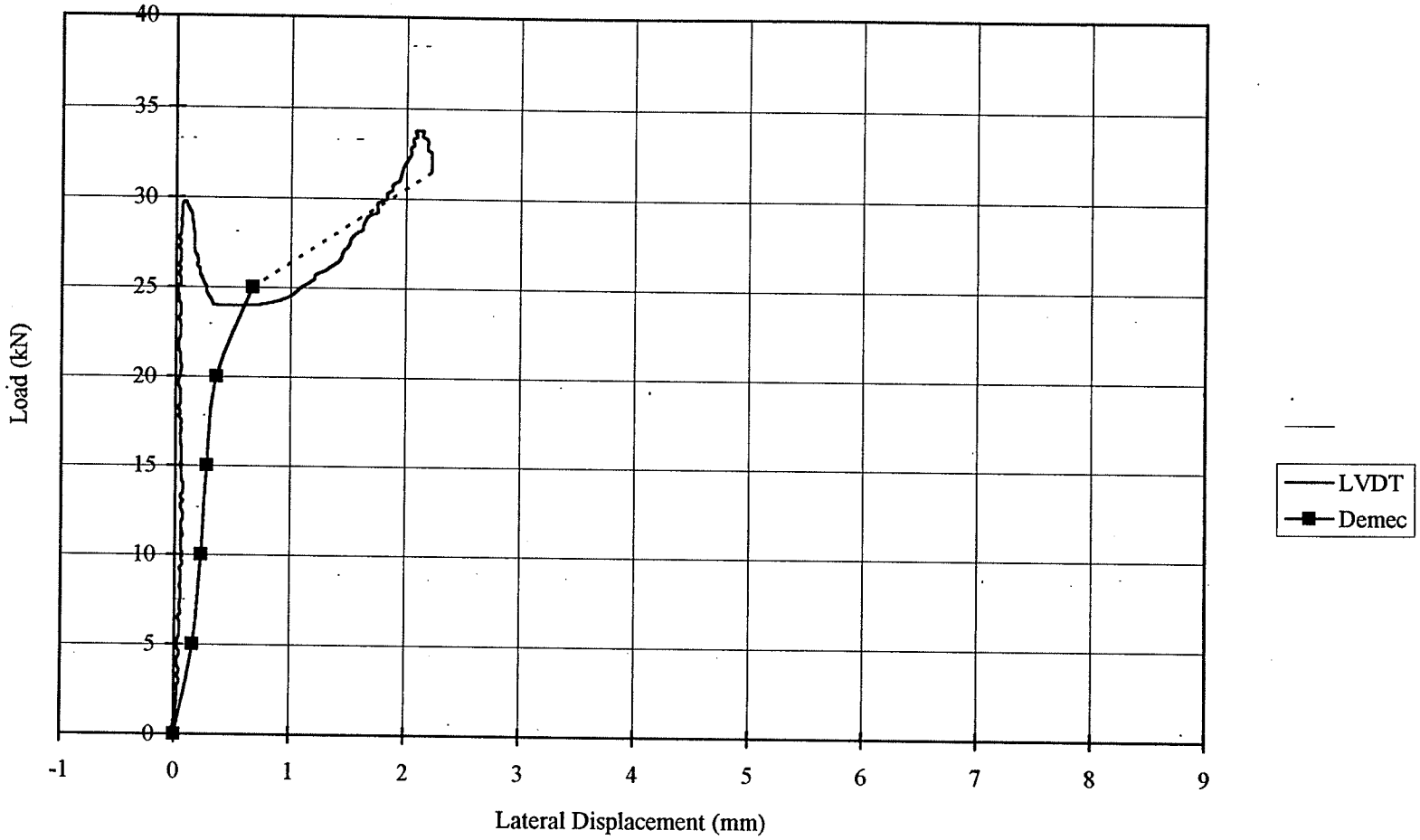

Figure A8: Load Versus Lateral Displacement for Specimen IS-N-1

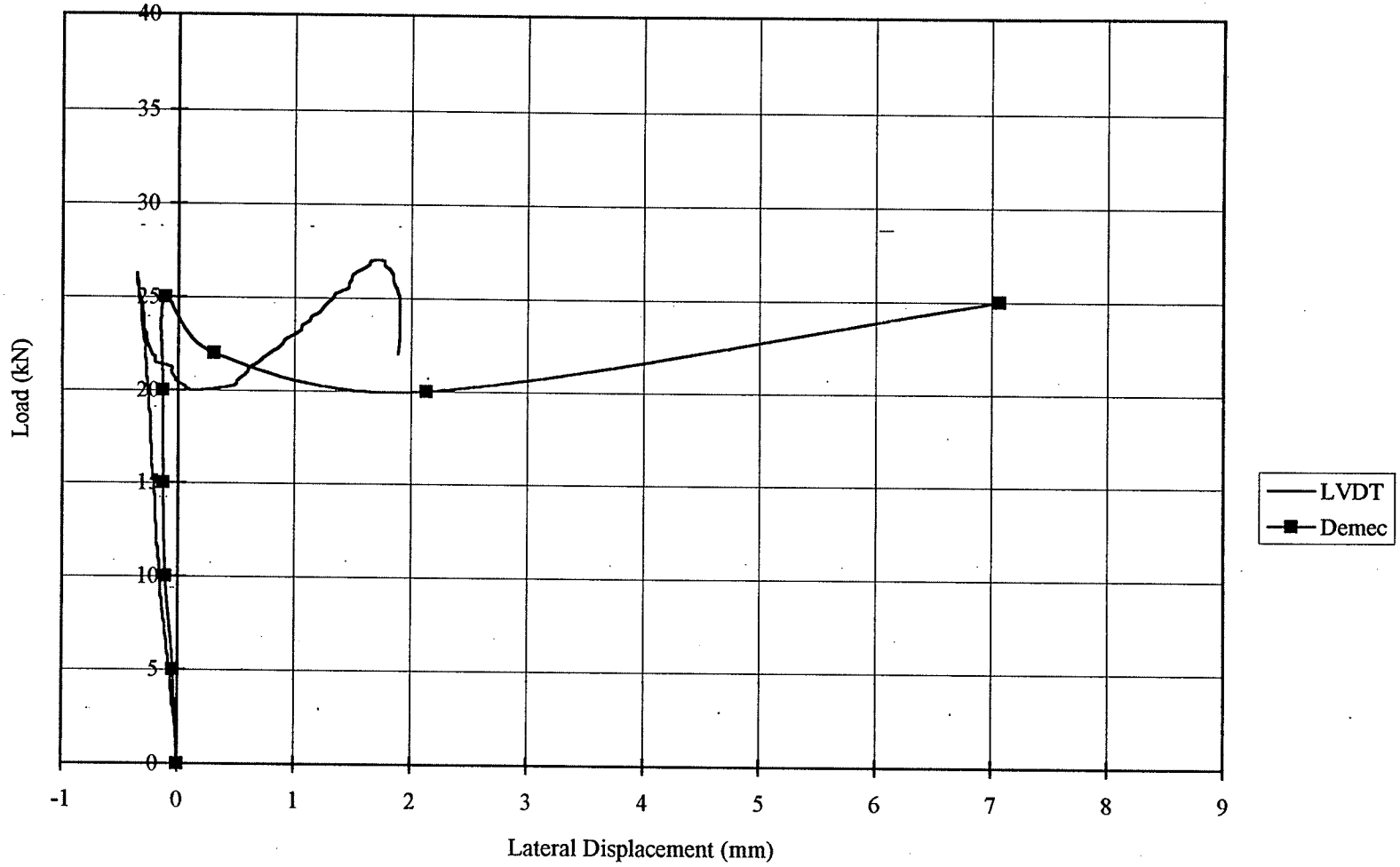

Figure A9: Load Versus Lateral Displacement for Specimen IS-N-2

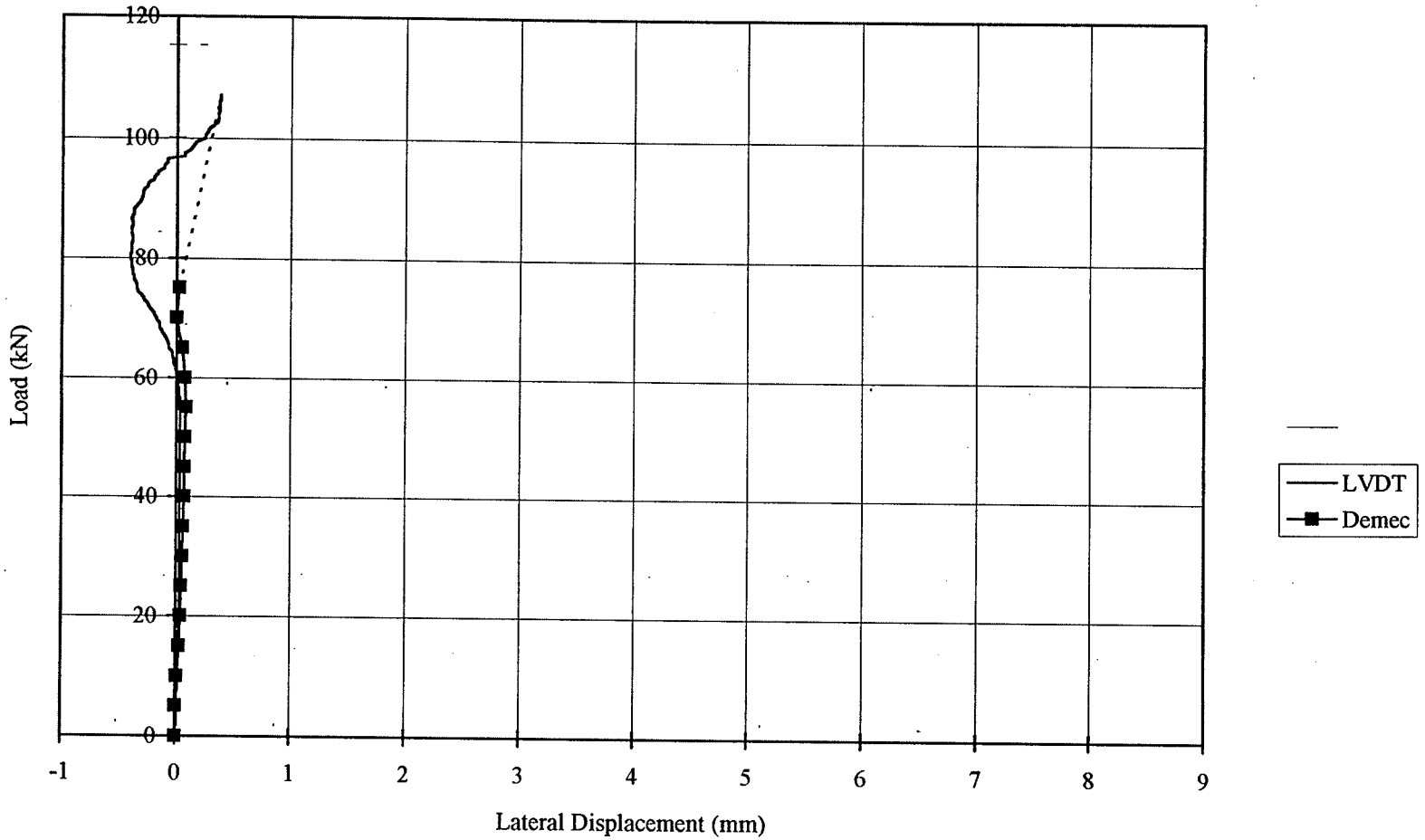

Figure A10: Load Versus Lateral Displacement for Specimen ST-N-1

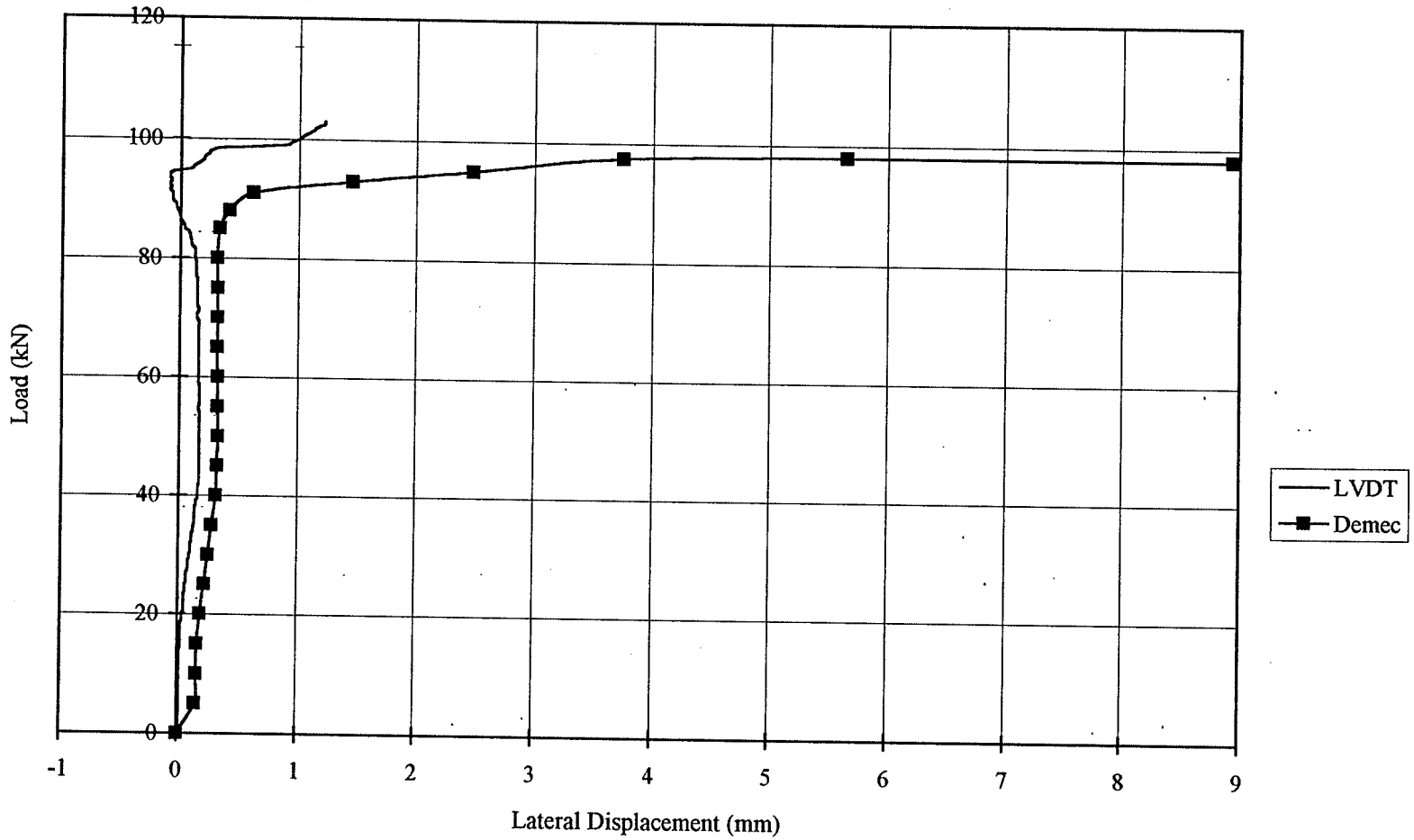

Figure A11: Load Versus Lateral Displacement for Specimen ST-N-2

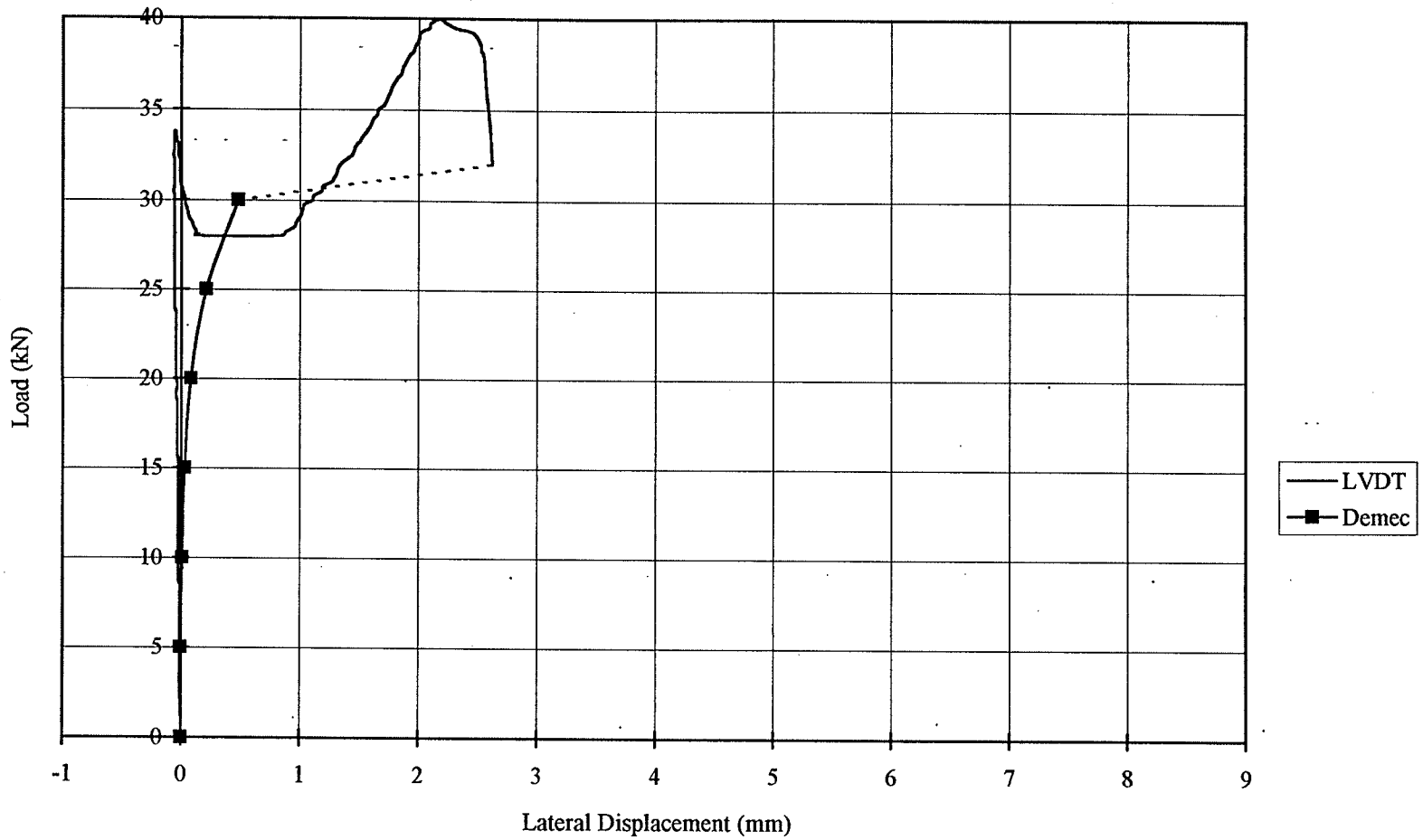

Figure A12: Load Versus Lateral Displacement for Specimen IS-P-1

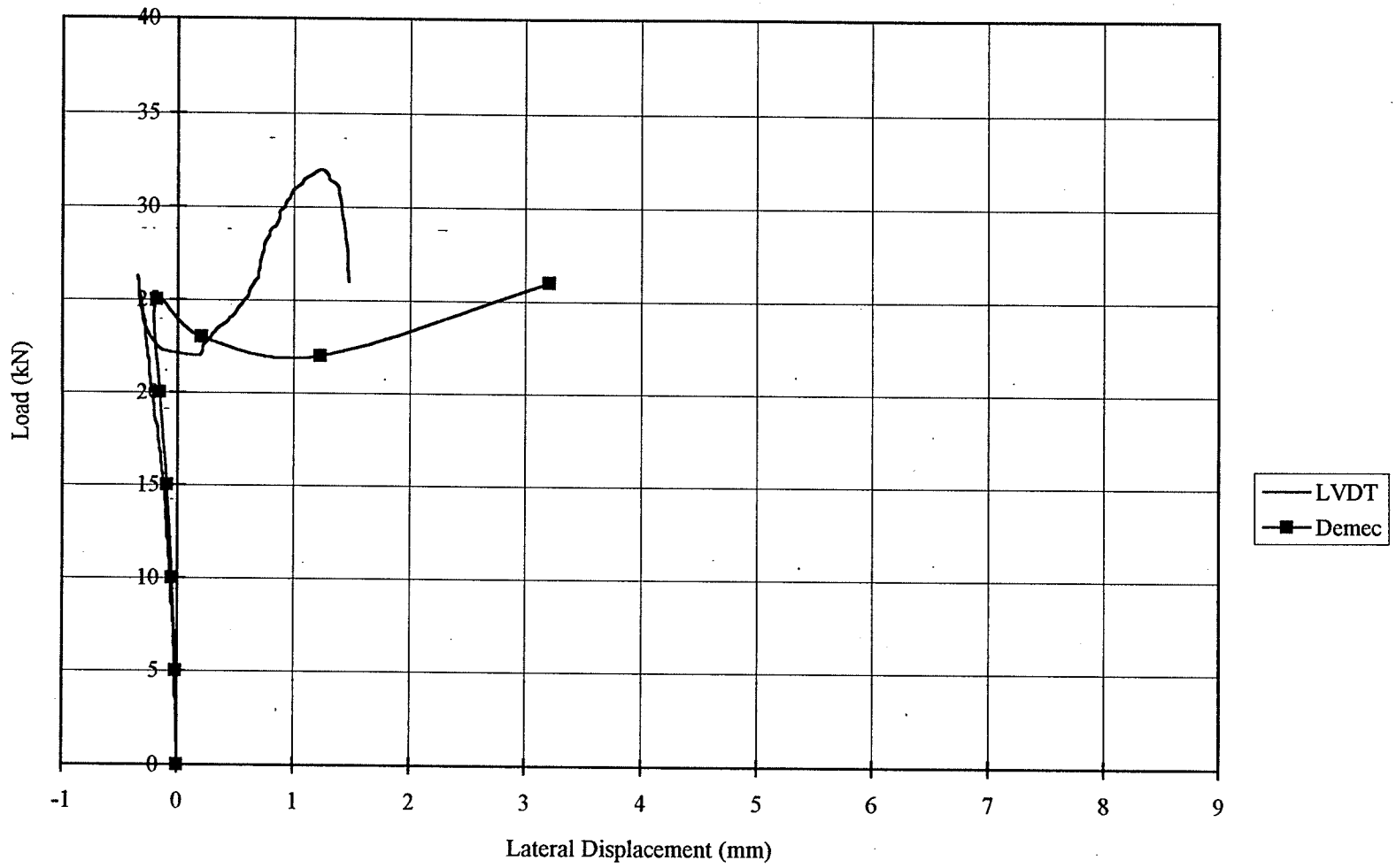

Figure A13: Load Versus Lateral Displacement for Specimen IS-P-2

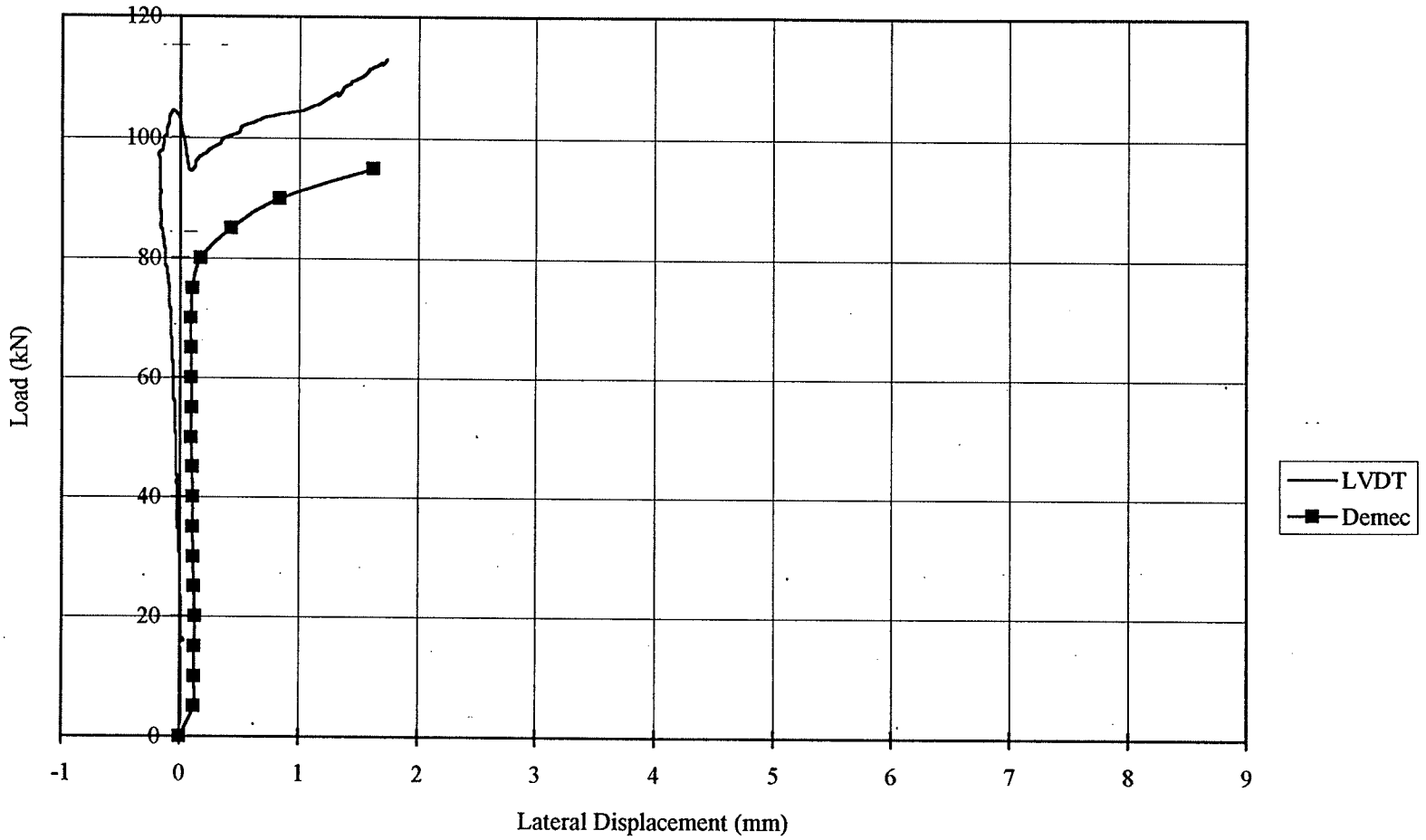

Figure A14: Load Versus Lateral Displacement for Specimen ST-P-1

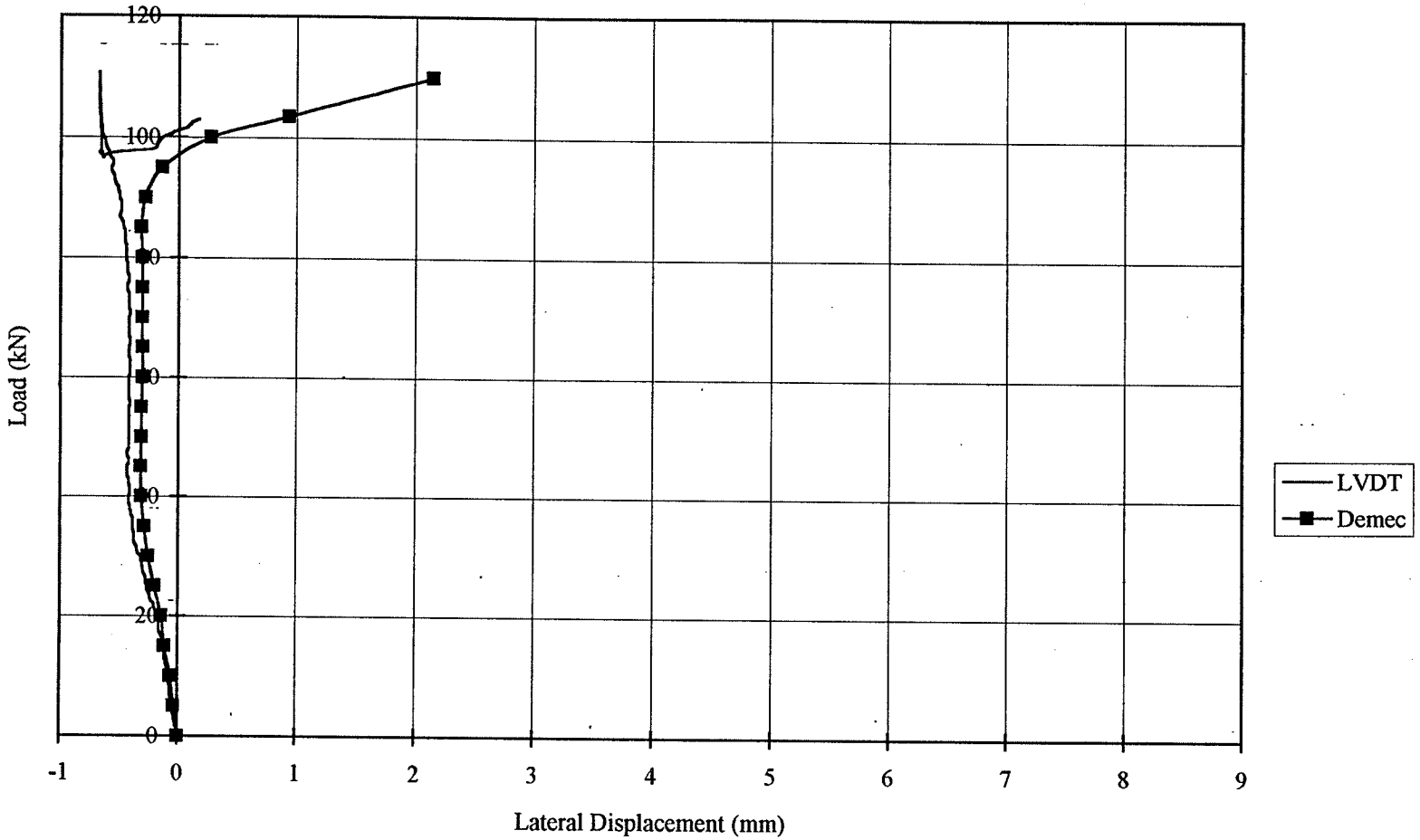

Figure A15: Load Versus Lateral Displacement for Specimen ST-P-2

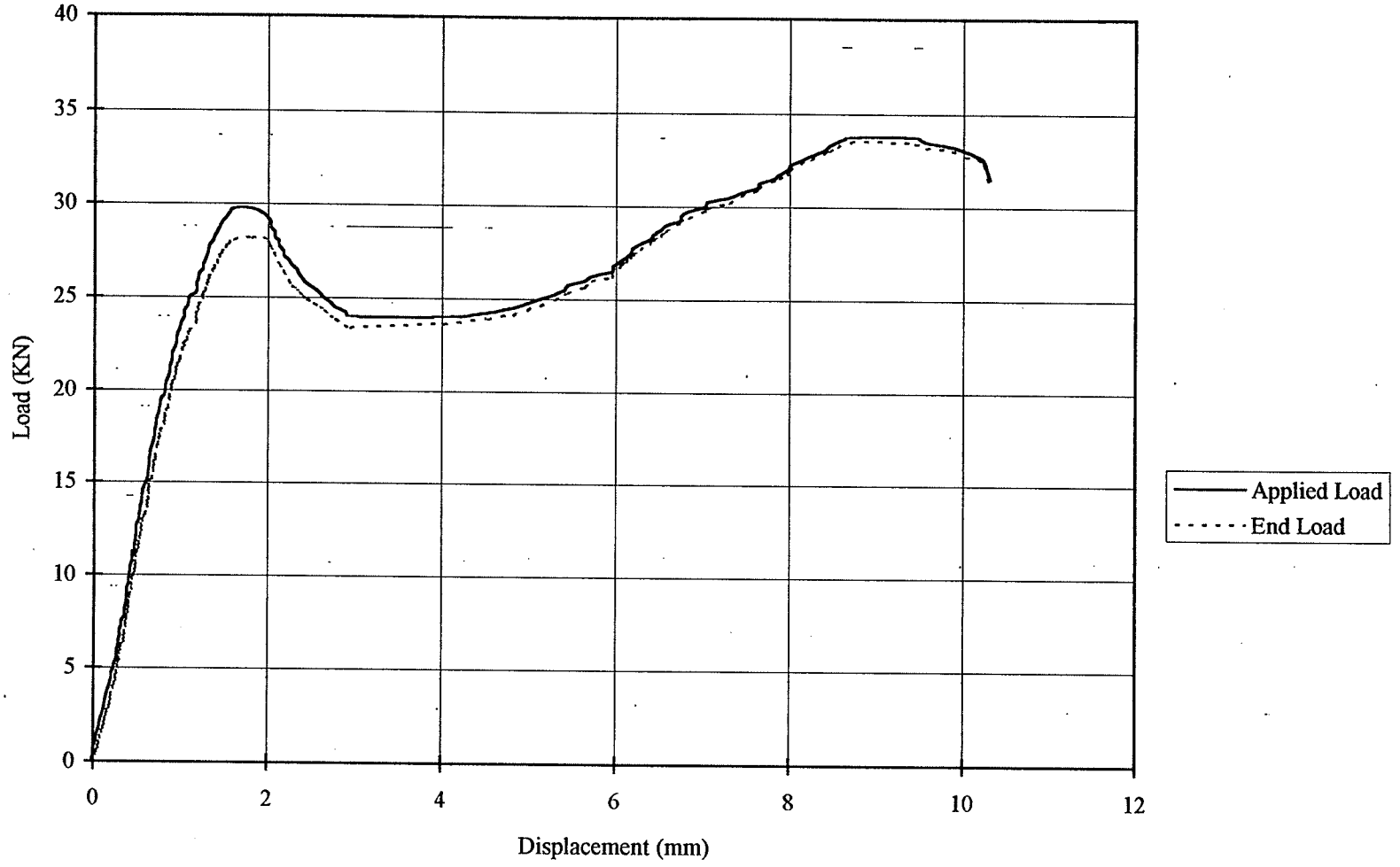

Figure A16: Comparison of Applied Load and End Load for Specimen IS-N-1

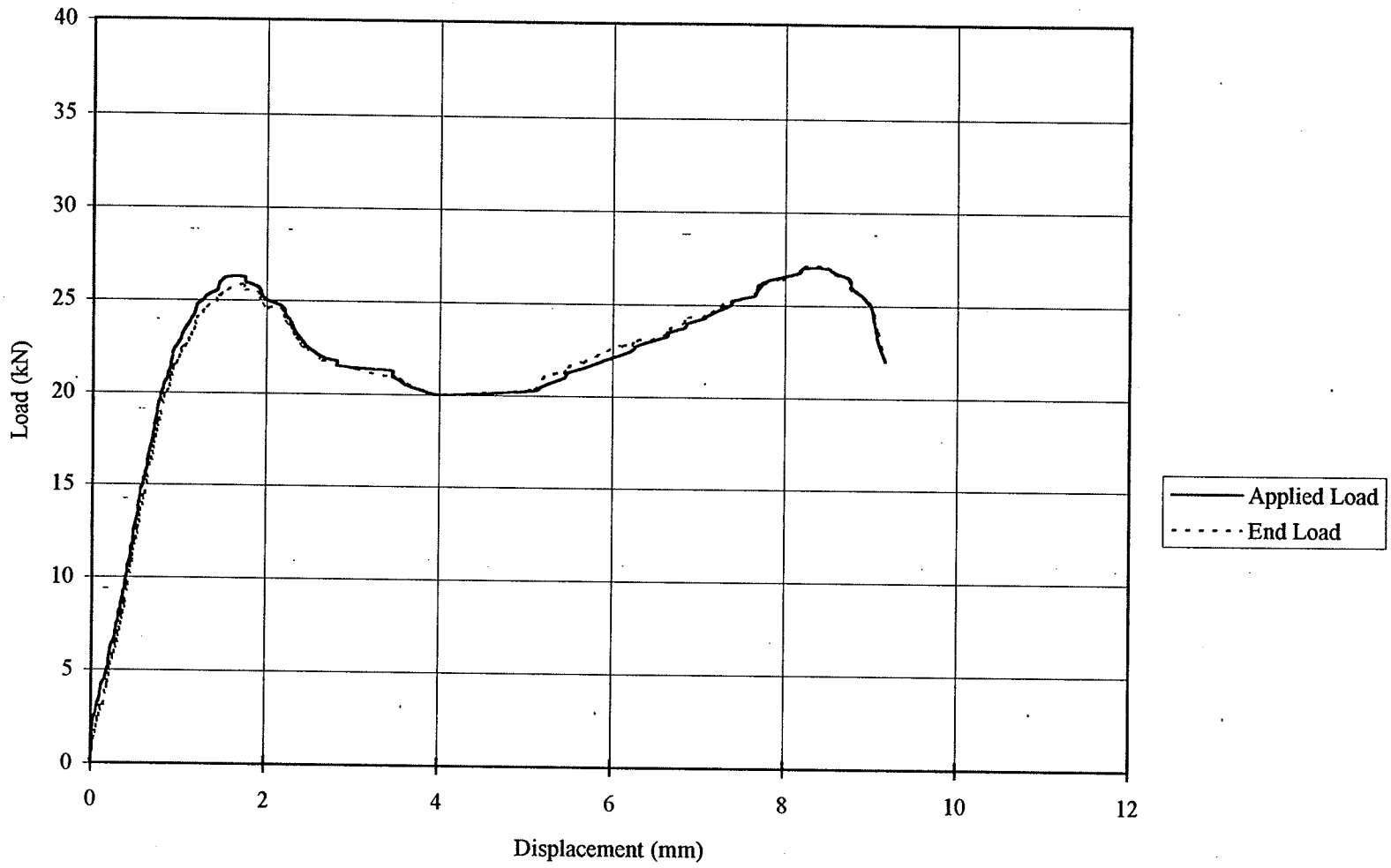

Figure A17: Comparison of Applied Load and End Load for Specimen IS-N-2

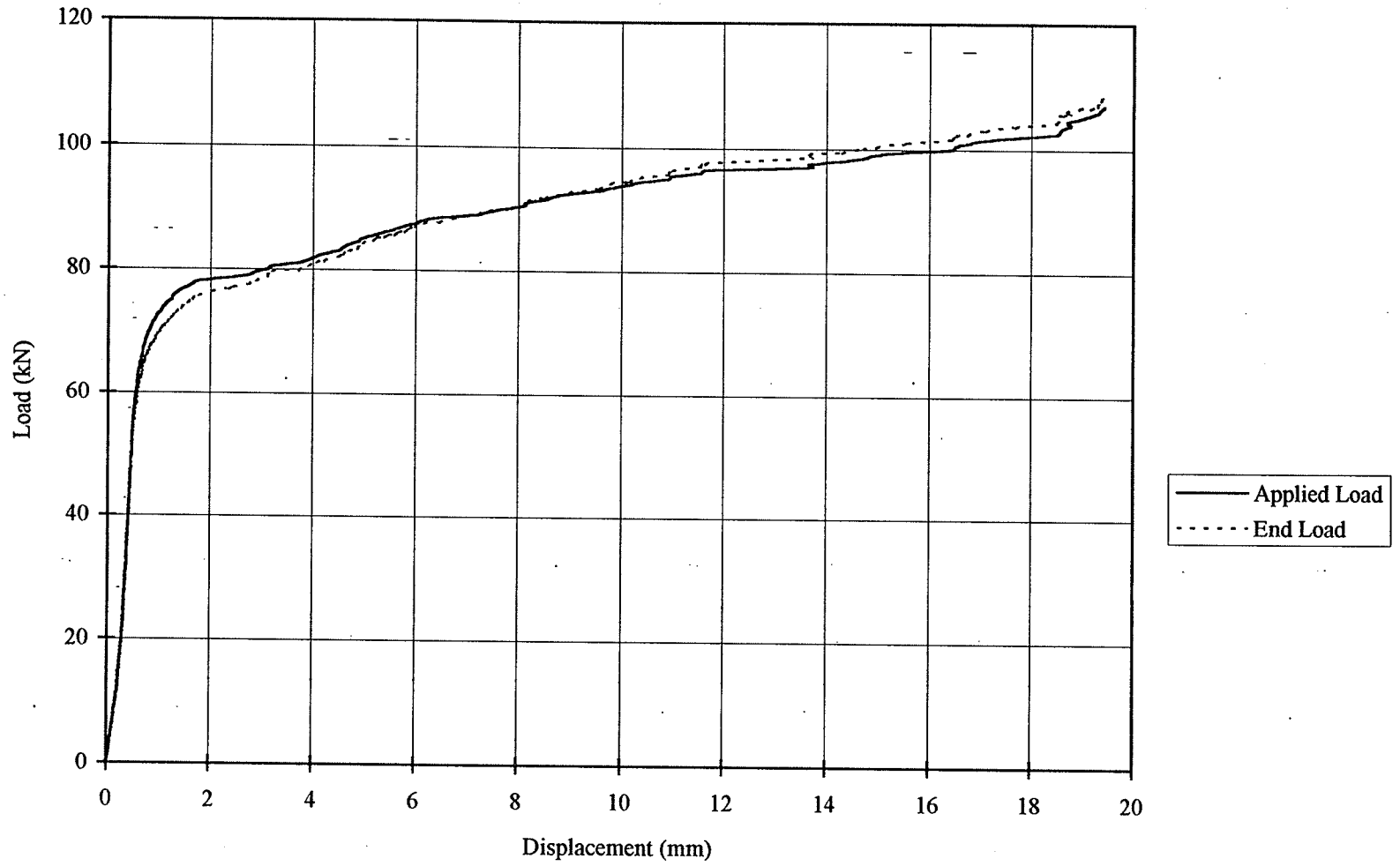

Figure A18: Comparison of Applied Load and End Load for Specimen ST-N-1

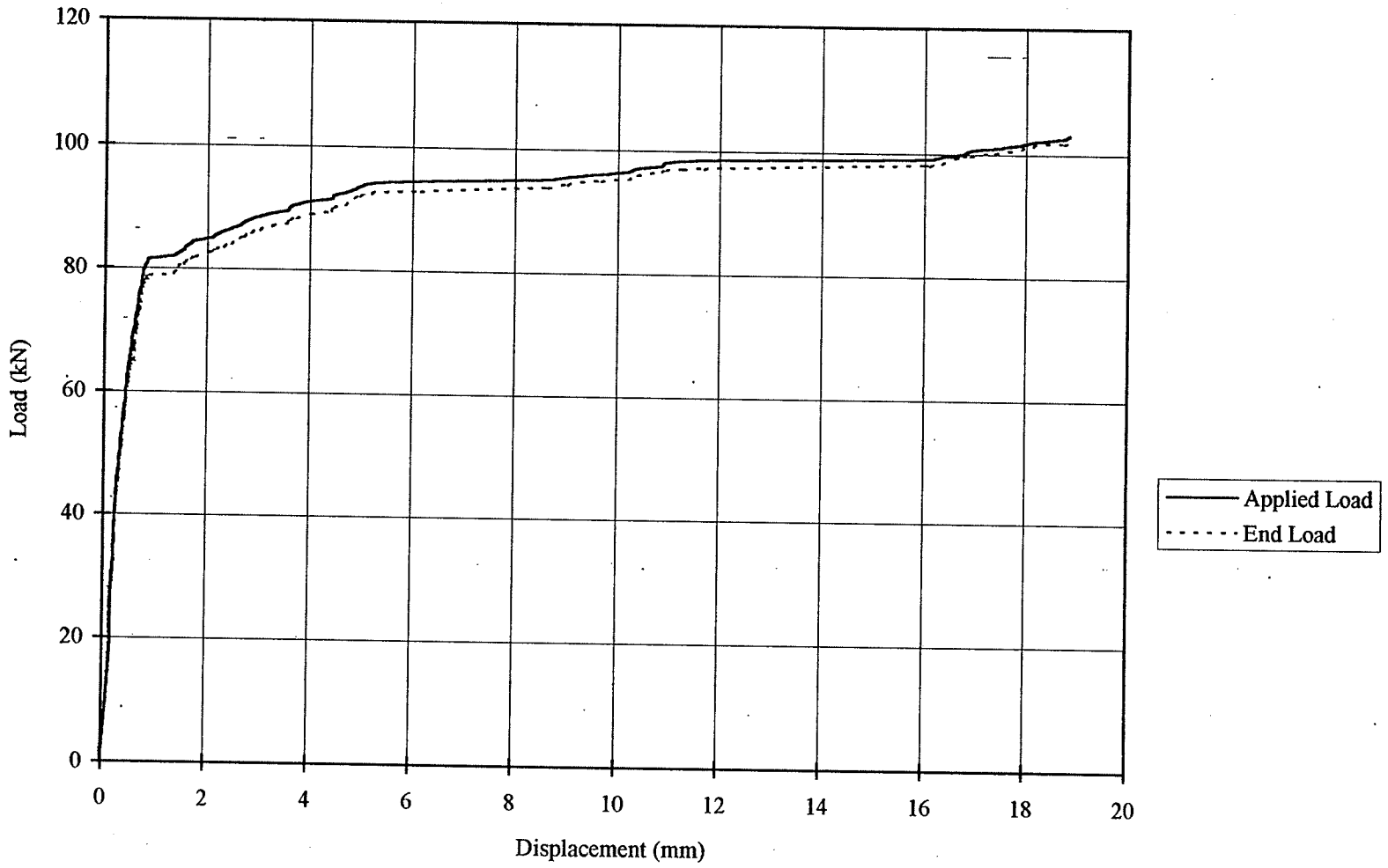

Figure A19: Comparison of Applied Load and End Load for Specimen ST-N-2

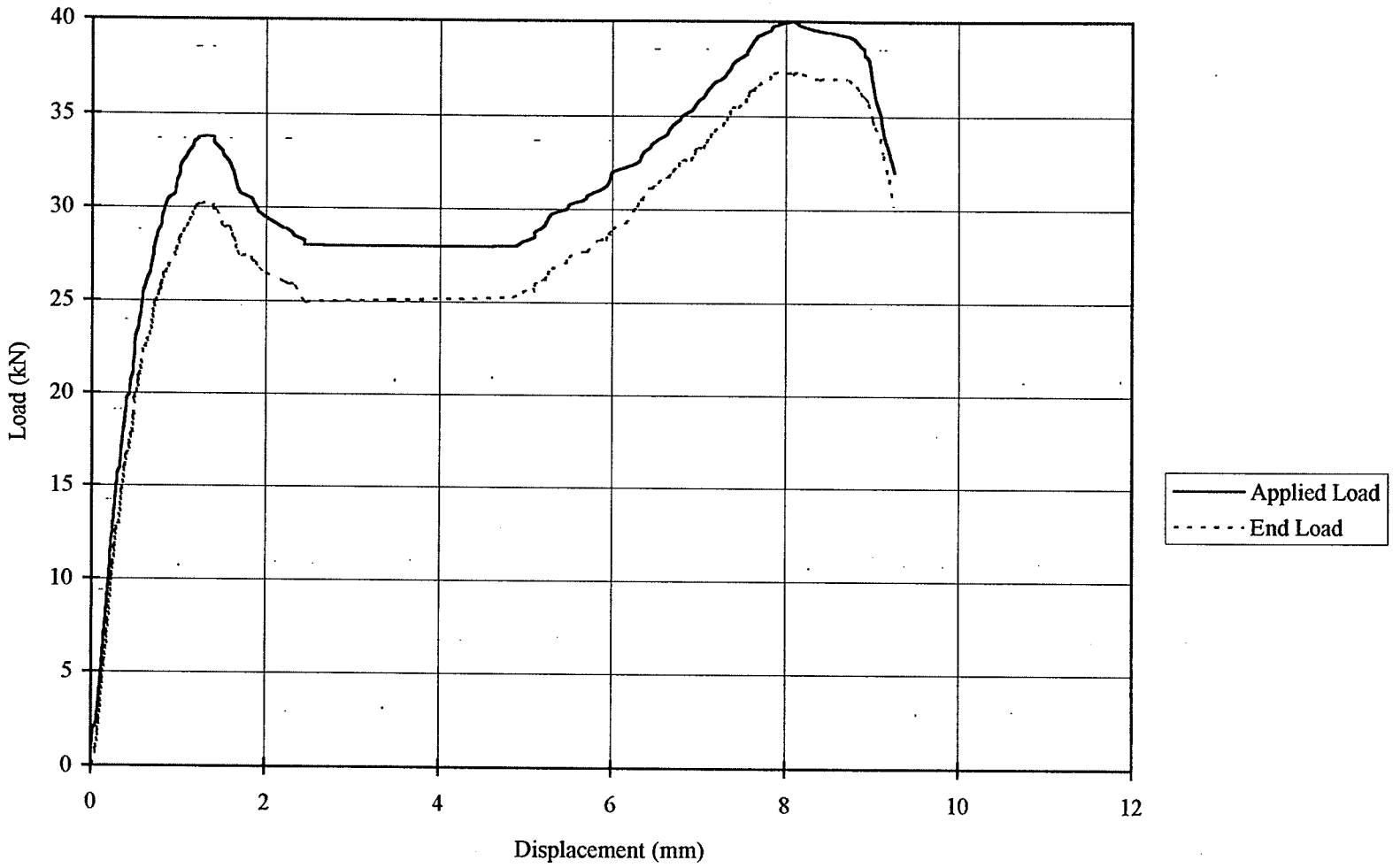

Figure A20: Comparison of Applied Load and End Load for Specimen IS-P-1

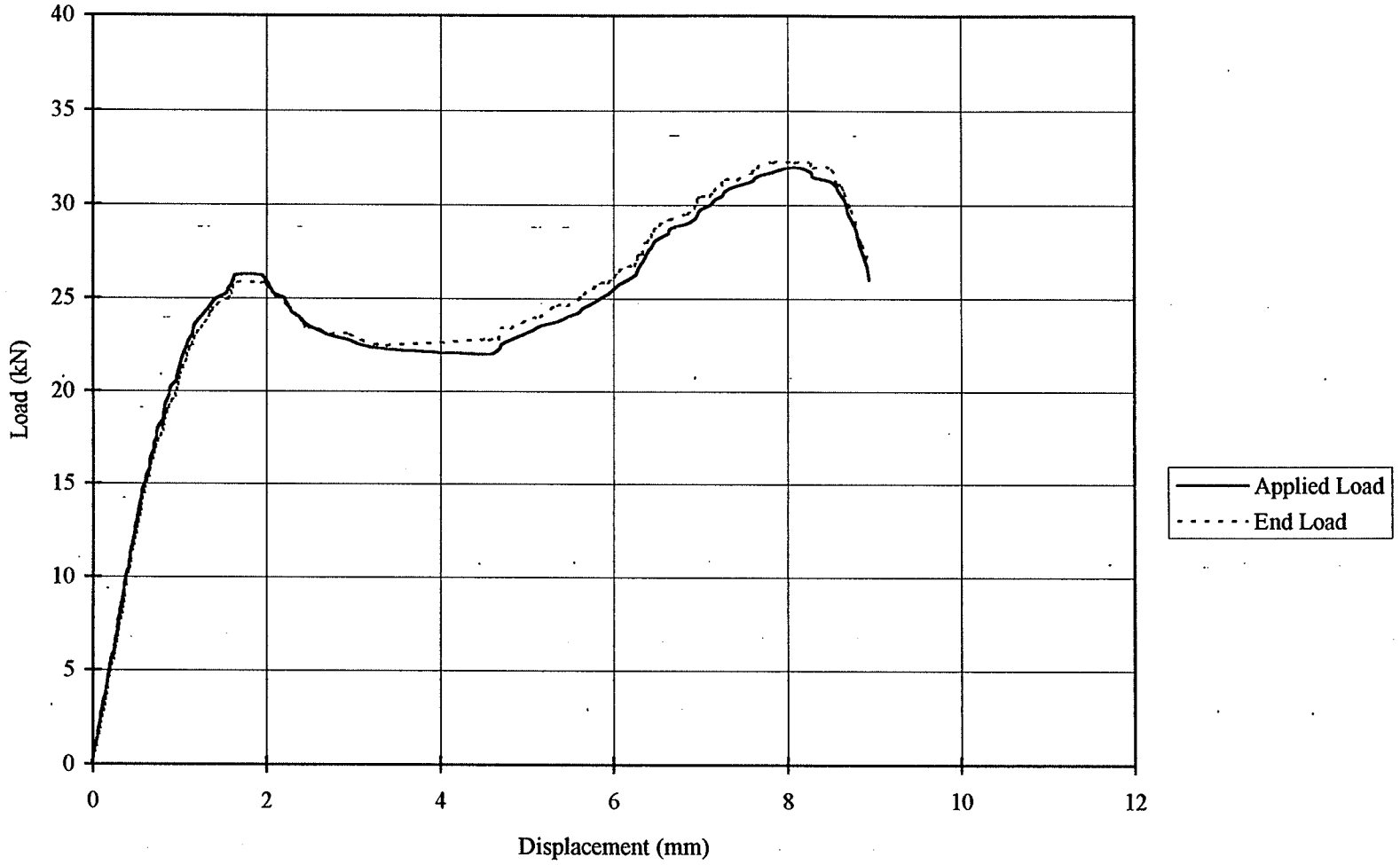

Figure A21: Comparison of Applied Load and End Load for Specimen IS-P-2

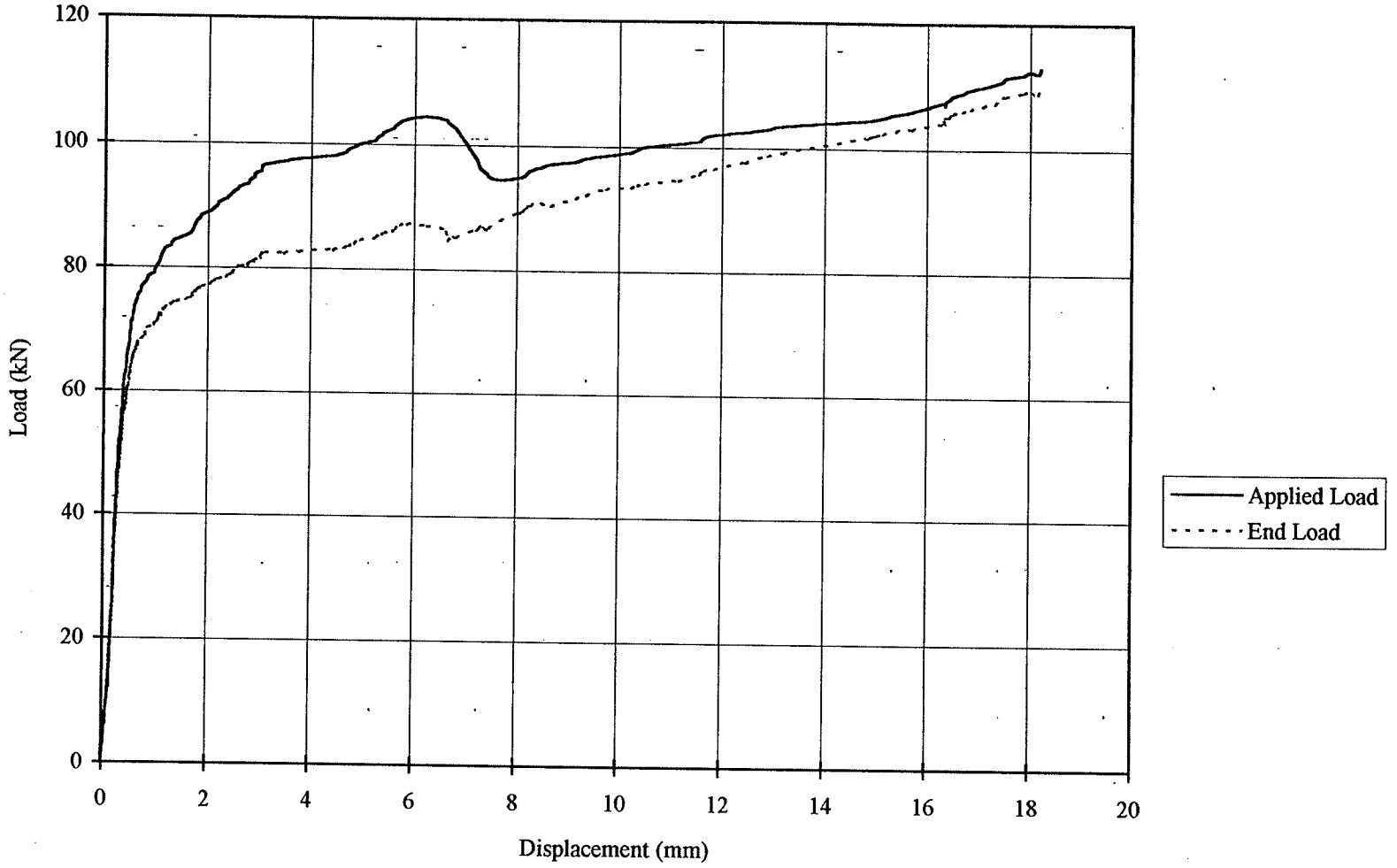

Figure A22: Comparison of Applied Load and End Load for Specimen ST-P-1

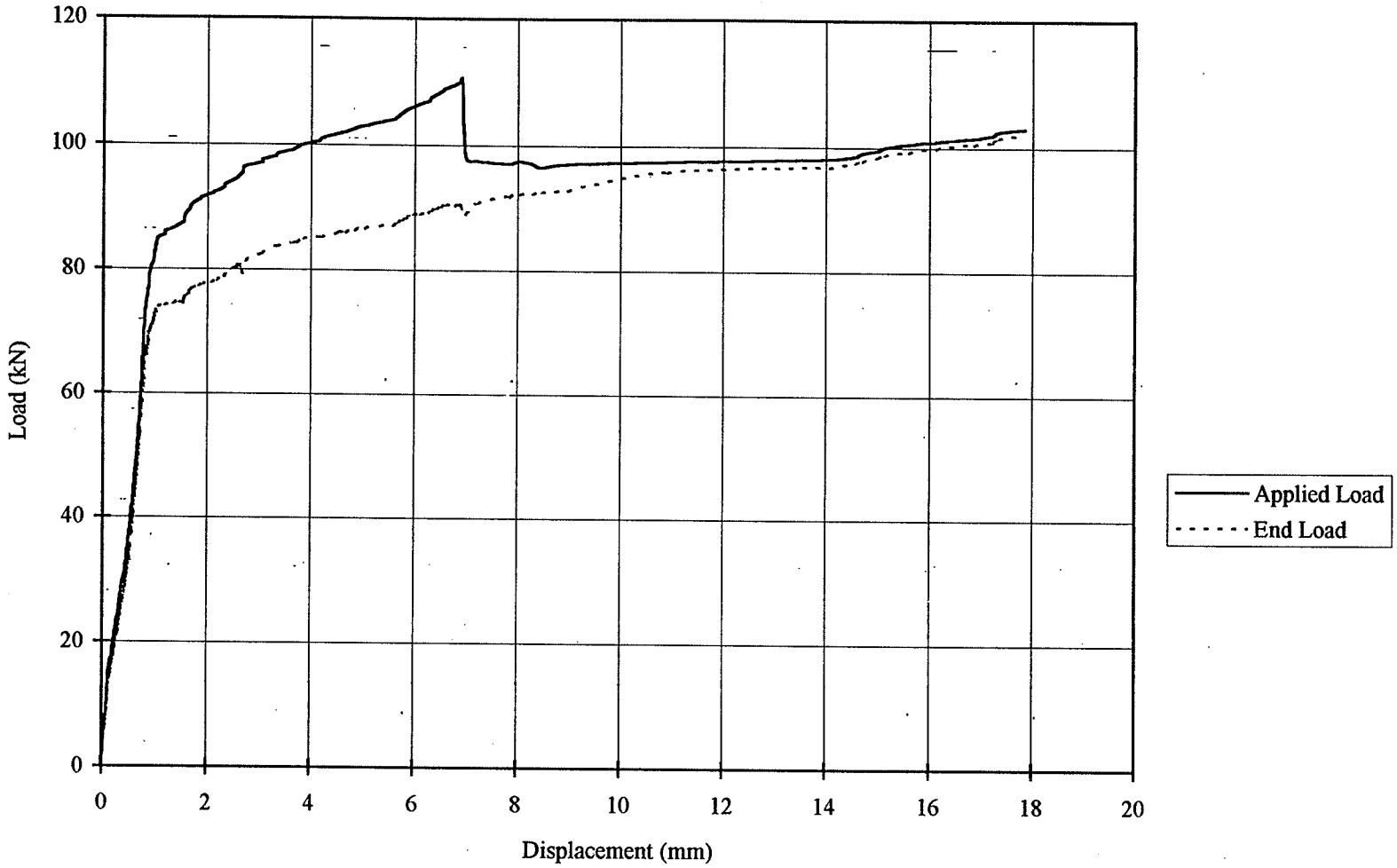

Figure A23: Comparison of Applied Load and End Load for Specimen ST-P-2